

Quantum Transport Theory of Strongly Correlated Matter

Assa Auerbach and Sauri Bhattacharyya

^a*Physics Department Technion 32000 Haifa Israel.*

Abstract

This report reviews recent progress in computing Kubo formulas for general interacting Hamiltonians. The aim is to calculate electric and thermal magneto-conductivities in strong scattering regimes where Boltzmann equation and Hall conductivity proxies exceed their validity. Three primary approaches are explained.

1. Degeneracy-projected polarization formulas for Hall-type conductivities, which substantially reduce the number of calculated current matrix elements. These expressions generalize the Berry curvature integral formulas to imperfect lattices.
2. Continued fraction representation of dynamical longitudinal conductivities. The calculations produce a set of thermodynamic averages, which can be controllably extrapolated using their mathematical relations to low and high frequency conductivity asymptotics.
3. Hall-type coefficients summation formulas, which are constructed from thermodynamic averages.

The thermodynamic formulas are derived in the operator Hilbert space formalism, which avoids the opacity and high computational cost of the Hamiltonian eigenspectrum. The coefficients can be obtained by well established imaginary-time Monte Carlo sampling, high temperature expansion, traces of operator products, and variational wavefunctions at low temperatures.

We demonstrate the power of approaches 1–3 by their application to well known models of lattice electrons and bosons. The calculations clarify the far-reaching influence of strong local interactions on the metallic transport near Mott insulators. Future directions for these approaches are discussed.

arXiv:2406.02677v1 [cond-mat.str-el] 4 Jun 2024

Contents

I	Introduction	5
1	Why calculate conductivities?	5
2	Lingering issues clarified	5
2.1	Are DC Hall conductivities <i>on-shell</i> or <i>off-shell</i> expressions?	5
2.2	What is the origin of magnetization subtractions in α_{xy} and κ_{xy} ? Must we compute them?	6
2.3	Can DC dissipative transport coefficients be expressed in terms of static thermodynamic coefficients?	6
2.4	What are the effects of a Mott insulator phase on the longitudinal and Hall transport of a nearby metal?	6
3	Organization of the report	6
II	Brief history of weak scattering	7
4	Drude theory	8
5	Boltzmann equation	8
5.1	Example: The square lattice	9
5.2	Conductivity relations at low temperatures	10
6	Memory Function Formalism	10
7	Limits of weak scattering approaches	11
III	Kubo Formulas	12
8	Polarizations and Currents	12
9	Examples: Hamiltonians and polarizations	12
10	Kubo formulas in Lehmann Representation	15
10.1	Non-interacting conductivities	15
11	The Tricky DC limit	16
12	Onsager relations	17
13	Hall conductivity proxies	18
13.1	Chern number	18
13.2	Streda formula	19
14	Kubo formulas in operator Hilbert space	20

14.1	Equilibrium Susceptibilities	20
14.2	The Liouvillian and its inverse	20
14.3	Dynamical linear response functions	21
14.4	Electric and Thermal conductivities	22
IV	DPP Hall conductivities	23
15	Derivation of DPP formulas	23
15.1	The Magnetization terms	24
16	DPP formulas for non-interacting Hamiltonians	25
17	Berry curvature integrals	25
18	DPP formula for confined Landau levels	28
19	DPP Hall conductivity in a disordered metal	29
20	Physical consequences of DPP formulas	30
V	Continued fractions of longitudinal conductivities	31
21	Moments expansion	31
21.1	Krylov bases	32
21.2	The continued fraction representation	34
22	From moments to recurrences	34
22.1	Single Mode Spectra	35
23	From recurrences to conductivities	36
23.1	Freud's high order asymptotics	36
23.2	Termination functions	38
23.3	Low frequency behavior	38
23.4	Addition of spectral functions with different frequency scales	40
23.5	Variational Extrapolation of Recurrences	41
VI	Hall coefficients summation formulas	43
24	Magnetic Field Expansion of Hall-type Conductivity	43
25	Hall Coefficient	45
25.1	Weak scattering limit	46
26	Modified Nernst Coefficient	46

27 Thermal Hall coefficient	47
28 Calculating the correction terms	47
29 Optimization of thermodynamic approaches	48
29.1 The Separability problem	48
29.2 Renormalized Hamiltonians at low temperatures	49
VII Strongly Correlated Electrons	51
30 The Hubbard Model	51
31 The tJ Model	51
31.1 Linear Resistivity slope	52
31.2 Hall map for large U/t	54
31.3 Hall coefficient corrections	55
32 Discussion	56
VIII Strongly Correlated Bosons	57
33 The Bose Hubbard model	57
33.1 Weak interactions	58
33.2 Strong interaction	58
34 Hard Core Bosons on the square lattice	60
34.1 Superconducting phase	60
34.2 Metallic phase: longitudinal conductivity	62
34.3 Metallic phase: Hall coefficient	65
34.4 Hall coefficient corrections	66
35 Discussion	66
IX Summary and Future Directions	67
36 Acknowledgements	67

Part I

Introduction

1. Why calculate conductivities?

Theorists commonly describe phases of matter by their order parameters, since they can be calculated by tried and tested algorithms of equilibrium statistical mechanics. These “*thermodynamic methods*” include stochastic series expansions [1], worm algorithm of Quantum Monte-Carlo simulations [2], and variational methods such as density matrix renormalization group [3, 4], projected entangled-pair states [5] and tensor networks [6].

Experimentalists on the other hand, commonly probe phases of matter by transport measurements. For example: Hall coefficients can characterize the current-carriers’ density (near band extrema). Temperature dependent resistivity may herald the onset of superconductivity or charge localization. Quantized Hall conductivity is associated with topologically ordered ground states.

Electric, thermo-electric and thermal transport coefficients, σ , α , $\bar{\alpha}$ and κ , are defined by linear response equations,

$$\begin{aligned}\mathbf{j} &= \sigma \cdot (\mathbf{E} - \nabla\mu/e) + \alpha \cdot (-\nabla T) \quad , \\ \mathbf{j}_Q &= T\bar{\alpha} \cdot (\mathbf{E} - \nabla\mu/e) + \kappa \cdot (-\nabla T) \quad .\end{aligned}\tag{1}$$

\mathbf{j} and \mathbf{j}_Q are the electric and thermal currents respectively. $\mathbf{E} - \nabla\mu/e$ and ∇T are the electrochemical field and temperature gradient respectively. In Eq. (1), the wavevector \mathbf{q} and frequency ω dependence of all variables are suppressed.

For systems described by weakly scattered Bloch-band quasiparticles, the Boltzmann equation [7, 8] and diagrammatic perturbation theory [9] are adequate. For incompressible quantum Hall phases [10] and topological insulators [11], proxies such as the Chern number [12, 13] and Streda formula [14] yield the Hall conductivity.

However, for strongly correlated gapless systems which exhibit “bad metal” phenomenology [15], quasiparticle descriptions may fail. The only Hamiltonian-based alternative to weak scattering approaches is the computation of the Kubo formulas [16]. However, dynamical Kubo formulas may be forbiddingly difficult. Exact diagonalizations entail exponentially large memory costs, and analytic continuation of Quantum Monte Carlo data to real frequencies is ill-posed at low frequencies [17]. Simplifications of Kubo formulas which apply to gapless phases are in dire need.

This Report reviews recent advances which sidestep some of the Kubo formula difficulties, and render conductivity calculations in the presence of strong interactions more accessible.

2. Lingering issues clarified

Before delving into details, we list certain questions which have permeated the common lore of transport theory, and are resolved in this Report.

2.1. Are DC Hall conductivities on-shell or off-shell expressions?

In the Lehmann (eigenstates) representation of Kubo formulas, *on-shell* expressions involve current matrix elements j_{nm}^α between quasi-degenerate states (i.e. whose energies’ separation $E_n - E_m$ vanishes in the large volume limit). On-shell expressions are implemented by taking

$$\lim_{\varepsilon \rightarrow 0} \lim_{\mathbf{q} \rightarrow 0} \lim_{\mathcal{V} \rightarrow \infty} \text{Im} \frac{1}{E_n(\mathcal{V}) - E_m(\mathcal{V}) - i\varepsilon} \rightarrow \pi \lim_{\mathbf{q} \rightarrow 0} \lim_{\mathcal{V} \rightarrow \infty} \delta(E_n(\mathcal{V}) - E_m(\mathcal{V})) \quad .\tag{2}$$

Real longitudinal conductivities turn out to be on-shell expressions.

In contrast, Hall-type (antisymmetric transverse) conductivities, involve sums over the *real* part of energy denominators, i.e.

$$\text{Re} \frac{1}{E_n - E_m - i\varepsilon} = \frac{E_n - E_m}{(E_n - E_m)^2 + \varepsilon^2} \quad .\tag{3}$$

By blithely setting $\varepsilon \rightarrow 0$, and neglecting $O(\varepsilon^2)$ terms, one may be wrongly led to believe that “Hall conductivities are off-shell expressions”, i.e. that they include J_{nm}^α which connect between well separated energies in the large volume limit.

This statement is misleading. As shown below by the degeneracy projected polarization (DPP) formulas in Part IV, on open boundary conditions (OBC), terms of order ε^2 in (3) are *essentially important* in the DC limit! In fact, Hall-type conductivities with OBC are *purely on-shell expressions*. Physically, this implies that at low temperatures, the Hall current is carried by low energy gapless excitations, which may be located in the bulk or at the system’s edges.

Off-shell Kubo formulas have been used in the literature, most notably by Thouless *et al* [12] in their seminal derivation of the quantized Hall conductance of perfectly periodic lattices. However, they are only valid in limited cases such as a gapped ground state with periodic boundary conditions (PBC), as discussed in Section 13.

2.2. What is the origin of magnetization subtractions in α_{xy} and κ_{xy} ? Must we compute them?

The infamous magnetization corrections for α_{xy} and κ_{xy} [18, 19] (which inconveniently diverge at zero temperature) are an artifact of introducing a static “gravitational field” $\psi_{\omega=0}$ in lieu of the temperature gradient $-\nabla T$, which is a *non-equilibrium* statistical force. The static ψ produces superfluous magnetization currents which must be subtracted from the Kubo formula in the DC limit [18, 19]. However, magnetization subtractions can be eliminated using the DPP formulas for α_{xy} and κ_{xy} as shown in subsection 15.1. The magnetization terms also fall out of the Hall coefficient summation formulas of Part VI.

2.3. Can DC dissipative transport coefficients be expressed in terms of static thermodynamic coefficients?

At first thought, one may suspect that expressions involving on-shell scattering rates (i.e. Fermi’s golden rule), may not be applicable to calculations of static thermodynamic averages.

On the other hand, it has long been realized that some dynamical conductivities may be computed by continued fraction representations [20, 21], which are constructed from the conductivity moments which are a set of thermodynamic averages. The price to pay is a necessary *extrapolation* of the calculated moments up to infinite order. While this may turn out to be a daunting task, extrapolation is occasionally facilitated by appealing to mathematical relations, which are reviewed in Section 23. These relations connect between high order moments and high frequency limits of the dynamical conductivity.

In a different approach, Part VI derives thermodynamic summation formulas for the low magnetic field Hall-type coefficients. Truncation of this sum may sometimes be justified by calculating leading order corrections, as demonstrated in the model examples of Part VII and Part VIII.

2.4. What are the effects of a Mott insulator phase on the longitudinal and Hall transport of a nearby metal?

Strong local interactions effects give rise to the Mott insulator and extend deep into the nearby metallic phase. The effects include large high temperature linear resistivity slopes, and Hall coefficient sign reversal and divergence at low doping of the Mott insulator. These effects are captured by thermodynamic Kubo formula calculations of the two dimensional t-J model and Hard Core Bosons model, in Part VII and Part VIII respectively.

3. Organization of the report

In Part II, we present a brief review of Drude, Boltzmann, and memory functional transport theories which apply to Hamiltonians of weakly scattered quasiparticles. In Parts III-VI, we lay the mathematical basis for approaches applicable to strongly interacting Hamiltonians. First, in Part III, the Kubo formula with its proper DC order of limits is defined. The reversal of that order of limits in Chern number and Streda formula proxies is discussed.

New approaches are derived, starting from Part IV, where the DPP formulas for DC Hall type conductivities are presented. The DPP formulas reduce to Berry curvature integrals in the disorder-free limit. Part V derives the continued

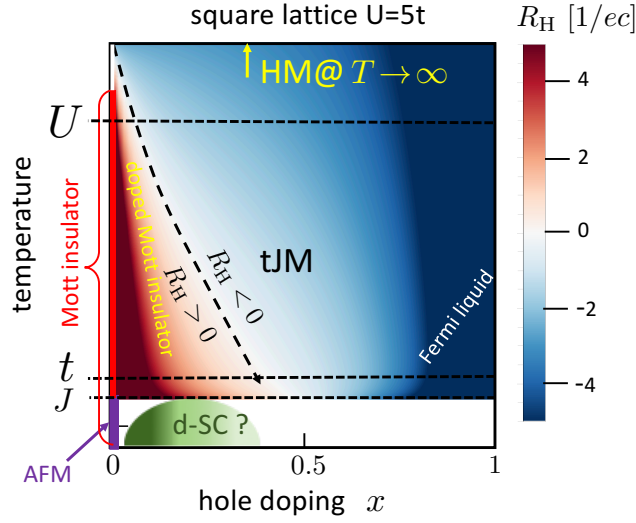


Figure 1: Hall coefficient map for the strongly interacting Hubbard model on the square lattice. The Hall coefficient was calculated [22] using the thermodynamic summation formula reviewed in Part VI. The model and its parameters are defined in Part VII. The anomalous (reddish-brown) region near the Mott insulator is a consequence of the strong local electron-electron interactions which affect the current commutation relations and produce the sign reversal and divergence. At low temperatures (beyond the present analysis), we mark the region of antiferromagnetic (AFM) order, and a hypothetical region of d -wave superconductivity (d-SC) [3, 23, 24].

fraction conductivities from the moments expansion, and presents viable extrapolation schemes. Part VI derives the Hall coefficient summation formulas.

Part VII demonstrates recent application [22] of the continued fraction conductivity and Hall coefficient summation formula to strongly interacting electrons near a Mott insulator, as modelled by the two dimensional Hubbard and t-J Hamiltonians. The resulting Hall coefficient map is depicted in Fig. 1. Part VIII demonstrates the application of the same formulas to obtain the resistivity and Hall coefficient of strongly interacting lattice bosons.

Part IX summarizes the Report. A discussion of strategies for optimizing the thermodynamic approaches is given. Future applications and directions of research are proposed.

Part II

Brief history of weak scattering

Perturbative calculations of Kubo formulas for DC conductivities of metals suffer from the singular effect of scattering. At leading order in impurity concentration an infinite resummation of diagrams is needed to obtain a finite longitudinal conductivity at finite impurity concentration [9].

Older (and simpler) alternatives for the weak scattering regimes are to apply the Drude and Boltzmann approaches. In this Report, unless otherwise specified, we use units of $\hbar = k_B = 1$.

4. Drude theory

Drude theory [25] is particularly useful for lightly doped semiconductors. It is based on a Fermi gas of electrons of mass m^* and charge e whose kinetic energy is described by the single particle dispersion,

$$\epsilon_{\mathbf{k}} = \frac{\mathbf{k}^2}{2m^*} . \quad (4)$$

Collisions with disorder and other electrons are introduced by a scattering time τ . Solving for the single electron equation of motion in a time dependent field, the dynamical longitudinal conductivity is

$$\sigma_{xx}^{\text{Drude}}(\omega) = \frac{ne^2}{m^*} \frac{\tau}{1 + (\omega\tau)^2} . \quad (5)$$

where e is the electron charge. The DC conductivities in a uniform magnetic field $\mathbf{B} = B\hat{\mathbf{z}}$ are

$$\begin{aligned} \sigma_{xx}^{\text{dc}} &= \frac{ne^2}{m^*} \frac{\tau}{1 + (\omega_c\tau)^2} , \\ \sigma_{xy}^{\text{dc}} &= \frac{ne^2}{m^*} \frac{\omega_c\tau^2}{1 + (\omega_c\tau)^2} , \end{aligned} \quad (6)$$

where $\omega_c = \frac{eB}{m^*c}$ is the cyclotron frequency, and c is the speed of light. The zero field Hall coefficient is defined as,

$$R_{\text{H}}^{\text{Drude}} \equiv - \lim_{B \rightarrow 0} \frac{\rho_{xy}(B)}{B} = \frac{1}{\sigma_{xx}^{\text{dc}}(0)} \left. \frac{d\sigma_{xy}^{\text{dc}}}{dB} \right|_{B=0} = \frac{1}{nec} . \quad (7)$$

Thus, $R_{\text{H}}^{\text{Drude}}$ is proportional to the inverse charge density. We note that $R_{\text{H}}^{\text{Drude}}$, in contrast to σ_{xy} , is independent of dynamical parameters m^* and τ . Later, in Part VI, the expression of the Hall coefficient in terms of thermodynamic coefficients is shown to be a general feature of non-separable Hamiltonians.

5. Boltzmann equation

The single band Boltzmann equation (BE) [7, 8, 26] for the quasiparticle distribution function deviation $\delta f_{\mathbf{k},r}$ is based on small deviations from the Fermi-Dirac distribution $f_0(\epsilon_{\mathbf{k}} - \mu)$, where $\epsilon_{\mathbf{k}}$ is the non-interacting Bloch band dispersion, \mathbf{k} is a wavevector within the Brillouin zone (BZ), and μ is the chemical potential. In the presence of an externally imposed electrochemical field $\mathbf{E} - \frac{1}{e}\nabla\mu$ and temperature gradient $-\nabla T$, the BE is,

$$\frac{\partial \delta f}{\partial t} + \dot{\mathbf{k}} \cdot \frac{\partial \delta f}{\partial \mathbf{k}} + \dot{\mathbf{x}}_{\mathbf{k}} \cdot \left[-\nabla\mu - \frac{\epsilon_{\mathbf{k}} - \mu}{T} \nabla T \right] \left(\frac{\partial f_{\mathbf{k}}^0}{\partial \epsilon} \right) = \mathcal{I}_{\mathbf{k}}^1[\delta f] . \quad (8)$$

where the semiclassical equations of motion are,

$$\begin{aligned} \dot{\mathbf{x}}_{\mathbf{k}} &= \nabla_{\mathbf{k}} \epsilon_{\mathbf{k}} - \dot{\mathbf{k}} \times \boldsymbol{\Omega}_{\mathbf{k}} , \\ \dot{\mathbf{k}} &= e\mathbf{E} - \frac{e}{c} \dot{\mathbf{r}}_{\mathbf{k}} \times \mathbf{B} . \end{aligned} \quad (9)$$

The band and spin indices are suppressed. The band Berry curvature $\boldsymbol{\Omega}_{\mathbf{k}}$, which modifies the velocity [26, 27] is given by,

$$\boldsymbol{\Omega}_{\mathbf{k}} \equiv i \langle \nabla_{\mathbf{k}} u_{\mathbf{k}} | \times | \nabla_{\mathbf{k}} u_{\mathbf{k}} \rangle , \quad (10)$$

where $|u_{\mathbf{k}}\rangle$ is the periodic part of the Bloch state. $\mathcal{I}_{\mathbf{k}}^1$ is the collision integral which is commonly simplified by the relaxation time approximation,

$$\mathcal{I}_{\mathbf{k}}^1[f] = -\frac{\delta f_{\mathbf{k}}}{\tau_{\mathbf{k}}} . \quad (11)$$

Weak electron-electron and electron-phonon interactions can be incorporated into BE by renormalizing the $\mathbf{v}_{\mathbf{k}}$, and contributing to the quasiparticle scattering rate $1/\tau_{\mathbf{k}}$.

In the absence of time-reversal symmetry breaking in the equilibrium density matrix, the electric and thermal currents are given respectively by

$$\begin{aligned}\mathbf{j} &= \sum_{\mathbf{k} \in \text{BZ}} \mathbf{v}_{\mathbf{k}} \delta f_{\mathbf{k}} \quad , \\ \mathbf{j}_Q &= \sum_{\mathbf{k} \in \text{BZ}} (\epsilon_{\mathbf{k}} - \mu) \mathbf{v}_{\mathbf{k}} \delta f_{\mathbf{k}} \quad ,\end{aligned}\tag{12}$$

where BZ is the Brillouin zone. Using the solution of Eq. (8) in (12), for C_4 symmetric bands, yields BE expression for the DC longitudinal and Hall conductivities,

$$\begin{aligned}\sigma_{xx}^{\text{dc}} &= \frac{e^2}{c\mathcal{V}} \sum_{\mathbf{k}} \left(-\frac{\partial f}{\partial \epsilon} \right) (v_{\mathbf{k}}^x)^2 \tau_{\mathbf{k}} \quad , \\ \sigma_{xy}^{\text{dc}} &= \frac{e^3 B}{c\mathcal{V}} \sum_{\mathbf{k} \in \text{BZ}} \left(-\frac{\partial f_{\mathbf{k}}^0}{\partial \epsilon} \right) v_{\mathbf{k}}^y \tau_{\mathbf{k}} \left(v_{\mathbf{k}}^y \frac{\partial}{\partial k_x} - v_{\mathbf{k}}^x \frac{\partial}{\partial k_y} \right) (v_{\mathbf{k}}^x \tau_{\mathbf{k}}) \quad .\end{aligned}\tag{13}$$

For an isotropic (energy dependent) scattering time $\tau_{\mathbf{k}} = \tau(\epsilon_{\mathbf{k}})$, one obtains simplified expressions at low temperatures relative to the Fermi energy ϵ_F ,

$$\begin{aligned}\sigma_{xx}^{\text{dc}} &= \tau(\epsilon_F) \chi_{\text{csr}} \quad , \\ \sigma_{xy}^{\text{dc}} &= \tau^2(\epsilon_F) \frac{e^3}{c\mathcal{V}} \sum_{\mathbf{k} \in \text{BZ}} \left(-\frac{\partial f_{\mathbf{k}}^0}{\partial \epsilon} \right) \left(v_{\mathbf{k}}^y \left(v_{\mathbf{k}}^y \frac{\partial}{\partial k_x} - v_{\mathbf{k}}^x \frac{\partial}{\partial k_y} \right) v_{\mathbf{k}}^x \right) \quad ,\end{aligned}\tag{14}$$

where the conductivity sum rule (CSR) is,

$$\chi_{\text{csr}} = \frac{e^2}{\mathcal{V}} \sum_{\mathbf{k} \in \text{BZ}} \left(-\frac{\partial f_{\mathbf{k}}^0}{\partial \epsilon} \right) (v_{\mathbf{k}}^x)^2 \quad .\tag{15}$$

The Hall coefficient acquires a scattering time independent expression [8],

$$R_{\text{H}}^{\text{Boltz}} = \frac{e^3}{c\chi_{\text{csr}}^2 \mathcal{V}} \sum_{\mathbf{k}} \left(-\frac{\partial f_{\mathbf{k}}^0}{\partial \epsilon} \right) \left(v_{\mathbf{k}}^y \left(v_{\mathbf{k}}^y \frac{\partial}{\partial k_x} - v_{\mathbf{k}}^x \frac{\partial}{\partial k_y} \right) v_{\mathbf{k}}^x \right) \quad .\tag{16}$$

Eq. (16) generalizes Drude's result (7) to non-spherical Fermi surfaces.

5.1. Example: The square lattice

The square lattice (SL) tight binding model is,

$$H^{\text{SL}} = - \sum_{\langle ij \rangle, s=\uparrow, \downarrow} t_{ij} (c_{is}^\dagger c_{js} + c_{js}^\dagger c_{is}) \quad ,\tag{17}$$

where c_{is}^\dagger creates an electron on site i with spin s . $\langle ij \rangle$ are nearest neighbor bonds on the square lattice (SL), and electron occupation per site is $n_{is} = c_{is}^\dagger c_{is}$.

The Hall coefficients given by Eq. (16) and related band structure contours are depicted in Fig. 2 for nearest neighbor (nn) and next nearest neighbor (nnn) model.

The most important prediction of Boltzmann theory is that the Hall coefficient is everywhere continuous and diverges only toward the full and empty band limits.

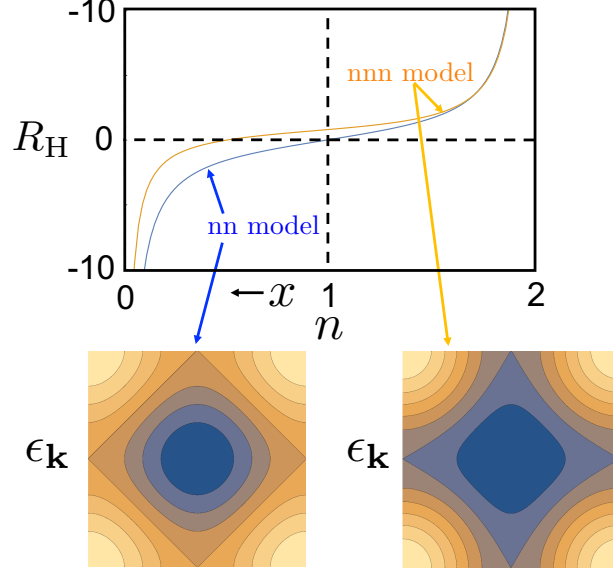


Figure 2: Hall coefficient R_H , as given by Boltzmann equation of the weakly scattered ($U = 0$) square lattice, given by Eq. (16) at $T = 0$. n is the electron filling, and x is the hole doping concentration customarily used in describing cuprate superconductors. The nearest neighbor (nn) model has particle-hole antisymmetry about $n = 1$. Next nearest neighbor (nnn) hopping moves the Hall sign reversal toward lower electron density.

5.2. Conductivity relations at low temperatures

For C_4 symmetric bands, the isotropic lifetime leads to simple relations between for the longitudinal electric, thermoelectric and thermal conductivities, which can be expanded at low temperatures as

$$\begin{aligned}
 \sigma_{xx}^{\text{dc}}(T) &= \sigma_{xx}^{\text{dc}}(0) \left(1 + \frac{\pi^2 (k_B T)^2}{8 \mu^2} + \dots \right) \\
 \alpha_{xx}^{\text{dc}}(T) &= \frac{\sigma_{xx}^{\text{dc}}(0) \pi^2 (k_B T)^2}{e^2 2 \mu} + \dots \\
 \kappa_{xx}^{\text{dc}}(T) &= \frac{\sigma_{xx}^{\text{dc}}(0) \pi^2}{e^2 3} (k_B T)^2 + \dots
 \end{aligned} \tag{18}$$

As $T \rightarrow 0$, one obtains the Wiedemann-Franz law

$$\frac{\kappa}{\sigma T} = \frac{\pi^2}{3} (k_B/e)^2 = 2.45 \times 10^{-8} \text{V}^2 \text{K}^{-2} \quad . \tag{19}$$

6. Memory Function Formalism

The Memory Function (MF) formalism [28, 29, 30] is closely related to the OHS formulation of dynamical response functions as described in Section 14.

A primary goal of the MF was to obtain the dynamical response of a set of “slow operators” which nearly commute with the Hamiltonian, by integrating out all the “fast operators” to obtain a self energy, called ‘memory matrix’ $M(z)$. Götze-Wölfle [31] have applied the MF to evaluate the longitudinal conductivity in a weakly scattered parabolic band of effective mass m^* ,

$$\sigma_{xx}(\omega) = \frac{ne^2}{m^*} \text{Re} \frac{i}{z - M(z)/\frac{ne^2}{m^*}} \quad , \tag{20}$$

where $M(z)$ is the current-current correlation function. They consider a white noise random potential V , whose ensemble average is

$$\langle V_{\mathbf{q}} V_{-\mathbf{q}'} \rangle_{\text{dis}} = w^2 \delta_{\mathbf{q}, -\mathbf{q}'} \quad , \quad (21)$$

and its commutator with the current is

$$[j^x, V_{\mathbf{q}}] = -i \frac{\hbar}{m} q_x V_{\mathbf{q}} \quad . \quad (22)$$

At low temperatures, MF recovers Drude result (5),

$$\sigma_{xx} = \frac{ne^2\tau}{m^*} \quad . \quad (23)$$

The MF scattering rate agrees with Fermi's golden rule,

$$\frac{\hbar}{\tau} = \pi \mathcal{N}(\epsilon_F) w^2 \quad , \quad (24)$$

where $\mathcal{N}(\epsilon_F)$ is the density of electron states at the Fermi energy.

More generally, the MF separation of timescales can facilitate obtaining the low temperature and frequency conductivities by renormalization of the dynamical response functions onto the low energy Hilbert space.

In Part V, the memory function $M(z)$ can be related to the first order termination function $\Delta_1^2 G_{11}^>(z)$ in the continued fraction of the longitudinal conductivity.

7. Limits of weak scattering approaches

BE describes transport by quasiparticles in the conduction band, with velocity $\mathbf{v}_{\mathbf{k}}$ at wavevector \mathbf{k} near the Fermi surface. For elastic scattering in dimensions one and two, BE is invalidated by wavefunction localization [32, 33, 34, 35]. The collision integral of Eq. (8) describes incoherent scattering processes which do not lead to localization.

The validity of BE depends on the existence of well defined quasiparticles. Inelastic scattering broadens the quasiparticle energies and wavevectors by $1/\tau$ and $2\pi/l$. The BE therefore requires

$$\epsilon_F \tau \gg 1 \quad , \quad k_F l \gg 1 \quad . \quad (25)$$

The criteria (25) have been related by Ioffe and Regel (IR) [36] to experimental values of the resistivity. Using the simplified Drude theory of a parabolic band, $\epsilon_F = \hbar^2 k_F^2 / 2m^*$, and $n = k_F^3 / 3\pi^2$, and by (5), one obtains an upper bound on value of resistivity which can be explained by Boltzmann equation,

$$\rho_{xx} = \frac{m^*}{ne^2\tau} = \frac{3\lambda_F}{2} \frac{\hbar}{e^2} \frac{1}{k_F l} \leq \rho_{xx}^{\text{IR}}|_{k_F l=1} \quad . \quad (26)$$

For typical cubic metals with $\lambda_F \sim 1\text{nm}$, the IR limit is $\rho_{xx}^{\text{IR}} \simeq 40\mu\Omega \text{ cm}$.

In metals, ρ_{xx} usually increases with temperature due to enhanced inelastic scattering. Many metals (see review in [37]) exhibit resistivity saturation at the values not far above the IR limit.

However, resistivity in certain strongly correlated metals exceeds this limit as temperature is raised, which has been dubbed ‘‘bad metal’’ behavior [15]. Boltzmann equation fails to account for this regime.

In semimetals and semiconductors with a small interband gap Δ_{ib} , interband matrix elements of the current must be included when

$$\Delta_{\text{ib}} \tau < 1 \quad . \quad (27)$$

This leads to a multi-band BE, which involves coupled equations for intra-band and inter-band distribution functions [38, 39, 40]. The equations are in general unwieldy. In the presence of disorder and electron-phonon scattering, a microscopic knowledge of inter-band temperature dependent scattering rates, and inter-band current matrix elements, is required.

Part III

Kubo Formulas

8. Polarizations and Currents

Kubo's formulation [16] of dynamical linear response, provides a rigorous approach to calculating conductivities of a microscopic model Hamiltonian H_0 which is supported on a finite d -dimensional volume \mathcal{V} .

The underlying assumption of Kubo's linear response theory is that local equilibrium is established throughout the sample. In other words, the currents' equilibration length and time scales are much shorter than those of the driving fields.

Following Luttinger [18, 41, 42], it is also assumed that the same electric and thermal currents which are driven by slowly varying *statistical* forces, such as $-\nabla\mu$ and $-\nabla T$, can be induced by *mechanical* electric and "gravitational" forces, \mathbf{E} and ψ respectively, which couple linearly to the Hamiltonian,

$$H(t) = H_0 - \Theta(t) \int \frac{d^d q}{(2\pi)^d} \left(\mathbf{P}_q \mathbf{E}_{-q}(t) + \frac{1}{T} \mathbf{Q}_q \psi_{-q}(t) \right) . \quad (28)$$

The polarizations which couple to the external force fields are,

$$\begin{aligned} \text{Electric polarization :} \quad \mathbf{P}_q &= e \int_{\mathcal{V}} d^d x e^{-iq \cdot \mathbf{x}} \mathbf{x} n(\mathbf{x}) , \\ \text{Thermal polarization :} \quad \mathbf{Q}_q &= \int_{\mathcal{V}} d^d x e^{-iq \cdot \mathbf{x}} \mathbf{x} (h(\mathbf{x}) - \mu n(\mathbf{x})) . \end{aligned} \quad (29)$$

$n(\mathbf{x})$ is particle density and $h(\mathbf{x})$ is a local decomposition of the Hamiltonian which satisfies,

$$H_0 = \int d^d x h(\mathbf{x}) . \quad (30)$$

The Kubo formulas for conductivities require knowledge of H_0 and its polarization operators of Eq. (29). The electric and thermal currents are derived by Heisenberg's equations,

$$\begin{aligned} \mathbf{j}_q &= i [H_0, \mathbf{P}_q] , \\ (\mathbf{j}_Q)_q &= i [H_0, \mathbf{Q}_q] . \end{aligned} \quad (31)$$

We note that the polarizations (29) depend on the choice of coordinate \mathbf{x} . However, any finite shift in the origin $\mathbf{x} \rightarrow \mathbf{x} + \mathbf{a}$ drops out of the commutators in Eqs. (31). For PBC, uniform polarizations can be defined as a $\mathbf{q} \rightarrow 0$ limit after taking volume to infinity, as shown later in Eqs. (59).

9. Examples: Hamiltonians and polarizations

The explicit forms of polarizations are shown for five generic models of many particle systems.

1. The Hamiltonian of N_p interacting Schrödinger particles (bosons or fermions) in first quantization notation is,

$$H_0^{\text{particles}} = \sum_{i=1}^{N_p} \frac{\mathbf{P}_i^2}{2m} + \sum_i V(\mathbf{x}_i) + \sum_{i<j} U(\mathbf{x}_i - \mathbf{x}_j) , \quad (32)$$

where $[\mathbf{x}_i^\alpha, \mathbf{p}_j^\beta] = i\hbar\delta_{ij}\delta_{\alpha\beta}$. The polarizations are given by,

$$\begin{aligned} P_{\mathbf{q}}^\alpha &= -|e| \sum_{i=1}^{N_p} \mathbf{x}_i^\alpha e^{-i\mathbf{q}\cdot\mathbf{x}_i} \quad , \\ Q_{\mathbf{q}}^\alpha &= \sum_{i=1}^{N_p} \frac{1}{2} \left\{ x_i^\alpha e^{-i\mathbf{q}\cdot\mathbf{x}_i}, \frac{\mathbf{p}_i^2}{2m} \right\} + \sum_i x_i^\alpha e^{-i\mathbf{q}\cdot\mathbf{x}_i} \left(V(\mathbf{x}_i) + \sum_{i<j} U(\mathbf{x}_i - \mathbf{x}_j) \right) \quad . \end{aligned} \quad (33)$$

2. Particles on a lattice L with electric charge e^* , local occupation n_i , and hermitian two-site interaction terms:

$$\begin{aligned} H_0^{\text{lattice}} &= \sum_{ij \in L} O_{ij} \quad , \\ P_{\mathbf{q}}^\alpha &= -|e^*| \sum_{i \in L} e^{-i\mathbf{q}\cdot\mathbf{x}_i} x_i^\alpha n_i \quad , \\ Q_{\mathbf{q}}^\alpha &= \sum_{i \in L} e^{-i\mathbf{q}\cdot\mathbf{x}_i} x_i^\alpha \left(\left(\sum_{j \in L} O_{ij} \right) - \mu n_i \right) \quad . \end{aligned} \quad (34)$$

3. General non-interacting (NI) normal Hamiltonians in second quantized form as

$$H^{\text{NI}} = \sum_l \epsilon_l a_l^\dagger a_l \quad , \quad [a_l, a_{l'}^\dagger]_{\pm} = \delta_{ll'} \quad . \quad (35)$$

where a_l^\dagger creates a particle of charge e^* in single-particle eigenstate $|l\rangle$ with energy ϵ_l . $[\bullet, \bullet]_{\pm}$ denotes an anticommutator (commutator) for fermions (bosons).

The polarizations are given by the bilinear forms,

$$\begin{aligned} P_{\mathbf{q}}^\alpha &= ie^* \frac{\partial}{\partial q^\alpha} \sum_{l'l'} \langle l|e^{-i\mathbf{q}\cdot\mathbf{x}}|l'\rangle a_l^\dagger a_{l'} \quad , \\ Q_{\mathbf{q}}^\alpha &= i \frac{\partial}{\partial q^\alpha} \sum_{l'l'} \frac{\epsilon_l + \epsilon_{l'} - 2\mu}{2} \langle l|e^{-i\mathbf{q}\cdot\mathbf{x}}|l'\rangle a_l^\dagger a_{l'} \quad . \end{aligned} \quad (36)$$

4. Non-interacting normal Hamiltonians of bosons or fermions with M basis states $\{|\mathbf{R}, i\rangle\}$ per unit cell at lattice site $\mathbf{R} \in L$:

$$\langle \mathbf{R}, i | \mathbf{R}', i' \rangle = \delta_{\mathbf{R}, \mathbf{R}'} \delta_{i, i'} \quad . \quad (37)$$

In a periodic crystal (PC), the Hamiltonian is given by

$$H^{\text{PC}} = \sum_{\mathbf{k} \in \text{BZ}} \sum_{ij=1}^M (h_{ij}(\mathbf{k}) - \mu \delta_{ij}) a_{\mathbf{k}, i}^\dagger a_{\mathbf{k}, j} \quad . \quad (38)$$

$a_{\mathbf{k}, i}^\dagger |0\rangle = |\mathbf{k}, i\rangle$ creates a fermion (boson) state of wavevector $\mathbf{k} \in \text{BZ}$ of lattice L , and basis state i . After taking $\mathcal{V} \rightarrow \infty$, the polarization operators of Eq. (36) may be represented by continuous derivatives with respect to \mathbf{q} ,

$$\begin{aligned} P_{\mathbf{q}}^\alpha &= e \sum_{\mathbf{k}ij} a_{\mathbf{k}, i}^\dagger (i\nabla_{\mathbf{q}}^\alpha a_{\mathbf{k}+\mathbf{q}, j}) \quad , \\ Q_{\mathbf{q}}^\alpha &= \sum_{\mathbf{k}ij} a_{\mathbf{k}, i}^\dagger \left\{ \left(\frac{h_{ij}(\mathbf{k}) + h_{ij}(\mathbf{k} + \mathbf{q})}{2} - \mu \delta_{ij} \right), i\nabla_{\mathbf{q}}^\alpha \right\} a_{\mathbf{k}+\mathbf{q}, j} \quad . \end{aligned} \quad (39)$$

5. Coupled Harmonic Oscillators (CHO) Eq. can describe collective bosonic modes such as phonons [43] and magnons [44] in an insulator. A general CHO Hamiltonian which linearly couples to an external orbital magnetic field is,

$$H^{\text{CHO}} = \frac{1}{2} \sum_i \frac{p_i^2}{m_i} + \frac{1}{2} \sum_{i,j} u_i D_{ij} u_j + \sum_{\alpha=x,y,z} B^\alpha \cdot \sum_{i,j} p_i M_{ij}^\alpha u_j \quad , \quad (40)$$

where $i \rightarrow \mathbf{x}_i$, $s(i)$ denotes both site and polarization indices, where and $[u_i, p_j] = i\delta_{ij}$ are canonically conjugated coordinates. m_i and D_{ij} are local mass and force constants. H^{CHO} can include lattice imperfections, impurities with different masses m_i , and boundaries. The magnetic field \mathbf{B} breaks time reversal symmetry by coupling between u_i and p_j as represented by a magnetization matrix \mathbf{M} . The thermal polarization is,

$$Q_q^\alpha = \sum_{i=1}^N e^{iq \cdot \mathbf{x}_i} x_i^\alpha \left(\frac{p_i^2}{2m_i} + \frac{1}{2} u_i \sum_j D_{ij} u_j + \frac{1}{2} p_i \sum_j \sum_{\alpha=x,y,z} B^\alpha \cdot \sum_j M_{i,j}^\alpha u_j \right) . \quad (41)$$

The thermal current is obtained by Eq. (31). Using second quantized operators,

$$a_i = \frac{1}{\sqrt{2}} (u_i + ip_i), \quad a_i^\dagger = \frac{1}{\sqrt{2}} (u_i - ip_i), \quad [a_i, a_j^\dagger] = \delta_{ij} \quad , \quad (42)$$

the Hamiltonian is written in a duplicated Bogoliubov form,

$$H^{\text{CHO}} = \frac{1}{2} \sum_{ij=1}^N (a_i^\dagger, a_i) H_{ij} \begin{pmatrix} a_j \\ a_j^\dagger \end{pmatrix} \equiv \frac{1}{2} \sum_{ij} (a_i^\dagger, a_i) \begin{pmatrix} H_{ij}^N & H_{ij}^A \\ (H_{ij}^A)^* & (H_{ij}^N)^* \end{pmatrix} \begin{pmatrix} a_j \\ a_j^\dagger \end{pmatrix} + \text{const} \quad , \quad (43)$$

where the constant comes from the ordering the operators a, a^\dagger . The duplicated form allows us to choose H^N to be hermitian, and H^A to be a symmetric matrix.

H^{CHO} can be diagonalized by a Bogoliubov transformation¹ defined by a symplectic matrix S_{in} of size $2N \times 2N$,

$$\begin{pmatrix} a_i \\ a_i^\dagger \end{pmatrix} = \sum_{n=1}^N S_{in} \begin{pmatrix} b_n \\ b_n^\dagger \end{pmatrix} = \sum_{n=1}^N \begin{pmatrix} U_{in} & V_{in}^* \\ V_{in} & U_{in}^* \end{pmatrix} \begin{pmatrix} b_n \\ b_n^\dagger \end{pmatrix} \quad , \quad (44)$$

where $[b_n, b_{n'}^\dagger] = \delta_{nn'}$, since

$$S^\dagger JS = S JS^\dagger = J, \quad J \equiv \begin{pmatrix} \mathbb{1}_N & 0 \\ 0 & -\mathbb{1}_N \end{pmatrix} \quad (45)$$

and $\mathbb{1}_N$ is a unit matrix of size N . Using S ,

$$H^{\text{CHO}} = \frac{1}{2} \sum_{ij} (b_n^\dagger, b_n) \begin{pmatrix} \varepsilon_n & 0 \\ 0 & \varepsilon_n \end{pmatrix} \begin{pmatrix} b_n \\ b_n^\dagger \end{pmatrix} . \quad (46)$$

Using the relation $S^{-1} = JS^\dagger J$, S is determined from H^{CHO} by the equations,

$$\begin{aligned} S^\dagger HS &= \begin{pmatrix} \varepsilon & 0 \\ 0 & \varepsilon \end{pmatrix} \\ \Rightarrow HS &= (S^\dagger)^{-1} \begin{pmatrix} \varepsilon & 0 \\ 0 & \varepsilon \end{pmatrix} = JSJ \begin{pmatrix} \varepsilon & 0 \\ 0 & \varepsilon \end{pmatrix} \\ JHS &= S \begin{pmatrix} \varepsilon & 0 \\ 0 & -\varepsilon \end{pmatrix} . \end{aligned} \quad (47)$$

U, V are readily obtained numerically by computing the *right eigenvectors* of the (non hermitian) matrix JH , and retaining those which belong to the positive spectrum $\varepsilon_n > 0$. (Existence of complex eigenvalues is possible: they reflect an instability of the harmonic Hamiltonian). The upper left block yields the eigenvalue equation, for $n = 1, \dots, N$:

$$\begin{aligned} \sum_{j=1}^N H_{ij}^N U_{jn} + H_{ij}^A V_{jn} &= U_{in} \varepsilon_n \\ \sum_{j=1}^N -(H_{ij}^A)^* V_{jn} - (H_{ij}^N)^* U_{jn} &= V_{in} \varepsilon_n \quad , \end{aligned} \quad (48)$$

¹We thank Dan Arovav for sharing with us his impeccable notes

where the eigenvectors (U_{in}, V_{in}) must be normalized as,

$$\forall n \in [1, \dots, N] : \sum_{i=1}^N (|U_{in}|^2 + |V_{in}|^2) = 1 \quad . \quad (49)$$

Using Eqs. (42) and (44), (p_i, u_i) are transformed into the eigenmode representation b_n^\dagger, b_n , the thermal polarization (41) is given by,

$$\mathbf{Q}_q = \frac{1}{2} \sum_{n, n'=1}^N (b_n^\dagger, b_n) \begin{pmatrix} \mathbf{Q}_q^N & \mathbf{Q}_q^A \\ (\mathbf{Q}_q^A)^* & (\mathbf{Q}_q^N)^* \end{pmatrix} \begin{pmatrix} b_{n'} \\ b_{n'}^\dagger \end{pmatrix} \quad . \quad (50)$$

10. Kubo formulas in Lehmann Representation

Henceforth we use unified notations

$$\begin{aligned} (\mathbf{P}, \mathbf{Q}) &\rightarrow (\mathbf{P}_1, \mathbf{P}_2) \\ (\mathbf{j}, \mathbf{j}_Q) &\rightarrow (\mathbf{J}_1, \mathbf{J}_2) \quad . \end{aligned} \quad (51)$$

In the Lehmann (eigenstate) representation, the currents' response functions are given by the sums,

$$\begin{aligned} L_{ij}^{\alpha\beta}(\mathbf{q}, \omega + i\varepsilon) &= -\frac{i}{\mathcal{V}} \sum_{mn} \frac{\rho_m - \rho_n}{E_n - E_m} \left(\frac{\langle n|(J_i^\alpha)_{-\mathbf{q}}|m\rangle \langle n|(J_j^\beta)_{\mathbf{q}}|m\rangle}{E_n - E_m - \omega - i\varepsilon} \right) \\ &= \frac{1}{\mathcal{V}} \sum_{mn} \frac{\rho_m - \rho_n}{E_n - E_m} \operatorname{Im} \left(\frac{\langle n|(J_i^\alpha)_{-\mathbf{q}}|m\rangle \langle n|(J_j^\beta)_{\mathbf{q}}|m\rangle}{E_n - E_m - \omega - i\varepsilon} \right) \\ &\quad - \frac{i}{\mathcal{V}} \sum_{mn} \frac{\rho_m - \rho_n}{E_n - E_m} \operatorname{Re} \left(\frac{\langle n|(J_i^\alpha)_{-\mathbf{q}}|m\rangle \langle n|(J_j^\beta)_{\mathbf{q}}|m\rangle}{E_n - E_m - \omega - i\varepsilon} \right) \quad . \end{aligned} \quad (52)$$

where E_m and $|m\rangle$ are the eigenenergies and eigenstates of H_0 , with $\rho_m = e^{-\beta E_m} / Z$ as Boltzmann's weights. $\alpha, \beta \in (x, y, z)$ are the Cartesian components of the currents.

The complex uniform ($\mathbf{q} = 0$) dynamical conductivities which correspond to the transport equations (1), are calculable by the Kubo formulas,

$$\begin{aligned} \text{electric conductivity :} \quad \sigma_{\alpha\beta}(\omega) &= \lim_{\mathbf{q} \rightarrow 0} \lim_{\mathcal{V} \rightarrow \infty} L_{11}^{\alpha\beta}(\mathbf{q}, \omega + i\varepsilon) \quad , \\ \text{thermoelectric conductivities :} \quad \alpha_{\alpha\beta}(\omega) &= \frac{1}{T} \lim_{\mathbf{q} \rightarrow 0} \lim_{\mathcal{V} \rightarrow \infty} L_{12}^{\alpha\beta}(\mathbf{q}, \omega + i\varepsilon) \quad , \\ \bar{\alpha}_{\alpha\beta}(\omega) &= \frac{1}{T} \lim_{\mathbf{q} \rightarrow 0} \lim_{\mathcal{V} \rightarrow \infty} L_{21}^{\mathbf{q}, \alpha\beta}(\omega + i\varepsilon) \quad , \\ \text{thermal conductivity :} \quad \kappa_{\alpha\beta}(\omega) &= \frac{1}{T} \lim_{\mathbf{q} \rightarrow 0} \lim_{\mathcal{V} \rightarrow \infty} L_{22}^{\alpha\beta}(\mathbf{q}, \omega + i\varepsilon) \quad . \end{aligned} \quad (53)$$

Straightforward computation of Eqs. (52) for general many-body Hamiltonians is generally a daunting task. Exact diagonalizations (ED) of H_0 may increase exponentially with \mathcal{V} even for a single eigenstate and eigenenergy. The difficulty is compounded by the apparent necessity to compute many current matrix elements.

10.1. Non-interacting conductivities

ED is of course more manageable for non-interacting bosons and fermions. For the single particle Hamiltonian (35) and polarizations Eq. (36), using Eq. (31), the current matrix elements are,

$$\begin{aligned} \langle l|j_{\mathbf{q}}^\alpha|l'\rangle &= i e(\epsilon_l - \epsilon_{l'}) \langle l|x^\alpha e^{i\mathbf{q}\cdot\mathbf{x}}|l'\rangle \quad , \\ \langle l|(j_Q)_{\mathbf{q}}^\alpha|l'\rangle &= i(\epsilon_l - \epsilon_{l'}) \frac{(\epsilon_l + \epsilon_{l'} - 2\mu)}{2} \langle l|x^\alpha e^{i\mathbf{q}\cdot\mathbf{x}}|l'\rangle \quad . \end{aligned} \quad (54)$$

The Kubo formulas reduce to sums over single particle eigenstates,

$$L_{ij}^{\alpha\beta}(\mathbf{q}, \omega + i\varepsilon) = \frac{1}{\mathcal{V}} \sum_{l'l''} \frac{n(\varepsilon_{l'}) - n(\varepsilon_l)}{\varepsilon_l - \varepsilon_{l'}} \left(\frac{\langle l|(J_i^\alpha)_{-\mathbf{q}}|l'\rangle \langle l''|(J_j^\beta)_{\mathbf{q}}|l\rangle}{\varepsilon_l - \varepsilon_{l'} - \omega - i\varepsilon} \right) , \quad (55)$$

where

$$n(\varepsilon) = \frac{1}{e^{\beta(\varepsilon - \mu)} \pm 1} , \quad (56)$$

for fermions (bosons) with a plus (minus) sign.

11. The Tricky DC limit

DC transport coefficients require taking the orders of limits carefully. Since for any time independent Hamiltonian on a finite volume ($\mathcal{V} < \infty$) the density matrix is in equilibrium. By definition, it cannot support any dissipative (entropy generating) steady-state transport currents. As argued by Luttinger [41], the DC steady state (which he called “rapid case”) can be achieved if the driving force satisfies $|\omega + i\varepsilon| > |\mathbf{q}|^2$, as both $\omega + i\varepsilon, |\mathbf{q}|$ are taken to zero, after we have taken $\mathcal{V} \rightarrow \infty$ to eliminate finite size gaps in the continuous thermodynamic spectrum.

For thermal transport, the statistical field $-\nabla T$ is replaced by Luttinger’s frequency dependent “gravitational” field $\psi(\omega)$ [41]. The legality of this substitution has been widely accepted [18, 42], although its rigorous conditions are still debated ²

In taking the DC limit, one must contend with the (superfluous) effects of the static gravitational field $\psi_{\omega=0}$. This force field may create an equilibrium circulating “magnetization current” in any finite system, which is not part of the transport current [18]. It contributes to $L_{ij}^{\alpha\beta}(\omega + i\varepsilon = 0)$ part of the Kubo formula which must be subtracted out *before* taking the DC limit.

In summary, the proper DC order of limits is given by

$$(L_{ij}^{\alpha\beta})^{\text{dc}} = \lim_{\omega+i\varepsilon \rightarrow i0^+} \lim_{\mathbf{q} \rightarrow 0} \lim_{\mathcal{V} \rightarrow \infty} (L_{ij}(\mathbf{q}, \omega + i\varepsilon, \mathcal{V}) - L_{ij}(\mathbf{q}, 0, \mathcal{V})) . \quad (57)$$

The causal decay of the real-time response function ensures that $L_{ij}(z)$ is analytic in the upper half plane ($\text{Im}(z) > 0$). Therefore the limit $\omega + i\varepsilon \rightarrow 0$ can be taken by a-priori setting $\omega = 0$, and sending $\varepsilon \rightarrow 0^+$ *after* sending $\mathcal{V} \rightarrow \infty$.

On finite volume, we can distinguish between OBC and PBC. For OBC, the uniform limit $\lim_{\mathbf{q} \rightarrow 0} (\mathbf{P}_i)_{\mathbf{q}}$ can be taken continuously, since the driving field is not required to be periodic between the boundaries. The DC limit is then simplified further to,

$$(L_{ij}^{\alpha\beta})^{\text{dc, OBC}} = \lim_{\varepsilon \rightarrow i0^+} \lim_{\mathcal{V} \rightarrow \infty} (L_{ij}(0, i\varepsilon, \mathcal{V}) - L_{ij}(0, 0, \mathcal{V})) , \quad (58)$$

where the uniform polarizations are given by Eqs. (29) by setting $\mathbf{q} = 0$ on any finite volume. In practice, as demonstrated in Part IV, Eq. (58) can be implemented by computing $L_{ij}(i\varepsilon(\mathcal{V}), \mathcal{V})$ on an increasing sequence of volumes $\{\mathcal{V}_i\}$, by choosing the $\varepsilon(\mathcal{V}_i)$ to be larger than the finite-size eigenenergy gaps in the Kubo formula.

On finite PBC lattices, the force fields must be continuous, and therefore their wavevectors \mathbf{q} are discretized. Therefore, in contrast to OBC, the order of limits on PBC must be taken by Eq. (57). Furthermore, since the uniform polarization cannot be taken continuously on $\mathcal{V} < \infty$, the limit is taken after $\mathcal{V} \rightarrow \infty$, i.e.

$$\begin{aligned} \mathbf{P}_{\mathbf{q}=0}^\alpha &= ie \lim_{\mathbf{q} \rightarrow 0} \lim_{\mathcal{V} \rightarrow \infty} \frac{1}{q^\alpha} \int_{\mathcal{V}} d^d x e^{-i\mathbf{q}\cdot\mathbf{x}} n(\mathbf{x}) , \\ \mathbf{Q}_{\mathbf{q}=0}^\alpha &= i \lim_{\mathbf{q} \rightarrow 0} \lim_{\mathcal{V} \rightarrow \infty} \frac{1}{q^\alpha} \int_{\mathcal{V}} d^d x e^{-i\mathbf{q}\cdot\mathbf{x}} (h(\mathbf{x}) - \mu n(\mathbf{x})) . \end{aligned} \quad (59)$$

An alternative to using the uniform polarization, the uniform *electric* current on a finite volume PBC can be defined as the derivative of the free energy with respect to an enclosed Aharonov-Bohm flux, see Eq. (71). No such definition exists for the thermal current.

²Challenges to the equality of the current response to “mechanical forces” and “statistical forces” have been made by e.g. Ref [45].

12. Onsager relations

Under time reversal (TR) symmetry, the following operators get transformed as,

$$\begin{aligned} H(\mathbf{B}) &\rightarrow H(-\mathbf{B}) \\ \mathcal{L}(\mathbf{B}) &\rightarrow -\mathcal{L}(-\mathbf{B}) \\ J_i &\rightarrow -J_j \quad . \end{aligned} \tag{60}$$

In the Kubo formulas, the order of operators J_i, J_j gets transposed under time reversal, and the complex frequency gets transformed as

$$z \rightarrow -z^* \quad . \tag{61}$$

We note that the imaginary frequency (which describes dissipation) keeps its sign, since the entropic arrow of time remains in the future direction. If time reversal symmetry is not spontaneously broken, (i.e. there is no spin or orbital magnetization at zero magnetic field), Onsager's relations yield,

$$L_{ij}^{\alpha\beta}(\mathbf{B}; \omega + i\varepsilon) = L_{ji}^{\beta\alpha}(-\mathbf{B}; -\omega + i\varepsilon) \quad . \tag{62}$$

For $\mathbf{B} \parallel \hat{\mathbf{z}}$, and $\hat{\mathbf{x}}$ the longitudinal conductivities in the DC limit $\omega = 0$ are symmetric in \mathbf{B} ,

$$\begin{aligned} \sigma_{xx}^{\text{dc}}(\mathbf{B}) &\underbrace{=}_{\text{Onsager}} \sigma_{xx}^{\text{dc}}(-\mathbf{B}) \\ \alpha_{xx}^{\text{dc}}(\mathbf{B}) &\underbrace{=}_{\text{Onsager}} \bar{\alpha}_{xx}^{\text{dc}}(-\mathbf{B}) \underbrace{=}_{C_{2x}} \bar{\alpha}_{xx}^{\text{dc}}(\mathbf{B}) \\ \kappa_{xx}^{\text{dc}}(\mathbf{B}) &\underbrace{=}_{\text{Onsager}} \kappa_{xx}^{\text{dc}}(-\mathbf{B}) \quad . \end{aligned} \tag{63}$$

wherev C_{2x} is a π rotation about the z axis. Thus the longitudinal conductivities are even in magnetic field at low fields. For the transverse conductivities we write,

$$L^{xy,\pm} = \frac{1}{2} (L^{xy} \pm L^{yx}) \quad , \tag{64}$$

where the antisymmetric part is usually called *the Hall conductivity*.

By Onsager relations (62),

$$\begin{aligned} \sigma_{xy,\pm}^{\text{dc}}(\mathbf{B}) &= \pm \sigma_{xy,\pm}^{\text{dc}}(-\mathbf{B}) \quad , \\ \kappa_{xy,\pm}^{\text{dc}}(\mathbf{B}) &= \pm \kappa_{xy,\pm}^{\text{dc}}(-\mathbf{B}) \quad . \end{aligned} \tag{65}$$

For general crystal structures, $\alpha_{xy,\pm} \neq \bar{\alpha}_{xy,\pm}$, and σ_{xy} has no special symmetry under $x \leftrightarrow y$. For the case of C_4 symmetry about $\hat{\mathbf{z}}$, $\sigma_{xy} = \sigma_{y,-x} = -\sigma_{yx}$. which implies that the symmetric transverse conductivities vanish,

$$\sigma_{xy,+}^{\text{dc}} = \alpha_{xy,+}^{\text{dc}} = \kappa_{xy,+}^{\text{dc}} \underbrace{=}_{C_4} 0 \quad . \tag{66}$$

In addition, by Onsager relations and C_4 symmetry the two transverse thermoelectric coefficients in Eq. (1) coincide,

$$\alpha_{xy}^{\text{dc}}(\mathbf{B}) \underbrace{=}_{C_4} \bar{\alpha}_{xy}^{\text{dc}}(\mathbf{B}) \quad . \tag{67}$$

Eqs. (65), (67), facilitate four-probe Hall coefficient measurements by antisymmetrizing the transverse voltage with respect to magnetic field.

13. Hall conductivity proxies

For general Hamiltonians, the Kubo formula (52) for the DC Hall conductivity σ_{xy}^{dc} is computationally challenging. Hence, two simpler proxy formulas for σ_{xy}^{dc} have been very popular: (i) The Chern conductivity $\sigma_{xy}^{\text{Chern}}$ and (ii) the Streda conductivity $\sigma_{xy}^{\text{Streda}}$. We emphasize that these proxies are only valid under restricted conditions, since they reverse the DC order of limits prescribed by Eq. (57).

13.1. Chern number

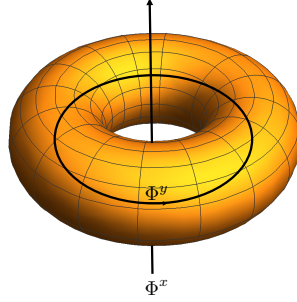


Figure 3: The Gauged Torus setup for a Chern number calculation. The charged system is placed on the surface of the torus, which is penetrated by a uniform magnetic field. Two Aharonov-Bohm fluxes Φ^x, Φ^y which thread the holes of the torus serve as adiabatic parameters of the ground state wavefunction Ψ_0 .

One considers a Hamiltonian

$$H = H_0(\mathbf{B}, \theta^x, \theta^y) \quad , \quad (68)$$

which describes particles with charge e placed on the surface of a torus of area $\mathcal{V} = L_x \times L_y$, with PBC. A uniform magnetic field \mathbf{B} penetrates the surface, and two Aharonov-Bohm fluxes $\Phi^\alpha, \alpha = x, y$ are threaded through the x and y holes of the torus, as depicted in Fig. 3. The fluxes are parametrized by,

$$\Phi^\alpha = \frac{\Phi_0}{2\pi} \theta^\alpha \quad , \quad \theta_\alpha \in [0, 2\pi] \quad , \quad (69)$$

where $\Phi_0 = hc/e$ is the flux quantum.

The Chern number of the ground state $|\Psi_0\rangle$ defined by an integral over the Berry curvature with respect to the angles θ_x, θ_y :

$$\begin{aligned} C_{xy} &= \frac{1}{\pi} \int_0^{2\pi} \int_0^{2\pi} d\theta_x d\theta_y \text{Im} \langle \frac{\partial}{\partial \theta_x} \Psi_0 | \frac{\partial}{\partial \theta_y} \Psi_0 \rangle = \frac{1}{2\pi} \oint_0^{2\pi} d\theta \cdot \text{Im} \langle \Psi_0 | \nabla_\theta \Psi_0 \rangle \\ &= \text{Chern number (integer)} \quad . \end{aligned} \quad (70)$$

The Chern number is a topological integer which characterizes a gapped Quantum Hall ground state $|\Psi_0\rangle$.

First order perturbation of the ground state w.r.t. the interaction

$$H' = -\frac{\hbar}{e} \sum_\alpha j_0^\alpha \frac{\theta^\alpha}{L_\alpha} \quad (71)$$

yields,

$$\frac{\partial}{\partial \theta_\alpha} |\Psi_0\rangle = \frac{\hbar}{eL_\alpha} \sum_{m \neq 0} |\Psi_m\rangle \frac{\langle \Psi_m | j_0^\alpha | \Psi_0 \rangle}{E_m - E_0} \quad . \quad (72)$$

Thus the Chern number can be related to the finite volume, zero frequency $\mathbf{q} = 0$ Kubo formula for σ_{xy} as given by the real part of Eq. (52):

$$\begin{aligned}\sigma_{xy}^{\text{Kubo}}(\mathbf{q} = 0, i\varepsilon = 0, \mathcal{V})_{\theta_x, \theta_y} &= \frac{\hbar}{\mathcal{V}} \sum_{0m} \frac{\langle \Psi_0 | J_0^x | \Psi_m \rangle \langle \Psi_m | J_0^y | \Psi_0 \rangle - \langle \Psi_0 | J_0^y | \Psi_m \rangle \langle \Psi_m | J_0^x | \Psi_0 \rangle}{(E_m - E_0)^2} \\ &= \frac{2e^2}{\hbar} \text{Im} \left\langle \frac{\partial}{\partial \theta_x} \Psi_0 \middle| \frac{\partial}{\partial \theta_y} \Psi_0 \right\rangle .\end{aligned}\quad (73)$$

Thus,

$$\sigma_{xy}^{\text{Chern}} \equiv \frac{1}{(2\pi)^2} \int_0^{2\pi} d\theta_x \int_0^{2\pi} d\theta_y \sigma_{xy}^{\text{Kubo}}(\mathbf{q} = 0, i\varepsilon = 0, \mathcal{V})_{\theta_x, \theta_y} = \frac{e^2}{h} C_{xy} .\quad (74)$$

In other words, the flux-averaged Kubo formula yields an integer times e^2/h . The variation of the integrand $\sigma_{xy}^{\text{Kubo}}$, with flux parameters $\theta_x, \theta_y \in [0, 2\pi)$ is expected to vanish in the large volume limit. The double integral $\int \int \frac{d\theta_x d\theta_y}{(2\pi)^2}$ can be replaced by $\sigma_{xy}(0, \mathcal{V})$ at $\theta_x = \theta_y = 0$.

Historically, the topological relation between σ^{Chern} and the Chern number was initially discovered by Thouless, Kohmoto, Nightingale, and den Nijs, (TKNN) [12], for filled bands of non interacting, disorder-free electrons on a torus, penetrated by a unit-cell-commensurate magnetic field.

The Chern proxy $\sigma_{xy}^{\text{Chern}}$ for interacting Hamiltonians was derived by adiabatic transport theory by Avron and Seiler [13].

However, we must caution that $\sigma_{xy}^{\text{Chern}}$ *reverses* the proper DC order of limits prescribed by Eq. (57). Therefore the validity of this proxy is limited to the following conditions:

1. For the adiabatic theorem to apply [13], a finite gap $\Delta > 0$ between the ground state and all excitations must exist in the infinite volume limit.
2. The longitudinal conductivity must vanish $\sigma_{xx} = 0$. This can be ensured only at zero temperature if there are no gapless current carrying excitations and no inelastic scattering processes.
3. If disorder is present it should be weak enough to prevent gapless current-carrying states from percolating through the bulk of the sample.

That said, we emphasize that $\sigma_{xy}^{\text{Chern}}$ has been instrumental in mathematical and experimental characterization of Quantum Hall and topological insulator phases [11, 46].

13.2. Streda formula

The Streda formula proxy for σ_{xy} is obtained by reversing the DC order of limits of Eq. 57. In Ref. [47] it is shown that,

$$\begin{aligned}\sigma_{xy}^{\text{Streda}} &= \lim_{\mathbf{q} \rightarrow 0} \lim_{\mathcal{V} \rightarrow \infty} \lim_{i\varepsilon \rightarrow 0^+} \sigma_{xy}(\mathbf{q}, i\varepsilon) \\ &= c \lim_{\mathbf{q} \rightarrow 0} \lim_{\mathcal{V} \rightarrow \infty} (\rho_{\mathbf{q}} | M_{\mathbf{q}}^z) = c \left. \frac{\partial \rho}{\partial B} \right|_{\mu, T} = c \left. \frac{\partial m^z}{\partial \mu} \right|_{B, T} ,\end{aligned}\quad (75)$$

where m^z is the z-magnetization and ρ is the charge density. The last equation follows from a Maxwell relation. The Streda formula is often used to characterize quantum Hall phases and topological insulators by scanning compressibility measurements [48].

In general the Streda order of limits does not commute with the DC order of limits (57), and therefore

$$\sigma_{xy}^{\text{Streda}} = \lim_{\mathbf{q} \rightarrow 0} \lim_{\mathcal{V} \rightarrow \infty} \lim_{\omega \rightarrow 0} \sigma_{xy}(\mathbf{q}, \omega) \neq \lim_{\omega \rightarrow 0} \lim_{\mathbf{q} \rightarrow 0} \lim_{\mathcal{V} \rightarrow \infty} \sigma_{xy}(\mathbf{q}, \omega) = \sigma_{xy}^{\text{dc}} .\quad (76)$$

The conditions which may permit the use Streda's proxy is that the ground state is bulk-incompressible, and that the Hall angle is large, i.e. $\sigma_{xy}/\sigma_{xx} \gg 1$. Such conditions occur when there is a gap $\Delta > 0$ for excitations above the ground state, and the temperature is lower than this gap. A weaker condition is a pseudogap, where the density of charge excitations vanishes rapidly enough at low energies to allow reversal of the $\omega, \mathbf{q} \rightarrow 0$ order of limits in the Kubo formula.

14. Kubo formulas in operator Hilbert space

The Kubo formulas of Eq. (52) may be formulated as matrix elements in OHS. This formalism avoids the Lehmann representation, and proves to be convenient for further mathematical manipulation. Below, we shall use the OHS formalism to derive the DPP formulas in Part IV, the continued fractions in Section 21, and the Hall coefficient summation formulas in Part VI. We start with the formulation of susceptibilities as inner product in OHS. We then proceed to formulate dynamical response functions in OHS.

14.1. Equilibrium Susceptibilities

Given a static Hamiltonian and free energy,

$$H = H_0 - h_A A - h_B B, \quad F = -T \log \text{Tr} e^{-\beta H} . \quad (77)$$

A thermodynamic expectation value is given by,

$$\begin{aligned} \langle A \rangle &\equiv - \left. \frac{\partial F}{\partial h_A} \right|_{h_A=h_B=0} \\ &= \text{Tr}(\rho_0 A) , \end{aligned} \quad (78)$$

where Boltzmann weights are $\rho = e^{-\beta H_0} / \text{Tr} e^{-\beta H_0}$. Static susceptibilities with respect to A and B are,

$$\begin{aligned} \chi_{AB} &= - \left. \frac{\partial^2 F[h_A, h_B]}{\partial h_A \partial h_B} \right|_{h_A=h_B=0} \\ &= \int_0^\beta d\tau \langle A(\tau) B \rangle + \beta \langle A^{\text{diag}} B^{\text{diag}} \rangle - \beta \langle A \rangle \langle B \rangle \\ &= \sum_{m,n} \frac{\rho_m - \rho_n}{E_n - E_m} \langle n|A|m \rangle \langle m|B|n \rangle + \beta \langle A^{\text{diag}} B^{\text{diag}} \rangle - \beta \langle A \rangle \langle B \rangle . \end{aligned} \quad (79)$$

where $O^{\text{diag}} = \sum_n |n \rangle \langle n| O |n \rangle \langle n|$. In the second line $B(\tau) \equiv e^{\tau H_0} B e^{-\beta H_0}$. The last line of (79) is written in the Lehmann representation of H_0 . The vector space of linear operators $A \rightarrow |A \rangle$ which act within the Schroedinger Hilbert space of the Hamiltonian H_0 , is an OHS containing hyperstates $|A \rangle$, and closed under linear superpositions. Henceforth we consider general operators $A^{\text{diag}} = B^{\text{diag}} = 0$, whose susceptibility is

$$\begin{aligned} \chi_{AB} &= \sum_{nm} W_{nm} A_{nm}^* B_{nm} \equiv (A|B) , \\ W_{nm} &\equiv \frac{\rho_m - \rho_n}{E_n - E_m} \geq 0 . \end{aligned} \quad (80)$$

$(A|B)$ defines the Bogoliubov-Mori (BM) inner product, [28] which depends on H_0 (with its boundary conditions) and inverse temperature β . It obeys the Hilbert space conditions of (i) a positive norm, (ii) hermiticity and (iii) linearity,

$$\begin{aligned} \text{(i)} \quad &(A|A) \geq 0 , \\ \text{(ii)} \quad &(A|B) = (B|A)^* , \\ \text{(iii)} \quad &(A|aB + bC) = a(A|B) + b(A|C), \quad \forall a, b \in \mathbb{C} . \end{aligned} \quad (81)$$

All operators which commute with H_0 are identified with the null hyperstate of zero norm.

14.2. The Liouvillian and its inverse

In OHS, the Liouvillian hyperoperator \mathcal{L} , which generates the time evolution of hyperstates, is defined by,

$$\mathcal{L}|A \rangle = i[H_0, A] , \quad (82)$$

where A is any operator in the Hilbert space of H_0 .

Lemma 1. *The Liouvillian is a hermitian hyperoperator in OHS,*

Proof.

$$\begin{aligned}
(A|\mathcal{L}|B) &= \sum_{nm} \frac{\rho_m - \rho_n}{E_n - E_m} A_{nm}^* (E_m - E_n) B_{mn} = - \sum_{nm} (\rho_m - \rho_n) A_{nm}^* B_{mn} \\
&= \left(\sum_{nm} (\rho_n - \rho_m) \frac{E_m - E_n}{E_m - E_n} B_{mn}^* A_{mn} \right)^* = (B|\mathcal{L}|A)^* \\
&\Rightarrow \mathcal{L} = \mathcal{L}^\dagger \quad \square
\end{aligned} \tag{83}$$

where the summation indices are relabelled $mn \rightarrow nm$ in the last equation. \square

\mathcal{L} is therefore diagonalizable. Its eigenoperators are $|n\rangle\langle m|$ with real eigenvalues $E_n - E_m$. It is the generator of time evolution in the OHS, since

$$|A(t)\rangle = |e^{iH_0 t} A e^{-iH_0 t}\rangle = e^{i\mathcal{L}t} |A\rangle \quad . \tag{84}$$

The inverse Liouvillian $\left(\frac{1}{\mathcal{L}}\right)_\varepsilon'$ does not exist if the kernel of \mathcal{L} is non zero. Hence we define it with an imaginary infinitesimal ε prescription,

$$\left(\frac{1}{\mathcal{L} - i\varepsilon}\right)_\varepsilon \equiv \left(\frac{1}{\mathcal{L}}\right)_\varepsilon' + i \left(\frac{1}{\mathcal{L}}\right)_\varepsilon'' \quad , \tag{85}$$

where the real part of the inverse is the hyperoperator

$$\left(\frac{1}{\mathcal{L}}\right)_\varepsilon' \equiv \frac{\mathcal{L}}{\mathcal{L}^2 + \varepsilon^2} \quad , \tag{86}$$

and the imaginary part is

$$\left(\frac{1}{\mathcal{L}}\right)_\varepsilon'' \equiv \frac{\varepsilon}{\mathcal{L}^2 + \varepsilon^2} = \pi \delta_\varepsilon(\mathcal{L}) \quad . \tag{87}$$

The weight of the inner product, Eq. (80) can be expressed as

$$W_{nm} = \lim_{\varepsilon \rightarrow 0} \sum_{nm} \operatorname{Re} \left(\frac{\rho_m - \rho_n}{E_n - E_m + i\varepsilon} \right) \quad . \tag{88}$$

Using Eq. (86) we can write BM inner product in a representation independent form,

$$\begin{aligned}
(A|B) &= - \lim_{\varepsilon \rightarrow 0} \operatorname{Tr} \left[\rho, \left(\frac{1}{\mathcal{L}}\right)_\varepsilon' A^\dagger \right] B \\
&= - \lim_{\varepsilon \rightarrow 0} \operatorname{Tr} \rho \left[\left(\frac{1}{\mathcal{L}}\right)_\varepsilon' A^\dagger, B \right] \quad .
\end{aligned} \tag{89}$$

The advantage of Eq. (89) over Eq. (80) will be made clear during the mathematical manipulations of the Kubo formulas performed in the following Sections.

14.3. Dynamical linear response functions

Dynamical response functions are obtained in linear response by adding to the Hamiltonian H_0 a weak time-dependent field $h_B(t)$ coupled to an operator B . The field is turned at $t \geq 0$,

$$H(t) = H_0 - \Theta(t) h_B(t) B \quad . \tag{90}$$

At $t > 0$ the expectation value of an observable A^\dagger is

$$\langle A^\dagger \rangle(t) = \text{Tr} \rho(\beta) U^\dagger(t) A^\dagger U([h_B], t) = \int_0^t dt' R_{AB}(t, t') h_B(t') + \mathcal{O}(h_B^2) \quad , \quad (91)$$

where the density matrix $\rho = \frac{1}{Z} e^{-\beta H_0}$ and the evolution operator U satisfies $i\dot{U} = H(t)U$. Expanding U to linear order in h_B yields,

$$R_{AB}(t - t') = -i \text{Tr} \rho [A^\dagger(t - t'), B] \Theta(t - t') \quad , \quad (92)$$

where $A(t) = e^{iH_0 t} A e^{-iH_0 t}$, and using $[\rho, H_0] = 0$ to obtain $R_{AB}(t, t') = R_{AB}(t - t')$. The transform of (92) into the upper complex plane defines the complex response function,

$$\begin{aligned} R_{AB}(z) &= \int_0^\infty e^{-izt} R_{AB}(t) dt = \sum_{mn} \frac{\rho_m - \rho_n}{E_n - E_m - z} \langle n | A^\dagger | m \rangle \langle m | B | n \rangle \\ &= \left(A \left| \frac{\mathcal{L}}{\mathcal{L} - z} \right| B \right) \quad , \quad \text{Im}(z) > 0 \quad . \end{aligned} \quad (93)$$

14.4. Electric and Thermal conductivities

The Kubo formulas of Eq. (52) are matrix elements in OHS,

$$L_{ij}^{\alpha\beta}(\mathbf{q}, \omega + i\varepsilon) = \frac{1}{\mathcal{V}} R_{J_i^\alpha, J_j^\beta}(\omega + i\varepsilon) = -\frac{i}{\mathcal{V}} \left((J_i^\alpha)_\mathbf{q} \left| \frac{1}{\mathcal{L} - \omega - i\varepsilon} \right| (J_j^\beta)_\mathbf{q} \right) \quad . \quad (94)$$

The values of $\omega, i\varepsilon, \mathbf{q}, \mathcal{V}$ are all finite. The DC limit must to be taken carefully as required by Eq. (57).

Part IV

DPP Hall conductivities

15. Derivation of DPP formulas

For simplicity the magnetic field is chosen along the z axis and C_4 symmetry is assumed in the XY plane. According to Eq. (57), the DC Hall-type conductivities are given by,

$$\text{Re}(L_{ij}^{xy})^{\text{dc}} = \lim_{\varepsilon \rightarrow 0} \lim_{\mathbf{q} \rightarrow 0} \lim_{\mathcal{V} \rightarrow \infty} \left(\text{Re} L_{ij}^{xy}(\varepsilon, \mathcal{V}) - \text{Re} L_{ij}^{xy}(0, \mathcal{V}) \right) . \quad (95)$$

As mentioned before, the second term cancels the spurious magnetization currents which are created by the static component of the ‘‘gravitational’’ field $\psi(\omega = 0)$. In OHS notation,

$$\text{Re} L_{ij}^{xy}(\varepsilon, \mathcal{V}) \equiv \frac{1}{\mathcal{V}} \text{Im} \left(J_i^x \left| \left(\frac{1}{\mathcal{L}} \right)' \right| J_j^y \right) + \frac{1}{\mathcal{V}} \text{Re} \left(J_i^x \left| \left(\frac{1}{\mathcal{L}} \right)'' \right| J_j^y \right) \xrightarrow{0} \quad (C_4) \quad (96)$$

where \mathbf{q} -dependence of the currents is implicit. Under $\pi/2$ rotation in the plane $\text{Re} L_{ij}^{xy}(\varepsilon, \mathcal{V}) = -\text{Re} L_{ij}^{yx}(\varepsilon, \mathcal{V})$, and since the second term is symmetric under $x \leftrightarrow y$, it vanishes. In the Lehmann representation,

$$\text{Re} L_{ij}^{xy}(\varepsilon, \mathcal{V}) = \frac{1}{\mathcal{V}} \sum_{mn} \frac{\rho_m - \rho_n}{E_n - E_m} \text{Im} \left(\langle n | J_i^x | m \rangle \langle m | J_j^y | n \rangle \right) \left(\frac{E_m - E_n}{(E_m - E_n)^2 + \varepsilon^2} \right) . \quad (97)$$

At first glance, one might be tempted to discard $\mathcal{O}(\varepsilon^2)$ contributions in the denominator of Eq. (97). On OBC, this would be a gross error! As shown below, the DC limit is dominated by eigenstates with $|E_n - E_m| \leq \varepsilon$.

Using the identity (89),

$$\text{Re} L_{ij}^{xy}(\varepsilon, \mathcal{V}) = -\frac{1}{\mathcal{V}} \text{Im} \text{Tr} \rho \left[\left(\frac{1}{\mathcal{L}} \right)'_{\varepsilon'} J_i^x, \left(\frac{1}{\mathcal{L}} \right)'_{\varepsilon} J_j^y \right] . \quad (98)$$

To remain consistent with C_4 symmetry, on finite volumes we identify $\varepsilon' = \varepsilon$, while keeping the DC order of limits in Eq. (95). By Eq. (31),

$$\left(\frac{1}{\mathcal{L}} \right)'_{\varepsilon} J_j^{\alpha} = i(1 - \Theta_{\varepsilon}) P_j^{\alpha} \equiv i(P_j^{\alpha} - (\tilde{P}_j^{\alpha})_{\varepsilon}) \quad , \quad \alpha = x, y \quad (99)$$

Θ_{ε} is a Lorentzian degeneracy projector,

$$\Theta_{\varepsilon} = \frac{\varepsilon^2}{\mathcal{L}^2 + \varepsilon^2} \quad (100)$$

and $(\tilde{P}_j^{\alpha})_{\varepsilon} \equiv \Theta_{\varepsilon} P_j^{\alpha}$ are DPP’s (*degeneracy projected polarizations*), whose matrix elements in the Lehmann representation are restricted (at small ε) to connect quasi-degenerate eigenstates,

$$\langle n | (\tilde{P}_i^{\alpha})_{\varepsilon} | m \rangle = \langle n | P_i^{\alpha} | m \rangle \frac{\varepsilon^2}{|E_n - E_m|^2 + \varepsilon^2} . \quad (101)$$

Eq. (98) can be written as

$$\text{Re} L_{ij}^{xy}(\varepsilon, \mathcal{V}) = \frac{1}{\mathcal{V}} \text{Im} \text{Tr} \rho \left[P_i^x - (\tilde{P}_i^x)_{\varepsilon}, P_j^y - (\tilde{P}_j^y)_{\varepsilon} \right] . \quad (102)$$

Expansion of the terms in (102) we obtain a sum of four terms,

$$\text{Re} L_{ij}^{xy}(\varepsilon, \mathcal{V}) = \text{Re} L_{ij}^{xy}(\varepsilon = 0, \mathcal{V}) - L_b(\varepsilon) - L_c(\varepsilon) + L_d(\varepsilon) . \quad (103)$$

The first term, which is independent of ε and ε' is called a magnetization term,

$$\text{Re} L_{ij}^{xy}(\varepsilon = 0, \mathcal{V}) \equiv \frac{1}{\mathcal{V}} \text{Im} \text{Tr} \rho \left[P_i^x, P_j^y \right] . \quad (104)$$

The physical content of magnetization terms is discussed in Section 15.1. The magnetization term precisely cancels the second term in Eq. (95), and therefore does not need to be calculated for the Hall-type conductivity.

The remaining three terms are related to each other,

$$\begin{aligned}
L_b(\varepsilon) &= \frac{1}{\mathcal{V}} \text{Im Tr } \rho \left[P_i^x, (\tilde{P}_j^y)_\varepsilon \right] = \frac{1}{\mathcal{V}} \text{Im} \sum_n \rho_n \sum_m \langle n | P_i^x | m \rangle \langle m | P_j^y | n \rangle \left(\frac{\varepsilon^2}{(E_n - E_m)^2 + \varepsilon^2} \right) , \\
L_c(\varepsilon) &= \frac{1}{\mathcal{V}} \text{Im Tr } \rho \left[(\tilde{P}_i^x)_\varepsilon, P_j^y \right] = \frac{1}{\mathcal{V}} \text{Im} \sum_n \rho_n \sum_m \langle n | P_i^x | m \rangle \langle m | P_j^y | n \rangle \left(\frac{(\varepsilon')^2}{(E_n - E_m)^2 + (\varepsilon')^2} \right) , \\
L_d(\varepsilon) &= \frac{1}{\mathcal{V}} \text{Im Tr } \rho \left[(\tilde{P}_i^x)_{\varepsilon'}, (\tilde{P}_j^y)_\varepsilon \right] = \frac{1}{\mathcal{V}} \text{Im} \sum_n \rho_n \sum_m \langle n | P_i^x | m \rangle \langle m | P_j^y | n \rangle \left(\frac{\varepsilon^2}{(E_n - E_m)^2 + \varepsilon^2} \right)^2 . \quad (105)
\end{aligned}$$

L_b and L_c contain one DPP, and therefore a Lorentzian factor, $\varepsilon^2 / ((E_n - E_m)^2 + \varepsilon^2)$. L_d contains a Lorentzian square $(\varepsilon^2 / ((E_n - E_m)^2 + \varepsilon^2))^2$. The Lorentzian factor and its square can be effectively replaced for small ε by box projectors $\Theta(\pi\varepsilon/2 - |E_n - E_m|)$ and $\Theta(\pi\varepsilon/4 - |E_n - E_m|)$, respectively. Since we are taking $\varepsilon \rightarrow 0$, (after $\mathcal{V} \rightarrow \infty$), the three terms have the same DC limit,

$$\lim_{\varepsilon \rightarrow 0} L_b(\varepsilon) = \lim_{\varepsilon \rightarrow 0} L_c(\varepsilon) = \lim_{\varepsilon \rightarrow 0} L_d(\varepsilon) . \quad (106)$$

Thus, summing up Eq. (103) the DC Hall conductivities are given by the DPP formulas,

$$\begin{aligned}
\sigma_{xy}^{\text{dc}} &= - \lim_{\varepsilon \rightarrow 0} \lim_{\mathbf{q} \rightarrow 0} \lim_{\mathcal{V} \rightarrow \infty} \frac{1}{\hbar \mathcal{V}} \text{Im Tr } \rho \left[(\tilde{P}^x)_\varepsilon, (\tilde{P}^y)_\varepsilon \right] , \\
\alpha_{xy}^{\text{dc}} &= - \lim_{\varepsilon \rightarrow 0} \lim_{\mathbf{q} \rightarrow 0} \lim_{\mathcal{V} \rightarrow \infty} \frac{1}{\hbar \mathcal{V} k_B T} \text{Im Tr } \rho \left[(\tilde{P}^x)_\varepsilon, (\tilde{Q}^y)_\varepsilon \right] , \\
\kappa_{xy}^{\text{dc}} &= - \lim_{\varepsilon \rightarrow 0} \lim_{\mathbf{q} \rightarrow 0} \lim_{\mathcal{V} \rightarrow \infty} \frac{1}{\hbar \mathcal{V} k_B T} \text{Im Tr } \rho \left[(\tilde{Q}^x)_\varepsilon, (\tilde{Q}^y)_\varepsilon \right] . \quad (107)
\end{aligned}$$

Here we have restored the dimensionful dependence on \hbar and k_B for practical applications.

15.1. The Magnetization terms

The terms $L_{ij}^{\text{xy}}(\varepsilon = 0, \mathcal{V})$ in Eq. (104) cancel against their counterterms in Eq. (95). For electric Hall conductivity σ_{xy} , the magnetization term vanishes since the two polarizations commute: $[P^x, P^y] = 0$. The thermoelectric and thermal Hall magnetization terms do not vanish. For Schrödinger particles governed by $H^{\text{particles}}$, the polarization commutators can be readily calculated to yield,

$$\begin{aligned}
\lim_{\mathbf{q} \rightarrow 0} \lim_{\mathcal{V} \rightarrow \infty} L_{12}^{\text{xy}} &= \lim_{\mathbf{q} \rightarrow 0} \lim_{\mathcal{V} \rightarrow \infty} \frac{1}{\mathcal{V}} \text{Im} \langle \frac{[P^x, Q^y] + [Q^x, P^y]}{2} \rangle = - \lim_{\mathcal{V} \rightarrow \infty} \frac{1}{\mathcal{V}} \langle \sum_{i=1}^{N_p} \mathbf{x}_i \times \mathbf{j}(\mathbf{x}_i) \cdot \hat{\mathbf{z}} \rangle = -c \langle m^z \rangle , \\
\lim_{\mathbf{q} \rightarrow 0} \lim_{\mathcal{V} \rightarrow \infty} L_{22} &= \lim_{\mathbf{q} \rightarrow 0} \lim_{\mathcal{V} \rightarrow \infty} \frac{1}{\mathcal{V}} \text{Im} \langle [Q^x, Q^y] \rangle = - \lim_{\mathcal{V} \rightarrow \infty} \frac{1}{\mathcal{V}} \langle \sum_{i=1}^{N_p} \mathbf{r}_i \times \mathbf{j}_Q(\mathbf{x}_i) \cdot \hat{\mathbf{z}} \rangle = -2 \langle m_Q^z \rangle , \quad (108)
\end{aligned}$$

which agrees with Ref. [18, 19]. m^z and m_Q^z are the z -direction electric and thermal magnetization densities respectively.

The magnetization subtractions create considerable headache when computing the Kubo formulas from Eq. (52). Since L_{ij} are weighted by $\frac{1}{T}$ in Eqs. (53), any separate approximations of the two terms in Eq. (95) could result in an error which embarrassingly diverges at low temperature. (Heat conductivities should actually vanish at low temperatures by the third law of thermodynamics). Elimination of these subtractions from the DPP formulas (107) provides an essential simplification.

16. DPP formulas for non-interacting Hamiltonians

For a normal Hamiltonian of non-interacting fermions or bosons, Eq. (35), the DPP formula is

$$\begin{aligned} L_{ij}^{xy} &= -\lim_{\varepsilon \rightarrow 0} \lim_{\mathbf{q} \rightarrow 0} \lim_{\mathcal{V} \rightarrow \infty} \frac{1}{\mathcal{V}} \text{Im} \sum_l n(\varepsilon_l) \langle l | [\tilde{P}_i^x, \tilde{P}_j^y] | l \rangle \\ &= -\lim_{\varepsilon \rightarrow 0} \lim_{\mathbf{q} \rightarrow 0} \lim_{\mathcal{V} \rightarrow \infty} \sum_{l'l'} (n(\varepsilon_l) - n(\varepsilon_{l'})) \text{Im} \langle l | \tilde{P}_i^x | l' \rangle \langle l' | \tilde{P}_j^y | l \rangle . \end{aligned} \quad (109)$$

where the polarizations P_i^x, P_j^y are defined in (36), and their DPP's are given by

$$\langle l | \tilde{P}_i^\alpha | l' \rangle = \langle l | P_i^\alpha | l' \rangle \frac{\varepsilon^2}{\varepsilon^2 + (\varepsilon_l - \varepsilon_{l'})^2} . \quad (110)$$

At low temperatures, the factor $n(\varepsilon_l) - n(\varepsilon_{l'})$ ensures the sum is dominated by excitation energies at less than of order T from the chemical potential.

For a bosonic Hamiltonian of coupled harmonic oscillators (40), the thermal polarization is generally an anomalous bilinear form given by Eq. (50). The anomalous matrix blocks $Q_{A,\mathbf{q}}^\alpha, (Q_{A,\mathbf{q}}^\alpha)^*$ involve creation or annihilation of two positive energy states, such that $\varepsilon_l + \varepsilon_{l'} > 0$. Thus, there are no anomalous contributions to the DPP³. Thus we are left with the normal parts of the polarizations,

$$\langle l | \tilde{Q}_i^\alpha | l' \rangle = \sum_{l''} \left(\frac{\varepsilon^2}{\varepsilon^2 + (\varepsilon_l^{\text{diag}} - \varepsilon_{l''}^{\text{diag}})^2} \right) (Q_{N;\mathbf{q}}^\alpha)_{ll''} . \quad (111)$$

17. Berry curvature integrals

Hall-type conductivities for non-interacting periodic crystal Hamiltonians H^{PC} , defined in Eq. (38), can be expressed as Berry curvature integrals over BZ, where the band Berry curvature is defined in Eq. (10).

The relations between Berry curvature integrals and Hall conductivity [27], Transverse thermoelectric conductivity [49] and thermal Hall conductivity [19, 50], have been previously derived from semiclassical dynamics and also directly from the Kubo formula of perfectly periodic lattices (55).

Here we provide a somewhat simpler derivation (in our view) starting from the single-particle DPP formulas for periodic lattices. $U_{li}(\mathbf{k})$ is a unitary matrix which diagonalizes $h_{ij}(\mathbf{k})$ in H^{PC} , and defines the eigenmode operators,

$$b_{\mathbf{k}l}^\dagger = \sum_{i=1}^M U_{li}(\mathbf{k}) a_{\mathbf{k}i}^\dagger \quad l = 1, \dots, M \quad , \quad (112)$$

such that,

$$H^{\text{PC}} = \sum_{\mathbf{k} \in \text{BZ}} \sum_{l=1}^M (\varepsilon_{\mathbf{k}l} - \mu) b_{\mathbf{k}l}^\dagger b_{\mathbf{k}l} . \quad (113)$$

The uniform polarizations can be defined by sending $\mathbf{q} \rightarrow 0$ after $\mathcal{V} \rightarrow \infty$ in Eq. (39), (see Eq. (59):

$$\begin{aligned} P^\alpha &= e \sum_{\mathbf{k}ij} a_{\mathbf{k}i}^\dagger (i\nabla_{\mathbf{k}}^\alpha) a_{\mathbf{k}j} \quad , \\ Q^\alpha &= \frac{1}{2} \sum_{\mathbf{k}ij} a_{\mathbf{k}i}^\dagger \left\{ (h_{ij}(\mathbf{k}) - \mu \delta_{ij}), (i\nabla_{\mathbf{k}}^\alpha) \right\} a_{\mathbf{k}j} \quad . \end{aligned} \quad (114)$$

³Unlike their contribution to the magnetization terms. It is good to know that anomalous terms are projected out, since their commutator would lead to diverging contributions to the low temperature limit of κ_{xy} .

The DPP operators are constrained to act only within the same band l . Using Eq. (112), the electric DPP's are given by

$$\langle \mathbf{k}l | \tilde{P}_\varepsilon^\alpha | \mathbf{k}'l \rangle = e \frac{\varepsilon^2}{\varepsilon^2 + (\epsilon_{\mathbf{k}l} - \epsilon_{\mathbf{k}'l})^2} \left\{ \overbrace{\sum_i U_{li}^\dagger(\mathbf{k}) \left(i \nabla_{\mathbf{k}}^\alpha U_{il}(\mathbf{k}) \right)}^{A_l^\alpha(\mathbf{k})} + i \nabla_{\mathbf{k}'}^\alpha \right\} . \quad (115)$$

The vector function $\mathbf{A}_l(\mathbf{k})$ is the *Berry gauge field* [51] of eigenmode $|\mathbf{k}, l\rangle$,

$$\mathbf{A}_l(\mathbf{k}) \equiv i \sum_{j=1}^M U_{lj}(\mathbf{k}) \nabla_{\mathbf{k}}^\alpha U_{jl}^\dagger(\mathbf{k}) . \quad (116)$$

Similarly, the thermal DPP's are

$$\langle \mathbf{k}l | \tilde{Q}_\varepsilon^\alpha | \mathbf{k}'l \rangle = \frac{\varepsilon^2}{\varepsilon^2 + (\epsilon_{\mathbf{k}l} - \epsilon_{\mathbf{k}'l})^2} \left((\epsilon_{\mathbf{k}l} - \mu) \left(i \nabla_{\mathbf{k}'}^\alpha + A_l^\alpha(\mathbf{k}) \right) + \frac{i}{2} v_{\mathbf{k}l}^\alpha \right) , \quad (117)$$

where $\mathbf{v}_{\mathbf{k}l} = \nabla_{\mathbf{k}} \epsilon_{\mathbf{k}l}$. Note that on a finite volume, \mathbf{k} are discrete with intervals of $\delta \mathbf{k} = 2\pi/\mathcal{V}^{\frac{1}{d}}$. The DC limit is obtained by keeping $\varepsilon > \delta \mathbf{k}$, as $\mathcal{V} \rightarrow \infty$. The differentiability of $\epsilon_{\mathbf{k}l}$ and $U_{il}(\mathbf{k})$ allows us to set $\mathbf{k}' \rightarrow \mathbf{k}$ in Eqs. (115) and (117), which involve a relative correction of $\mathcal{O}(\varepsilon)$.

By (115) the commutator

$$\begin{aligned} \langle \mathbf{k}, l | [\tilde{P}_\varepsilon^x, \tilde{P}_\varepsilon^y] | \mathbf{k}, l \rangle &= i \nabla_{\mathbf{k}} \times \mathbf{A}_l(\mathbf{k}) \cdot \hat{\mathbf{z}} + \mathcal{O}(\varepsilon^2) \\ &= i \Omega^z(\mathbf{k}, l) , \end{aligned} \quad (118)$$

where we discarded $[\partial_{k_x}, \partial_{k_y}] = 0$ when acting on differentiable wavefunctions. $\Omega^z(\mathbf{k}, l)$ defines the Berry curvature field in the $\hat{\mathbf{z}}$ direction of eigenmode l .

By Eq. (107) the intrinsic Hall conductivity recovers the result of Chang and Niu [27],

$$\sigma_{xy}^{\text{dc}} = - \lim_{\varepsilon \rightarrow 0} \sum_l \int \frac{d^d k}{(2\pi)^d} n(\epsilon_{\mathbf{k}l}) \Omega_{\mathbf{k}l}^z . \quad (119)$$

This expression has been used to describe the anomalous Hall effect in ferromagnets [52]. Additional effects of impurities have been introduced semiclassically [53].

The thermal Hall DPP's have a slightly more complicated commutator,

$$\begin{aligned} \langle \mathbf{k}l | [\tilde{Q}_\varepsilon^x, \tilde{Q}_\varepsilon^y] | \mathbf{k}l \rangle &= i \langle \mathbf{k}l | \left(\epsilon_{\mathbf{k}l}^2 \nabla_{\mathbf{k}} \times \mathbf{A}_l(\mathbf{k}) + \epsilon_{\mathbf{k}l} \mathbf{v}_{\mathbf{k}l} \times \mathbf{A}_{\mathbf{k}l} + \epsilon_{\mathbf{k}l} \mathbf{v}_{\mathbf{k}l} \times \nabla \right) | \mathbf{k}l \rangle + \frac{i}{2} \epsilon_{\mathbf{k}l} \nabla \times \mathbf{v}_{\mathbf{k}l} + \mathcal{O}(\varepsilon) \\ &= i \epsilon_{\mathbf{k}l}^2 \nabla_{\mathbf{k}} \times \mathbf{A} + 2 \epsilon_{\mathbf{k}l} \mathbf{v}_{\mathbf{k}l} \times \mathbf{A}_{\mathbf{k}l} + \mathcal{O}(\varepsilon) . \end{aligned} \quad (120)$$

where $i \nabla_{\mathbf{k}} \times \mathbf{v}_{\mathbf{k}l} = 0$.

For convenience we define energy resolved conductivities by,

$$\begin{aligned} \tilde{\sigma}_{xy}(\varepsilon) &= - \frac{1}{\mathcal{V}} \sum_{\mathbf{k}l} \delta(\varepsilon - \epsilon_{\mathbf{k}l}) \Omega_{\mathbf{k}l}^z , \\ \tilde{\Sigma}_{xy}(\varepsilon) &= - \frac{1}{\mathcal{V}} \sum_{\mathbf{k}l} \delta(\varepsilon - \epsilon_{\mathbf{k}l}) (\nabla_{\mathbf{k}} \epsilon_{\mathbf{k}l}) \times \mathbf{A}_{\mathbf{k}l} \cdot \hat{\mathbf{z}} . \end{aligned} \quad (121)$$

In three dimensions, for fixed k_z , the δ function restricts the wavevectors to a circle on sphere of energy ε , such that

$$\sum_{\mathbf{k}_\perp l} \delta(\varepsilon - \epsilon_{\mathbf{k}l}) = \frac{1}{(2\pi)^2} \oint_{s \in \partial\{\epsilon_{k_z, \mathbf{k}_\perp l} \leq \varepsilon\}} \frac{ds}{|\nabla_{\mathbf{k}_\perp} \epsilon_{\mathbf{k}l}|} . \quad (122)$$

Thus, we use Stokes theorem to relate $\tilde{\Sigma}_{xy}$ to σ_{xy} by,

$$\begin{aligned}
\tilde{\Sigma}_{xy}(\epsilon) &= \frac{1}{(2\pi)^3} \sum_l \int dk_z \oint_{\partial\{s \in \epsilon_{k_z, k_{\perp}} \leq \epsilon\}} ds \cdot \mathbf{A}_l^z \\
&= \sum_l \int \frac{d^3k}{(2\pi)^3} \Theta(\epsilon - \epsilon_{\mathbf{k}l}) \Omega_l^z(\mathbf{k}) \\
&= \int_{-\infty}^{\epsilon} d\epsilon' \tilde{\sigma}_{xy}(\epsilon') \quad .
\end{aligned} \tag{123}$$

Thus, we arrive at the expression previously derived by Qin, Niu and Shi [19],

$$\begin{aligned}
\kappa_{xy}^{\text{dc}} &= \lim_{\epsilon \rightarrow 0} \lim_{\mathbf{q} \rightarrow 0} \lim_{\mathcal{V} \rightarrow \infty} \frac{1}{T} \int_{-\infty}^{\infty} d\epsilon n(\epsilon) \left(\epsilon^2 \tilde{\sigma}_{xy} + 2\epsilon \int_0^{\epsilon} d\epsilon' \tilde{\sigma}_{xy}(\epsilon') \right) \\
&= \frac{1}{T} \int_{-\infty}^{\infty} d\epsilon \left(-\frac{\partial n}{\partial \epsilon} \right) \epsilon^2 \tilde{\Sigma}_{xy}(\epsilon) \quad .
\end{aligned} \tag{124}$$

Similarly, the DPP formula for the thermoelectric conductivity of a clean C_4 -symmetric metallic band of electrons with charge $e < 0$, is given by

$$\alpha_{xy}^{\text{dc}} = -\lim_{\epsilon \rightarrow 0} \lim_{\mathbf{q} \rightarrow 0} \lim_{\mathcal{V} \rightarrow \infty} \frac{1}{2\mathcal{V}T} \sum_{\mathbf{k}l} n(\epsilon_{\mathbf{k}l}) \left([\tilde{P}_{\mathbf{k}l}^x, \tilde{Q}_{\mathbf{k}l}^y] + [\tilde{Q}_{\mathbf{k}l}^x, \tilde{P}_{\mathbf{k}l}^y] \right) \quad . \tag{125}$$

Using (118) and defining,

$$\begin{aligned}
\tilde{\sigma}_{xy}(\epsilon) &= -\frac{1}{\mathcal{V}} \sum_{\mathbf{k}l} \delta(\epsilon - \epsilon_{\mathbf{k}l}) \Omega_{\mathbf{k}l}^z \\
\tilde{\Sigma}_{xy}(\epsilon) &= \int_{-\infty}^{\epsilon} d\epsilon' \tilde{\sigma}_{xy}(\epsilon') \quad ,
\end{aligned} \tag{126}$$

one can express,

$$\alpha_{xy}^{\text{dc}} = \frac{1}{eT} \int_{-\infty}^{\infty} d\epsilon \left(-\frac{\partial n}{\partial \epsilon} \right) \epsilon \tilde{\Sigma}_{xy}(\epsilon) \quad . \tag{127}$$

For low temperatures Eqs. (124) and (127) for metals reduce to the relations,

$$\begin{aligned}
\kappa_{xy}^{\text{dc}} &\simeq \frac{\pi^2 k_B^2 T}{3e} \tilde{\sigma}_{xy}(\epsilon_F) \quad , \\
\alpha_{xy}^{\text{dc}} &\simeq \frac{\pi^2 k_B^2 T}{3e} \frac{d\tilde{\sigma}_{xy}}{d\epsilon_F} \quad .
\end{aligned} \tag{128}$$

these relations extend Mott relations [54] between electric and thermoelectric conductivities to bandstructures with Berry curvatures [49].

Introducing the effects of disorder in the anomalous Hall effect has been a major challenge in the field. The main difficulty is to extend the semiclassical analysis to include effects of short range scattering [53, 55, 56, 57]. The general non-interacting DPP formulas (109) can feasibly study effects of disorder numerically.

18. DPP formula for confined Landau levels

We consider an electron in a uniform magnetic field \mathbf{B} , with vector potential \mathbf{A} , $\nabla \times \mathbf{A} = B\hat{z}$. In first quantized notation, the Landau operators are,

$$\Pi^\alpha \equiv p^\alpha - \frac{e}{c} A^\alpha \quad . \quad (129)$$

The Landau level (LL) raising and lowering operators are respectively,

$$a = \frac{l_B^2}{\hbar} (\Pi^x + i\Pi^y) \quad , \quad a^\dagger = \frac{l_B^2}{\hbar} (\Pi^x - i\Pi^y) \quad . \quad (130)$$

where $[a, a^\dagger] = 1$, and the Landau length is $l_B = \sqrt{\frac{\hbar c}{eB}}$.

The LL Hamiltonian is

$$H^{\text{LL}} = \frac{1}{2m} ((\Pi^x)^2 + (\Pi^y)^2) = \hbar\omega_c \left(a^\dagger a + \frac{1}{2} \right) \quad , \quad (131)$$

where the cyclotron frequency is $\omega_c = \frac{eB}{mc}$. The eigenenergies are

$$\epsilon_{k,\nu} = \hbar\omega_c \left(\nu + \frac{1}{2} \right) \quad , \quad k = 1, \dots, N_L \quad . \quad (132)$$

where the integer LL index is ν , and $N_L = \frac{BA}{\Phi_0}$ is the number of states per area A in each LL.

The guiding center operators are,

$$\begin{aligned} R^x &= x + \frac{l_B^2}{\hbar} \Pi^y \\ R^y &= y - \frac{l_B^2}{\hbar} \Pi^x \quad , \end{aligned} \quad (133)$$

where

$$[R^\alpha, \Pi^\beta] = 0, \quad [R^x, R^y] = -il_B^2 \quad . \quad (134)$$

The polarization operators are

$$\begin{aligned} P^x &= ex = eR^x - e \frac{l_B^2}{\hbar} \Pi^y \quad , \\ P^y &= ey = eR^y + e \frac{l_B^2}{\hbar} \Pi^x \quad . \end{aligned} \quad (135)$$

Since Π^x, Π^y change the LL index by ± 1 , while R^α connect states within each LL. Hence under degeneracy projection, the Π -operators are projected out, and DPP's are simply proportional to the guiding center operators,

$$\begin{aligned} \tilde{P}^x &= eR^x \quad , \\ \tilde{P}^y &= eR^y \quad . \end{aligned} \quad (136)$$

The DPP Hall conductivity formula (109) yields

$$\begin{aligned} \sigma_{xy}^{\text{dc}} &= -\frac{e^2}{\hbar^2 \mathcal{V}} \sum_{k,\nu} n(\epsilon_{k,\nu}) \text{Im} \langle k, \nu | [R^x, R^y] | k, \nu \rangle \\ &= \frac{eC}{B\mathcal{V}} \sum_{k,\nu} n(\epsilon_{\nu,k}) = \frac{n_e eC}{B} \quad , \end{aligned} \quad (137)$$

where $n_e(\mu, T, B)$ is the electron density.

While the sum in Eq. (137) includes all occupied states, Eq. (109) shows that the Hall conductivity can be written only in terms of states near the Fermi energy ϵ_F .

Where are these current carrying states? On finite systems with OBC, the semiclassical eigenenergies in each LL (which apply for smooth confining potential on the scale of l_B), reach the Fermi energy ϵ_F at the sample edges. Each LL band contributes one gapless edge mode. The Hall conductivity is precisely given by Eq. (137).

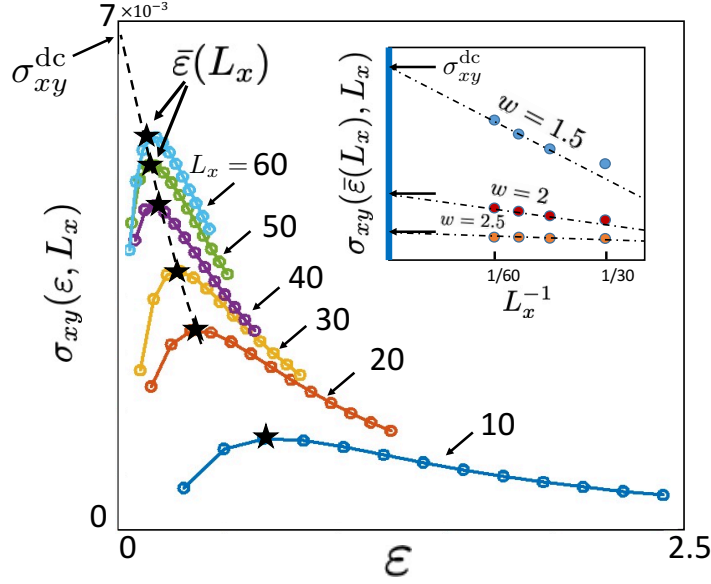


Figure 4: Extrapolation of numerical Hall conductivities of the square lattice Hamiltonian, Eq. (17). Disorder averaged σ_{xy} are plotted versus ϵ , for a sequence of linear dimensions L_x . Stars mark the values of $\bar{\epsilon}$ as defined in Eq. (139). The disorder strength is fixed at $w = 3$. The temperature, Fermi energy, and magnetic field are $T = 0.3$, $\epsilon_F = -1$ and $B = 0.025$ respectively. **Inset:** The DC limit σ_{xy}^{dc} (marked by black arrows) for three values of disorder strength.

19. DPP Hall conductivity in a disordered metal

In the weak disorder and magnetic field regime proxies such as Chern numbers and Streda formulas do not work, since disorder mixes Landau levels, and the longitudinal conductivity is finite. Since σ_{xy} strongly depends on the scattering lifetime, it is instructive to compare Boltzmann's theory to the Kubo formula by numerically calculating it via the DPP formalism. It also gives us a chance to demonstrate how the DC limit is taken in a metallic gapless system.

In Ref. [58], the weakly disordered square lattice (DSL) Hamiltonian was considered,

$$H^{\text{DSL}} = - \sum_{\langle ij \rangle} \left(e^{-iA_{ij}} c_i^\dagger c_j + \text{h.c.} \right) + \sum_i (w_i - \epsilon_F) c_i^\dagger c_i \quad , \quad (138)$$

where $w_i \in [-w/2, w/2]$ is a uniformly distributed random number and $B = \sum_{\square} A_{ij}$ is the magnetic flux per plaquette. Using the DPP formula (107), we compute the disordered averaged curves $\sigma_{xy}(\epsilon, L)$ for a sequence of linear sizes L , as shown in Fig. 4.

For each curve we determine $\bar{\epsilon}(L)$ by

$$\left. \frac{d\sigma_{xy}(\epsilon, L)}{d\epsilon} \right|_{\epsilon=\bar{\epsilon}} = 0 \quad , \quad (139)$$

which is marked by black star in Fig. 4. These values fit the function $\bar{\epsilon} \simeq 7(L_x)^{-1}$. This scaling is consistent with level spacings of one dimensional extended states.

The DC conductivity is estimated by graphically extrapolating the sequence,

$$\sigma_{xy}^{\text{dc}} = \lim_{L \rightarrow \infty} \sigma_{xy}(\bar{\epsilon}(L), L) \quad . \quad (140)$$

In the inset of Figure 4, we extrapolate the Hall conductivities at various values of disorder strength w to their their respective DC limits.

The DPP formula calculation [58] has found $\sigma_{xy}^{\text{dc}} \sim Bw^{-4}$, as depicted in Fig. 5. These results are consistent with DB and BE theories (6,13) which predict that $\sigma_{xy} \propto \omega_c \tau^2$ in the weak magnetic field regime $\omega_c \tau \ll 1$. The w^{-4} scaling is consistent with Fermi's golden rule for the disorder-driven scattering rate, Eq. (24), i.e. $\tau^{-1} \propto w^2$.

20. Physical consequences of DPP formulas

The first implication of Eqs. (107) is that the Hall conductivities are *on-shell* expressions which is in apparent contrast to the original Kubo formula (97). Furthermore, at low temperatures, the conductivity is dominated by the low energy excitations $|E_n - E_0| \leq O(T)$. Conceptual conclusions from the DPP formulas are:

1. A OBC system exhibiting a non-zero Hall-type conductivity possesses a quasi-degenerate (gapless) manifolds of eigenstates which are created by the presence of the magnetic field.
2. At low temperatures, since the DPP's involve low energy eigenstates, it is easy to see that α_{xy}^{dc} and κ_{xy}^{dc} vanish as $T \rightarrow 0$. It is also simple to verify for phonons and spin-wave models, that the anomalous (i.e. $a^\dagger a^\dagger, aa$) terms in the current operators.
3. These manifolds are subjected to the *non commutative geometry* generated by the DPP's. That is to say, since

$$\langle [\tilde{P}^\alpha, \tilde{P}^\beta] \rangle \propto i\sigma_{\alpha\beta}^{\text{dc}} . \quad (141)$$

then $\frac{1}{\sigma_{\alpha\beta}^{\text{dc}}} \tilde{P}^\beta$ acts as a conjugate momentum to \tilde{P}^α . The DPP's are therefore similar in spirit to the non-commuting guiding center coordinates which act within a quasi-degenerate Landau level in the strong magnetic field limit.

4. In quantum Hall and topological insulator phases, the Hall-current carrying states are supported on the OBC sample edges. For compressible metallic phases, the Hall current is carried on chiral extended states which percolate through the bulk. An explicit description of these states has been used by Chalker and Coddington model [59] to describe the quantum-percolation transition between Hall plateaux.
5. Finally, DPP formula for κ_{xy} proves that thermal Hall currents in insulators [60, 61, 62] are carried by extended chiral modes.

Numerical advantages.— The elimination of the higher eigenstates in the DPP formulas at low temperatures allows us to replace $H(B)$ by its effective Hamiltonian $H^{\text{eff}}(B)$ renormalized onto the lower energy Hilbert space. $H^{\text{eff}}(B)$ may be computationally easier to work with than H .

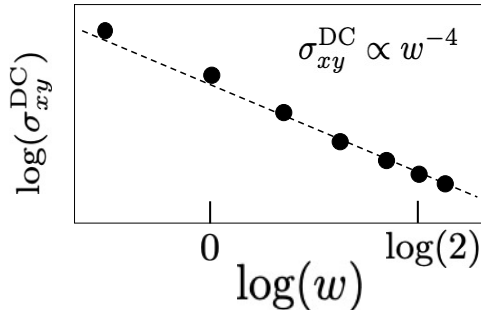


Figure 5: DC extrapolated Hall conductivity for weak magnetic field $B = 0.03$ and moderate disorder strength w , at Fermi energy $\epsilon_F = -1$. The Hall conductivity scales as w^{-4} as expected by Drude's theory $\sigma_{xy} \propto \omega_c \tau^2$.

Part V

Continued fractions of longitudinal conductivities

21. Moments expansion

Real longitudinal conductivities (in the x direction) are given by the real part of Eq. (94),

$$L_{ii}^{xx}(\omega) = \frac{1}{\mathcal{V}} \text{Im} \left(J_i^x \left| \left(\frac{1}{\mathcal{L} - \omega - i\varepsilon} \right) \right| J_i^x \right) = \frac{\pi}{\mathcal{V}} (J^x | \delta_\varepsilon(\mathcal{L} - \omega) | J^x) \quad , \quad i = 1, 2, 3 \quad . \quad (142)$$

where δ_ε is a broadened Dirac δ -function of width $\varepsilon > \mathcal{V}^{\frac{1}{d}}$. Henceforth we suppress $\varepsilon, \mathbf{q}, \mathcal{V}$ dependence, keeping in mind the eventual correct DC order of limits of Eq. (57). For the moments expansion we define a symmetrized mixed electric+thermal current as

$$J_3^x = (J_1^x + J_2^x)/2 \quad . \quad (143)$$

Thus, the thermoelectric conductivity can be written as a sum of auto-correlation functions,

$$\alpha_{xx}(\omega) = \frac{2}{T} L_{33}^{xx}(\omega) - \frac{1}{2} \sigma_{xx}(\omega) - \frac{1}{2} \kappa_{xx}(\mathbf{q}, \omega) \quad . \quad (144)$$

Henceforth we discuss $L_{ii}^{xx}(\omega)$ and suppress the currents' label i .

The moment of order $2k$ of L is

$$\begin{aligned} \mu_{2k} &= \int_{-\infty}^{\infty} \frac{d\omega}{\pi} L^{xx}(\omega) \omega^{2k} \\ &= \frac{1}{\mathcal{V}} \int_{-\infty}^{\infty} d\omega (J^x | \delta(\mathcal{L} - \omega) \mathcal{L}^{2k} | J^x) \\ &= \frac{1}{\mathcal{V}} (J^x | \mathcal{L}^{2k} | J^x) \quad . \end{aligned} \quad (145)$$

The $k = 0$ moment is the CSR,

$$\mu_0 = \frac{1}{\mathcal{V}} (J^x | J^x) \equiv \chi_{\text{csr}} \quad . \quad (146)$$

All odd moments vanish by antisymmetry of $mn \rightarrow nm$,

$$(J^x | \mathcal{L}^{2k+1} | J^x) = \sum_{mm} W_{mm} (E_m - E_n)^{2k+1} A_{nm}^* A_{nm} = 0 \quad . \quad (147)$$

Moments are thermodynamic expectation values of time-independent operators,

$$\begin{aligned} \mu_{2k} &= \frac{1}{\mathcal{V}} \left(J^x \left| \overbrace{[H_0, [H_0, \dots [H_0, J^x]] \dots]}^{2k} \right. \right) \\ &= \frac{1}{\mathcal{V}} \text{Im} \left([P^x, \overbrace{[H_0, [H_0, \dots [H_0, J^x]] \dots}]^{2k-1} \right) \quad , \end{aligned} \quad (148)$$

where we used Eq. (89) and P^x is the x -polarization corresponding to J^x by Eq. (31).

Moments are coefficients of the short time Taylor series of the real-time conductivity,

$$\begin{aligned} L^{xx}(t) &= \frac{1}{\pi} \int_{-\infty}^{\infty} d\omega L^{xx}(\omega) e^{i\omega t} = \frac{1}{\mathcal{V}} \langle J^x | e^{i\mathcal{L}t} | J^x \rangle \\ &= \sum_{k=0, \infty} \frac{(-1)^k \mu_{2k}}{(2k)!} t^{2k} . \end{aligned} \quad (149)$$

Unfortunately, a finite set of moments cannot, in general, determine the long time behavior of Eq. (149), and the low frequency behavior of Eq. (142).

The following constraints can be very helpful in guiding us to a viable extrapolation scheme to high orders.

1. Since $\delta_\varepsilon(\mathcal{L} - \omega)$ is a non-negative Hermitian hyperoperator, $L^{xx}(\omega) \geq 0$ is a non-negative spectral function.
2. $L^{xx}(\omega) = L^{xx}(-\omega)$, which therefore permits a finite DC conductivity at $\omega = 0$.
3. All the moments μ_{2k} are squares of norms $\|\mathcal{L}^k A\|^2$, and therefore non negative.
4. By thermodynamic arguments, the real-time conductivities of Eq. (149) should be continuous and differentiable for $t \in (-\infty, \infty)$. Also, they are expected to decay (relax) at long times. This ensures the analyticity of $L^{xx}(z)$ in the upper half plane $\text{Im}(z) > 0$.⁴ Thus, by (149), the asymptotic growth of the high order moments is bounded by,

$$\lim_{k \rightarrow \infty} \frac{\mu_{2k}}{(2k)!} < \infty . \quad (150)$$

21.1. Krylov bases

An orthonormal Krylov basis of hyperstates can be constructed from the current operator. We start with the normalized root (zeroth order) state,

$$|0\rangle \equiv \frac{J}{\sqrt{\langle J|J \rangle}} . \quad (151)$$

($|\bullet\rangle$) denotes normalized hyperstates, in contrast to non normalized hyperstates such as $|\bullet\rangle$.)

Higher order Krylov hyperstates are inductively generated by the equations

$$|n+1\rangle = \frac{1}{N_{n+1}} (\mathcal{L}|n\rangle - \Delta_n |n-1\rangle) , \quad N_{n+1} \equiv (\langle n|\mathcal{L}^2|n\rangle - \Delta_n^2)^{\frac{1}{2}} , \quad n = 1, 2, \dots \infty \quad (152)$$

where Δ_n is the *recurrent* of order n , which is equal to the matrix elements of the Liouvillian,

$$\Delta_n = \langle n|\mathcal{L}|n-1\rangle = \langle n-1|\mathcal{L}|n\rangle . \quad (153)$$

In order to evaluate Δ_n the following statements are verified:

1. The Liouvillian expectation values vanish in the Krylov basis. By construction of Eq. (152), even (odd) order Krylov hyperstates involve states with even (odd) powers $\mathcal{L}^n|J\rangle$. Hence we can expand any Krylov hyperstate as

$$|n\rangle = \sum_{k=0}^{\text{Int}(n/2)} a_{n-2k} \mathcal{L}^{n-2k} |0\rangle . \quad (154)$$

The expectation values of \mathcal{L} in Krylov hyperstates are,

$$\begin{aligned} \langle n|\mathcal{L}|n\rangle &= \sum_{k,k'=0}^{\text{Int}(n/2)} a_{n-2k} a_{n-2k'} \langle 0|\mathcal{L}^{n-2k} \mathcal{L} \mathcal{L}^{n-2k'} |0\rangle \\ &= \sum_{k,k'=0,n} a_k b_{k'} \langle 0|\mathcal{L}^{2(n-k-k')+1} |0\rangle = 0 , \end{aligned} \quad (155)$$

which follows from Eq. (147).

⁴The only notable exception is in a superconductor, where persistent currents do not decay. For superconductors, the zero frequency conductivity is excluded from $L^{xx}(\omega)$.

2. The Krylov basis is orthonormal,

$$\langle m|n \rangle = \langle n|m \rangle = \delta_{nm} \quad , \quad n, m = 0, 1, 2, \dots \infty \quad (156)$$

which is proven by induction using Eq. (152) starting from $n, m = 0$.

3. The Liouvillian representation in the Krylov basis is,

$$L_{nm} = \langle n|\mathcal{L}|m \rangle = \delta_{m,n-1}\Delta_n + \delta_{n,m-1}\Delta_{n+1} \quad , \quad (157)$$

$$= \begin{pmatrix} 0 & \Delta_1 & 0 & 0 & 0 & \dots \\ \Delta_1 & 0 & \Delta_2 & 0 & 0 & \dots \\ 0 & \Delta_2 & 0 & \Delta_3 & 0 & \dots \\ 0 & 0 & \Delta_3 & 0 & \Delta_4 & \dots \\ 0 & 0 & 0 & \Delta_4 & 0 & \dots \\ 0 & \vdots & \vdots & \vdots & \vdots & \dots \end{pmatrix}_{nm} \quad n, m = 0, 1, 2, \dots \infty \quad . \quad (158)$$

The matrix L_{nm} can be regarded as a tight binding hopping Hamiltonian on a half chain, with hopping parameters Δ_n .

4. The phases of $|n\rangle$ can be chosen such that we can gauge all the recurrences Δ_n to be real and positive.

$G_{nm}(z)$ is the ‘‘Liouvillian Green function’’,

$$G_{nm}(z) \equiv \langle n|(z - \mathcal{L})^{-1}|m \rangle \quad . \quad (159)$$

Since L is symmetric, so is $G_{nm}(z)$, which is in general complex. On the real axis $z \rightarrow \omega + i0^+$, $-\text{Im}G_{nm}(\omega + i\epsilon) = -G''_{nm}(\omega)$ is a *spectral function*. It is non-negative and symmetric in $\omega \rightarrow -\omega$. The real part of the complex function $G_{nm}(z)$ can be obtained from the spectral function by the Kramers-Kronig (KK) transform,

$$G'_{nm}(\omega) = \frac{1}{\pi} \int_{-\infty}^{\infty} d\omega' \frac{G''_{nm}(\omega')}{\omega - \omega'} \quad . \quad (160)$$

$G''_{nm}(\omega) = G''_{nm}(-\omega)$, and by Eq. (160), $G'_{nm}(0) = 0$. Non diagonal Green functions $G_{nm}(0 + i\epsilon)$ can be obtained from the inversion equation $(GL)_{nm} = \delta_{nm}$,

$$\sum_{m \geq 0} G_{nm}(0^+) L_{mn'} = \delta_{nn'} \quad . \quad (161)$$

For example,

$$\begin{aligned} \sum_m G_{0m}(0^+) L_{m1} &= G_{00}\Delta_1 + G_{02}\Delta_2 = 0, \Rightarrow G_{02}(0^+) = iG''_{00} \left(-\frac{\Delta_1}{\Delta_2} \right) \quad , \\ \sum_m G_{0m}(0^+) L_{m4} &= G_{02}(0^+)\Delta_3 + G_{04}(0^+)\Delta_4 = 0 + \Rightarrow G_{04}(0^+) = iG''_{00} \left(-\frac{\Delta_1}{\Delta_2} \right) \left(-\frac{\Delta_3}{\Delta_4} \right) \quad , \\ &\vdots \quad \quad \quad \vdots \quad \quad \quad \end{aligned} \quad (162)$$

and generally,

$$\begin{aligned} G_{0,2k}(0^+) &= G_{2k,0}(0^+) = iG''_{00} R_k \quad , \quad k = 0, 1, 2, \dots \\ R_k &= \prod_{k'=1}^k \left(-\frac{\Delta_{2k'-1}}{\Delta_{2k'}} \right) \quad . \quad (163) \end{aligned}$$

Another important relation is,

$$G_{1,n}(0^+) = \frac{\delta_{n,0}}{\Delta_1} \quad , \quad (164)$$

which is purely real. As a consequence, the matrix elements of the imaginary inverse Liouvillian do not connect to the first Krylov state:

$$\left\langle n \left| \left(\frac{1}{\mathcal{L}} \right)'' \right| 1 \right\rangle = \left\langle 1 \left| \left(\frac{1}{\mathcal{L}} \right)'' \right| n \right\rangle = 0 \quad . \quad (165)$$

This result will prove to be useful in Section 24.

21.2. The continued fraction representation

Since $z - L$ is a tridiagonal matrix, an iterative inversion can be used to invert G_{00} in Eq. (159), and express it as

$$\begin{aligned} G_{00}(z) &= \frac{1}{z - \Delta_1^2 G_{11}^>(z)} \quad , \\ G_{11}^>(z) &= \frac{1}{z - \Delta_2^2 G_{22}^>(z)} \quad , \\ &\vdots = \quad \vdots \quad , \end{aligned} \quad (166)$$

where $G_{mn}^>$ is the *termination Green function* on the half-chain with the sites $m \geq n$. The sequence of equations (166) comprises an infinite continued fraction (CF),

$$G_{00}(z) \simeq \frac{1}{z - \frac{\Delta_1^2}{z - \frac{\Delta_2^2}{z - \frac{\Delta_3^2}{\vdots}}}} \quad (167)$$

22. From moments to recurrences

The first question that comes to mind is: How do we obtain the recurrences $\Delta_1, \Delta_2 \dots \Delta_k$, from a given sequence of moments $\mu_0, \mu_2 \dots \mu_{2k}$?

Eq. (145) and (158) generate a sequence of identities:

$$\begin{aligned} \mu_{2k} &= \mu_0 \langle 0 | (L[\Delta])^{2k} | 0 \rangle \quad . \\ \frac{\mu_2}{\mu_0} &= \Delta_1^2 \quad , \\ \frac{\mu_4}{\mu_0} &= \Delta_1^4 + \Delta_1^2 \Delta_2^2 \quad , \\ \frac{\mu_6}{\mu_0} &= \Delta_1^6 + 2\Delta_1^4 \Delta_2^2 + \Delta_1^2 \Delta_2^4 + \Delta_1^2 \Delta_2^2 \Delta_3^2 \quad , \\ \frac{\mu_8}{\mu_0} &= \Delta_1^8 + 3\Delta_1^6 \Delta_2^2 + 3\Delta_1^4 \Delta_2^4 + \Delta_1^2 \Delta_2^6 + 2\Delta_1^4 \Delta_2^2 \Delta_3^2 + 2\Delta_1^2 \Delta_2^4 \Delta_3^2 + \Delta_1^2 \Delta_2^2 \Delta_3^4 + \Delta_1^2 \Delta_2^2 \Delta_3^2 \Delta_4^2 \quad , \\ &\vdots \quad \quad \quad \vdots \end{aligned} \quad (168)$$

Importantly, μ_{2k}/μ_0 depend only on the recurrents $\Delta_1, \Delta_2 \dots \Delta_k$. This allows us to solve for the recurrents iteratively, starting at $k = 1$. As a result we obtain the algebraic equations,

$$\begin{aligned}
\Delta_1^2 &= \bar{\mu}_2 \quad , \\
\Delta_2^2 &= \frac{\bar{\mu}_4}{\bar{\mu}_2} - \bar{\mu}_2 \quad , \\
\Delta_3^2 &= \frac{\bar{\mu}_4^2 - \bar{\mu}_2 \bar{\mu}_6}{\bar{\mu}_2^3 - \bar{\mu}_2 \bar{\mu}_4} \quad , \\
\Delta_4^2 &= \bar{\mu}_2 \frac{(\bar{\mu}_4^3 + \bar{\mu}_6^2 + \bar{\mu}_2^2 \bar{\mu}_8 - \bar{\mu}_4(2\bar{\mu}_2 \bar{\mu}_6 + \bar{\mu}_8))}{(\bar{\mu}_2^2 - \bar{\mu}_4)(\bar{\mu}_2 \bar{\mu}_6 - \bar{\mu}_4^2)} \quad , \\
&\vdots = \vdots
\end{aligned} \tag{169}$$

In general μ_{2k} increase very rapidly (of order $(2k)!$) with k , while Δ_k are much smaller numbers which increase at a much slower rate. The presence of subtractions in Eq. (169) imply that small relative errors in μ_{2k} may result in large relative errors in $\Delta_{k \geq k'}$ ⁵

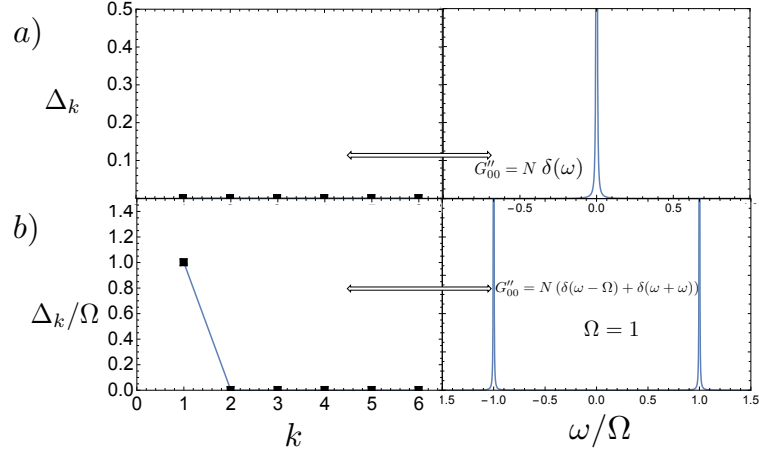


Figure 6: Single mode correlations.

22.1. Single Mode Spectra

Let us start with a single sharp mode at zero frequency as shown in Fig. 6(a),

$$-G''_{00}(\omega) = \pi \delta(\omega) \quad . \tag{170}$$

All the recurrents vanish identically, since $[H, A] = 0$.

$$\Delta_k^2 = 0 \quad , \quad \forall n \quad . \tag{171}$$

A single mode at finite frequency $|\Omega| > 0$ is shown in Fig. 6(b). It is described by

$$-G''_{00}(\omega) = \pi (\delta(\omega - \Omega) + \delta(\omega + \Omega)) / 2 \quad . \tag{172}$$

The only non-zero recurrent is $\Delta_1 = \Omega$. Physically this occurs when J^x is an eigen-operator of the Liouvillian

$$\mathcal{L}J^x = \Omega J^x \quad . \tag{173}$$

⁵We thank Snir Gazit for alerting us to this numerical challenge.

and therefore applying J^x to the Hamiltonian's ground state $|\Psi_0\rangle$ creates an eigenstate $J^x|\Psi_0\rangle$ with excitation energy Ω .

An approximation which *assumes* a spectral function which approximately is described by a δ -function, is the single mode approximation. This approximation was used by Feynman [63] to describe the roton minima in the spectrum of superfluid helium [63], by Girvin, Macdonald and Platzman [64] to describe the magneto-roton excitation of the Fractional Quantum Hall phase, in Refs. [65, 66] to approximate the Haldane gap in a spin-one chain model.

23. From recurrences to conductivities

The longitudinal conductivity of Eq. (142) is determined by the zeroth order spectral function,

$$\begin{aligned} L^{xx}(\omega) &= -\mu_0 \lim_{z \rightarrow \omega + i0^+} G''_{00}(z) \\ &= \pi\mu_0 \langle 0 | \delta(\mathcal{L} - \omega) | 0 \rangle \quad , \end{aligned} \quad (174)$$

where $L[\Delta_n]$ is the infinite tridiagonal matrix of Eq. (158), and $G_{00}(z)$ is defined as a CF in Eq. (167).

In practice, the calculation of Δ_n is limited to a finite sequence. However, truncating the CF at any finite order does not lead to a continuous function, but to a sequence of δ -functions. In effect, determining G''_{00} amounts to inversion of the moments series, which is in general an unsolved problem.

CF however allow us to design extrapolation schemes which may be suitable for certain class of physical problems, which provide additional information about the desired G''_{00} . For example, $-G''_{00}(\omega)$ is a positive and symmetric function, whose all its recurrences are finite, non-negative numbers.

Since extrapolation is a tricky art, it is useful to first learn about rigorous results relating high frequency asymptotics of G''_{00} and high order recurrences.

23.1. Freud's high order asymptotics

For a large class of smooth spectral function $-G''_{00}(\omega)$ with support on the whole frequency axis ⁶, Freud [67] has conjectured an asymptotic relation between the high frequency asymptotic fall-off of the spectral function, and the asymptotic behavior of the high order recurrences Δ_k as $k \rightarrow \infty$.

This conjecture was proven by Lubinsky, Mhaskar and Saff (LMS) [68], for spectral functions described by

$$-G''_{00}(\omega) = \exp(-Q(\omega)) \quad . \quad (175)$$

The fall-off exponent Q is assumed to satisfy the following conditions:

1. $Q(\omega) = Q(-\omega)$.
2. $Q'(\omega)$ exists for $\omega \neq 0$, and $\omega Q'(\omega)$ is bounded near the origin as $\omega \rightarrow 0^+$. Furthermore, Q'' exists for large enough ω .
3. For finite values of $C > 0, \alpha > 0$ at large enough ω ,

$$\begin{aligned} Q'(\omega) &> 0 \quad , \\ \omega^2 |Q''(\omega)| / Q'(\omega) &\leq C \quad , \\ \lim_{\omega \rightarrow \infty} (1 + \omega Q''(\omega) / Q'(\omega)) &= \alpha > 0 \quad . \end{aligned} \quad (176)$$

LMS proved that the corresponding recurrences Δ_n for Eq. (175) exhibit the asymptotic behavior,

$$\begin{aligned} \lim_{k \rightarrow \infty} \Delta_k &\sim a_\alpha k^{\frac{1}{\alpha}} \\ a_\alpha &= \frac{1}{2} \left(\frac{\sqrt{\pi} \Gamma\left(\frac{\alpha}{2}\right)}{\Gamma\left(\frac{\alpha+1}{2}\right)} \right)^{\frac{1}{\alpha}} \quad . \end{aligned} \quad (177)$$

⁶We thank Ari Turner for explaining to us the mathematical literature reviewed in this section

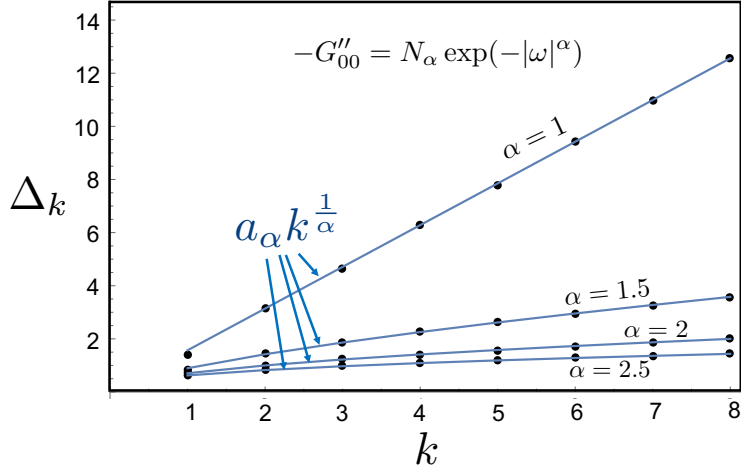


Figure 7: The recurrents of the pure stretched exponentials (black circles), and Freud's asymptotic expression (blue lines) as governed by Eq. (177). The differences between the values are plotted in Fig. 8.

Interestingly, for pure stretched exponential

$$Q(\omega, \alpha) = |\omega|^\alpha, \quad (178)$$

as shown in Figs. 7 and 8, the exact low order recurrents are close but slightly different from the analytic asymptotic values of Eq. (177), except for the pure Gaussian $\alpha = 2$, for which Eq. (177) is exact.

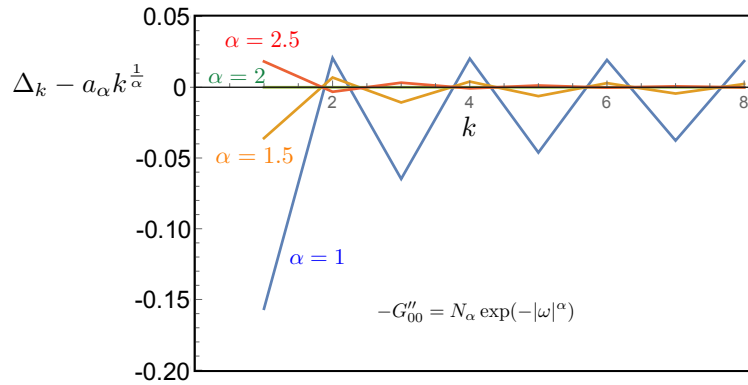


Figure 8: The difference between the true recurrents of the stretched exponential and asymptotic values of Eq. (177), which decrease with the order k . Note that the asymptotic values are exact only for the Gaussian $\alpha = 2$.

In general, since the moments and recurrents are non-negative, by Eqs. (168), the moments grow at least as fast as

$$\mu_{2k} \geq (k!)^{2/\alpha}. \quad (179)$$

Due to assumed continuity of $G_{00}(t)$ on the real-time axis, by Eq. (150), the moments cannot grow faster than $\mu_{2n} \leq (2n)!$.

This implies that for continuous and bounded response functions, the asymptotic power α of $Q(\omega)$ is limited to

$$1 \leq \alpha \leq \infty. \quad (180)$$

23.2. Termination functions

Assume that we have calculated a finite set of recurrents

$$\{\Delta\}_1^{k_{\max}} = (\Delta_1, \dots, \Delta_{k_{\max}}) \quad . \quad (181)$$

This finite set is not sufficient to describe the continuous function $G''_{00}(\omega)$. Extrapolation of recurrents is tantamount to finding an accurate termination function $\bar{G}_{k_{\max}}^>(z)$ such that,

$$G_{00}(z) \simeq \frac{1}{z - \frac{\Delta_1^2}{z - \frac{\Delta_2^2}{z - \frac{\Delta_{k_{\max}-1}^2}{z - \Delta_{k_{\max}}^2 \bar{G}_{k_{\max}}^>(z; [\alpha])}}} \quad . \quad (182)$$

$\bar{G}_{k_{\max}}^>(z)$ is the normalized CF which contains only the higher order recurrents $\bar{\Delta}_k, k \geq k_{\max} + 1$,

$$\bar{G}_{k_{\max}}^>(z) = \frac{1}{z - \frac{\bar{\Delta}_{k_{\max}+1}^2}{z - \frac{\bar{\Delta}_{k_{\max}+2}^2}{z - \frac{\bar{\Delta}_{k_{\max}+3}^2}{\vdots}}}} \quad . \quad (183)$$

If $\{\bar{\Delta}\}_k, k = 0, \dots, \infty$ are the known recurrents of a complex variational spectral function $\bar{G}_{00}(z)$. The variational recurrents are used to produce the termination function by iteratively inverting the CF of the complex function $\bar{G}_{00}(z)$,

$$\begin{aligned} \bar{G}_{11}^>(z) &= \frac{1}{\bar{\Delta}_1^2} \left(z - \frac{1}{\bar{G}_{00}(z)} \right) \\ \vdots &= \vdots \\ \bar{G}_{k_{\max}}^>(z) &= \frac{1}{\bar{\Delta}_{k_{\max}-1}^2} \left(z - \frac{1}{\bar{G}_{k_{\max}-1}^>(z)} \right) \quad . \end{aligned} \quad (184)$$

We emphasize that or the inversion, both real and imaginary parts of $\bar{G}_{00}(\omega + i\varepsilon)$ are required, where the real part is obtained by a Kramers-Kronig transformation, Eq. (160), of the imaginary part.

Termination functions can be used to study the effects of low order recurrents on the frequency dependence of $G''_{00}(\omega)$.

23.3. Low frequency behavior

By LMS theorem, the high order recurrents can determine high frequency decay of a large class of spectral functions. Conversely, low frequency behavior can be deduced in certain cases from the low order recurrents. We first demonstrate the low frequency effects of varying the first recurrent, and then we show the low frequency effects of alternating even-odd deviations of recurrents from their high order asymptotic behavior.

The recurrents of the semicircle spectral function function,

$$-G''_{00}(\omega) = \frac{1}{2\Delta^2} \sqrt{2\Delta^2 - \omega^2} \Theta(2\Delta^2 - \omega^2) \quad (185)$$

are,

$$\bar{\Delta}_k^{\text{sc}} = \Delta \quad , \quad k = 1, 2, \infty \quad . \quad (186)$$

The recurrences of a Gaussian spectral function are,

$$-G''_{00}(\omega) = \sqrt{\pi}e^{-\omega^2} \quad (187)$$

are,

$$\bar{\Delta}_k^{\text{Gauss}} = \sqrt{\frac{k}{2}} \quad , \quad k = 1, 2, \infty \quad . \quad (188)$$

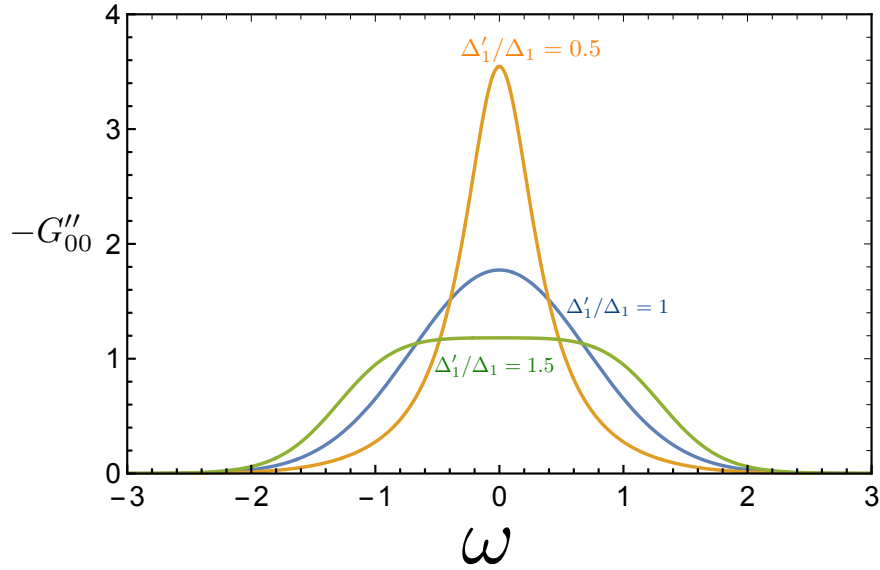


Figure 9: Changing just the first recurrent Δ'_1 in the Gaussian spectral function.

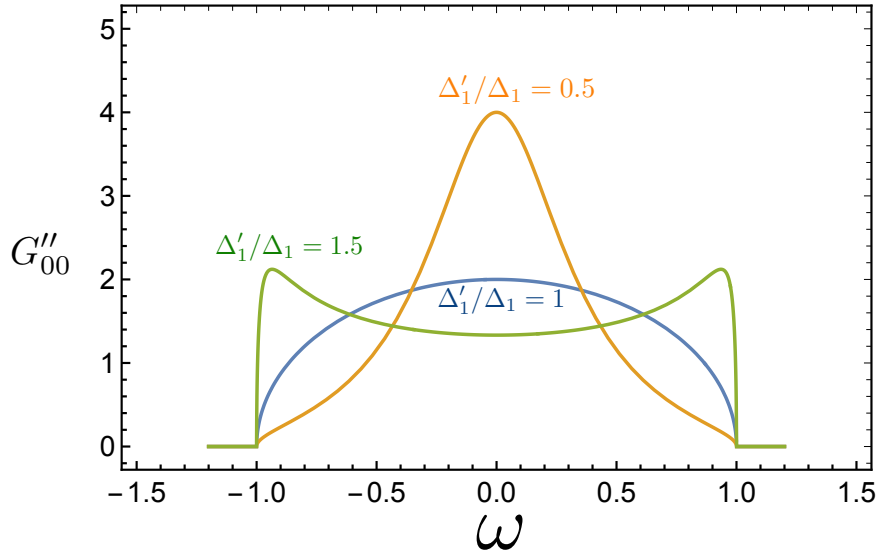


Figure 10: Changing just the first recurrent Δ'_1 in the semicircle spectral function.

As noted by the memory function approach, in the weak scattering limit, the first order recurrent plays an important role in determining the low frequency conductivity.

The first recurrent Δ_1 dominates the DC conductivity. This is demonstrated by varying Δ'_1 in Fig. 9, keeping the higher order recurrences the same. For both the Gaussian in Fig. 9, and the semicircle in Fig. 10, the DC limit of the resulting normalized modified functions vary with Δ'_1/Δ_1 as

$$\frac{G''_{00}(0)}{\bar{G}''_{00}(0)} = \frac{(\Delta'_1)^2}{\Delta_1^2} . \quad (189)$$

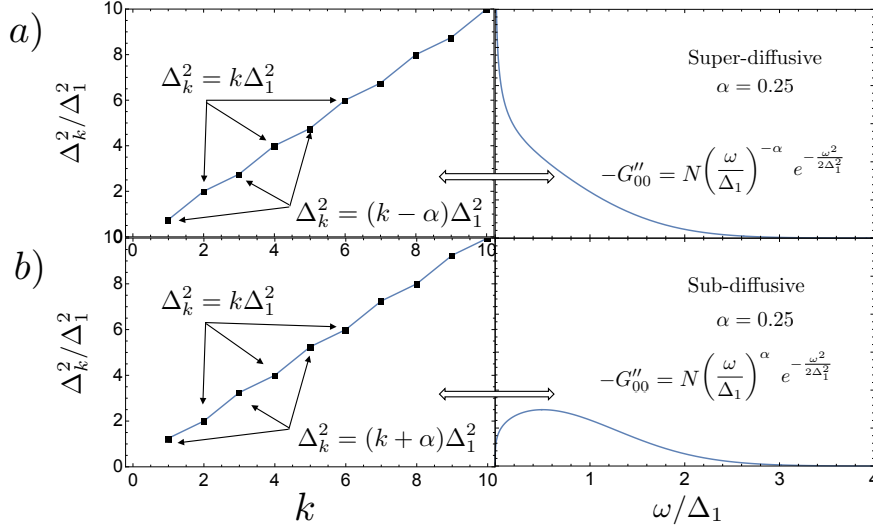


Figure 11: Continued fraction recurrences of PG functions. High frequency Gaussian tail is reflected in the average linear increase of Δ_k^2 . Low frequency divergence (vanishing) in the super-diffusive (sub-diffusive) functions is signalled in the the oscillation of even and odd recurrences starting at the lowest orders.

Stronger modifications of the low frequency behavior is produced by even-odd deviations of the recurrences from the asymptotic form. This is demonstrated by the power-law times Gaussian function (PG), as discussed in detail in Ref. [21],

$$-G''_{\text{PG}}(\omega) = \frac{\sqrt{2\pi}}{\Omega \Gamma\left(\frac{\beta+1}{2}\right)} \left| \frac{\omega}{\Omega} \right|^\beta \exp\left(-\frac{\omega^2}{\Omega^2}\right) . \quad (190)$$

The recurrences of the PG have been evaluated analytically,

$$\left(\Delta_k^{\text{PG}}\right)^2 = \frac{1}{2}(k + \beta) \delta_{k,\text{odd}} + \frac{1}{2}k \delta_{k,\text{even}} \quad (191)$$

and are plotted versus their low order recurrences in Fig. (11). The zero frequency conductivity vanishes or diverges depending on the sign of β . While the relative deviations from the asymptotic $k^{1/2}$ behavior at large k decreases, the effects of the low order recurrences are dramatic at low frequencies. A similar effect is seen numerically for power law functions times stretched exponentials at $\alpha \neq 2$ [21].

23.4. Addition of spectral functions with different frequency scales

The low frequency regime of the response function affects the behavior of the recurrences in a more complicated way than the high frequency asymptotics. For example we consider a sum of two semicircles with different energy scales $\Omega_2 \ll \Omega_1$

$$G''_{2\text{sc}}(\omega) = G''_{\text{sc}}(\omega; \Omega_1) \pm a_2 G''_{\text{sc}}(\omega; \Omega_2) , \quad (192)$$

where $G''_{\text{sc}}(\omega; \Omega)$ is given by Eq. (185). a_2 may be positive (for enhanced DC conductivity), or negative, for suppressed DC conductivity. The moments are additive,

$$\mu_{2k}^{2\text{sc}} = \mu_{2k}^{\text{sc}1} \pm a_2 \mu_{2k}^{\text{sc}1} . \quad (193)$$

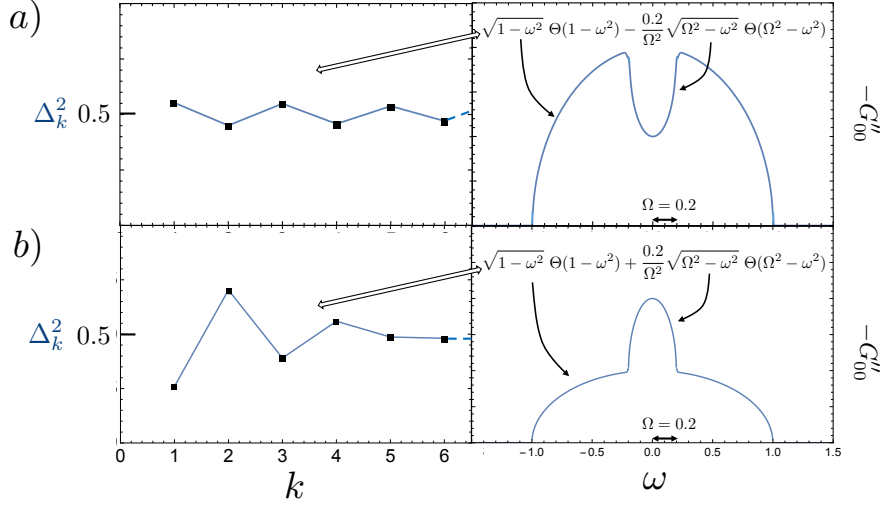


Figure 12: General example of low frequency effects. Top Frames: low frequency suppression of a semicircle function, corresponds to odd order recurrences larger than even orders. Bottom frame: low frequency enhancement corresponds to even order recurrences higher than odd orders. This is qualitatively similar to the effects seen in the recurrences of PGauss functions in Fig. 11

(where we must use $a_2 < 1$, since all moments must be non-negative). After hashing the algebraic relations (169), the combined recurrences are highly entangled. The effects of summing two spectral functions are shown in Fig. 12. The addition of two spectral functions results in even-odd oscillations of the recurrences which persist to high orders, although its signature is already observed at low orders.

23.5. Variational Extrapolation of Recurrences

Since nested commutators of the Hamiltonian with the current create a factorial growth of number of operators, the computational cost of high order moments and recurrences in many cases increases faster than exponentially.

Here we describe the Variational Extrapolation of Recurrences as a possible scheme which allows for a numerical test of its convergence.

Having computed $\Delta_1, \dots, \Delta_{n_{\max}}$, may lead to a reasonable guess for the possible asymptotic behavior at large and low frequencies. We choose a family of analytic variational spectral functions $\bar{G}''_{00}(\omega; \{\alpha\})$, which can be parametrized by variational parameters $\alpha_1, \dots, \alpha_{m_{\text{var}}}$.

Using Kramers-Kronig relation (160) find the real part of $\bar{G}_{00}(\omega + i0^+)$,

$$\bar{G}'_{00}(\omega; \{\alpha\}) = \frac{1}{\pi} \int_{-\infty}^{\infty} d\omega' \bar{G}''_{00}(\omega'; \{\alpha\}) \quad , \quad (194)$$

and calculate the variational recurrences $(\bar{\Delta}_1 \dots \bar{\Delta}_{n_{\max}})$ from the lowest $2n_{\max}$ moments of $\bar{G}''(\omega)$.

The variational parameters are obtained by minimizing the least squares function with respect to $\{\alpha\}$,

$$\chi^2 = \min_{\{\alpha_1, \dots, \alpha_{m_{\text{var}}}\}} \frac{1}{n_{\max} - n_{\min}} \sum_{n=n_{\min}+1}^{n_{\max}} \left(\frac{\Delta_n - \bar{\Delta}_n(\{\alpha\})}{\Delta_n} \right)^2 \quad . \quad (195)$$

The lower cut-off $n_{\min} \geq 1$ is chosen to preferentially fit the recurrences of \bar{G}_{00} to the higher orders of the calculated recurrences. The total number of variational parameters m_{var} must be smaller than $n_{\max} - n_{\min}$ to avoid overfitting.

Inverting Eq. (182) provides $\bar{G}^>_{n_{\max}, n_{\max}}(z)$ which directly provides the Variational Extrapolation of Recurrences (VER)

approximation for G_{00} ,

$$G_{00}^{\text{ver}}(z) \simeq \frac{1}{z - \frac{\Delta_1^2}{z - \frac{\Delta_2^2}{z - \dots \frac{\Delta_{k_{\max}-1}^2}{z - \Delta_{k_{\max}}^2 \tilde{G}_{k_{\max}}^>(z; [\alpha])}}} . \quad (196)$$

The spectral function is given by,

$$\text{Im } G_{00}^{\text{ver}}(\omega + i0^+) \simeq \text{Im} \frac{1}{\omega - \frac{\Delta_1^2}{\omega - \frac{\Delta_2^2}{\omega - \dots \frac{\Delta_{k_{\max}-1}^2}{\omega - \Delta_{k_{\max}}^2 \tilde{G}_{k_{\max}}^>(\omega + i0^+; [\alpha])}}} . \quad (197)$$

Eq. (197) shows that the imaginary part of G_{00} is due to the complex termination function with $\text{Im } \tilde{G}_{k_{\max}} \neq 0$. The quality of the VER can be tested by two criteria: (i) The χ^2 in (195) should be much less than unity. (ii) Computing some additional recurrences $\Delta_{k > k_{\max}}$ and comparing them to the extrapolated $\tilde{\Delta}_k$.

Part VI

Hall coefficients summation formulas

For simplicity, the magnetic field is chosen along the z axis and C_4 symmetry is assumed in the XY plane. The Hall-type coefficients are the electric Hall coefficient R_H , the Nernst Coefficient N , and the thermal Hall coefficient R_{TH} :

$$\begin{aligned} R_H &= \frac{1}{(\sigma_{xx}^{dc})^2} \left. \frac{d\sigma_{xy}^{dc}}{dB} \right|_{B=0} , \\ N &= \frac{1}{\sigma_{xx}^{dc}} \left. \frac{d\alpha_{xy}^{dc}}{dB} \right|_{B=0} - R_H \alpha_{xx}^{dc} , \\ R_{TH} &= \frac{1}{(\kappa_{xx}^{dc})^2} \left. \frac{d\kappa_{xy}^{dc}}{dB} \right|_{B=0} . \end{aligned}$$

The coefficients in Eq. (198) exist if we assume that

$$\lim_{B \rightarrow 0} \sigma_{xx} > 0 , \quad \lim_{B \rightarrow 0} \kappa_{xx} > 0 . \quad (198)$$

That is to say, the expressions apply to gapless dissipative phases, and do not apply to superconductor, insulator, or quantum Hall phases. In addition we also assume no spontaneous magnetization at zero magnetic field, which implies no anomalous Hall effect.

Straightforward Kubo formula calculations of Eq. (198) demand determination of both longitudinal and Hall conductivities. The summation formulas [47, 69] derived below, replaces the difficulties of DC Kubo formulas by calculations of thermodynamic coefficients.

24. Magnetic Field Expansion of Hall-type Conductivity

The derivative with respect to the magnetic field is very difficult to perform using the Lehmann representation, which requires taking derivatives of current operators, wavefunctions, and eigenenergies.

It is therefore much more convenient to differentiate by parts the DC Hall conductivities as written in Eq. (102),

$$\begin{aligned} \left(\frac{dL_{ij}^{xy}(\varepsilon, V)}{dB} \right)_{B=0} &= \frac{1}{\mathcal{V}} \text{Im} \frac{d}{dB} \text{Tr} \rho \left[P_i^x - (\tilde{P}_i^x)_\varepsilon, P_j^y - (\tilde{P}_j^y)_\varepsilon \right] \\ &= \cancel{\Xi_{TR}}^0 + \Xi_{\mathcal{L}} . \end{aligned} \quad (199)$$

We assume OBC in order to define uniform polarizations. OBC are also required to continuously vary the magnetic field B and avoid Dirac's quantization [70].

Ξ_{TR} vanishes under the trace by even time reversal symmetry of H_0, ρ, P_i^x, P_j^y at $B = 0$, and odd symmetry of $\frac{d\rho}{dB}, \frac{dP_i^x}{dB}, \frac{dP_j^y}{dB}$.

$$\begin{aligned} \Xi_{TR} &= \frac{1}{\mathcal{V}} \text{Im} \text{Tr} \frac{d\rho}{dB} \left[P_i^x - \tilde{P}_i^x, P_j^y - \tilde{P}_j^y \right] + \frac{1}{\mathcal{V}} \text{Im} \text{Tr} \rho \left[(1 - \Theta_\varepsilon) \frac{dP_i^x}{dB}, (1 - \Theta_\varepsilon) P_j^y \right] \\ &\quad + \frac{1}{\mathcal{V}} \text{Im} \text{Tr} \rho \left[(1 - \Theta_\varepsilon) P_i^x, (1 - \Theta_\varepsilon) \frac{dP_j^y}{dB} \right] = 0 . \end{aligned} \quad (200)$$

The remaining term $\Xi_{\mathcal{L}}$ is calculated by differentiating the hyper-projector (100) with respect to B ,

$$\begin{aligned}\frac{d\Theta_{\varepsilon}(B)}{dB} &= \frac{\varepsilon}{\mathcal{L}^2 + \varepsilon^2} (\mathcal{M}\mathcal{L} + \mathcal{L}\mathcal{M}) \frac{\varepsilon}{\mathcal{L}^2 + \varepsilon^2} \\ &= (-i) \frac{\varepsilon}{\mathcal{L}^2 + \varepsilon^2} \mathcal{M} \frac{\varepsilon}{\mathcal{L}^2 + \varepsilon^2} J_i + \frac{\varepsilon}{\mathcal{L}^2 + \varepsilon^2} \mathcal{L}\mathcal{M} \frac{\varepsilon}{\mathcal{L}^2 + \varepsilon^2} .\end{aligned}\quad (201)$$

The hypermagnetization is defined by

$$\mathcal{M} \equiv -\frac{\partial \mathcal{L}}{\partial B} = [M^z, \bullet] , \quad (202)$$

where $M^z = -\frac{dH_0}{dB}$.⁷

Thus we obtain,

$$\begin{aligned}\Xi_{\mathcal{L}} &= \frac{1}{\mathcal{V}} \text{ImTr}\rho \left(\left[P_i^x - (\tilde{P}_i^x)_{\varepsilon}, -\frac{d\Theta_{\varepsilon}}{dB} P_j^y \right] - \left[P_j^y - (\tilde{P}_j^y)_{\varepsilon}, -\frac{d\Theta_{\varepsilon}}{dB} P_i^x \right] \right) \\ &= \frac{1}{\mathcal{V}} \text{ImTr}\rho \left(\left[\left(\frac{1}{\mathcal{L}} \right)'_i J_i^x, \frac{\varepsilon}{\mathcal{L}^2 + \varepsilon^2} \mathcal{M}\mathcal{L} \frac{\varepsilon}{\mathcal{L}^2 + \varepsilon^2} P_j^y + i \frac{\varepsilon}{\mathcal{L}^2 + \varepsilon^2} \mathcal{L}\mathcal{M} \frac{\varepsilon}{\mathcal{L}^2 + \varepsilon^2} P_i^y \right] + (J_i^x \leftrightarrow J_j^y) \right) \\ &= -\frac{1}{\mathcal{V}} \text{Im} \left(J_i^x \left| \left(\frac{1}{\mathcal{L}} \right)''_i \mathcal{M} \left(\frac{1}{\mathcal{L}} \right)''_j \right| J_j^y \right) + \Xi_0(J_i^x, J_j^y) - (J_i^x \leftrightarrow J_j^y) .\end{aligned}\quad (203)$$

In the last row of (203), we applied Eq. (89) to reconstruct the OHS current matrix element. The vanishing of Ξ_0 is proven as follows. Using the hermiticity of \mathcal{L} (83), we can write:

$$\begin{aligned}\Xi_0 &= \frac{i}{\mathcal{V}} \text{Im} \left(J_i^x \left| \left(\frac{1}{\mathcal{L}} \right)''_i \mathcal{L}\mathcal{M} \left(\frac{1}{\mathcal{L}} \right)''_j \right| P_j^y \right) \\ &= \frac{i}{\mathcal{V}} \text{Im} \left(\mathcal{L} \left(\frac{1}{\mathcal{L}} \right)''_i J_i^x \left| \mathcal{M} \left(\frac{1}{\mathcal{L}} \right)''_j \right| P_j^y \right) .\end{aligned}\quad (204)$$

Next, we will prove that,

$$\left(\frac{1}{\mathcal{L}} \right)''_i \mathcal{L} |J_i^{\alpha}\rangle = 0 + \mathcal{O}(\varepsilon) . \quad (205)$$

The inner product of the hyperstate given by Eq. (205) with any Krylov basis hyperstate $\langle n; J_i^{\alpha} |$ belonging to the same root current is,

$$\begin{aligned}\langle n; J_i^{\alpha} | \left(\frac{1}{\mathcal{L}} \right)''_i \mathcal{L} |J_i^{\alpha}\rangle &= \sqrt{\chi_{\text{csr}}} \langle n; J_i^{\alpha} | \left(\frac{1}{\mathcal{L}} \right)''_i \mathcal{L} |0; J_i^{\alpha}\rangle \\ &= \sqrt{\chi_{\text{csr}}} \Delta_1 \text{Im} G_{n1} = 0 + \mathcal{O}(\varepsilon) ,\end{aligned}\quad (206)$$

since G_{n1} is purely real, as proven in Eq. (165).

In contrast to Eq. (205), the surviving terms in (203) do not vanish since,

$$\begin{aligned}\langle n; J_i^{\alpha} | \mathcal{L} \left(\frac{1}{\mathcal{L}} \right)''_i |P_i^{\alpha}\rangle &= \langle n; J_i^{\alpha} | \left(\frac{1}{\mathcal{L}} \right)''_i \mathcal{L} |P_i^{\alpha}\rangle \\ &= -i \sqrt{\chi_{\text{csr}}} \langle n; J_i^{\alpha} | \left(\frac{1}{\mathcal{L}} \right)''_i |1; J_i^{\alpha}\rangle \\ &= -i \sqrt{\chi_{\text{csr}}} \text{Im} G_{n,0} = -i \delta_{n,2k} \chi_{\text{csr}} G''_{00} R_k \neq 0 .\end{aligned}\quad (207)$$

⁷Note: Under TR, $M^z \rightarrow -M^z$, and the commutators in the response functions reverse their order $[A, B] \rightarrow [\text{TR}(B), \text{TR}(A)]$. Therefore the hypermagnetization \mathcal{M} is even under TR.

where the last identity uses Eq. (163).

Thus we obtain

$$\left(\frac{dL_{ij}^{xy}(\varepsilon, \mathcal{V})}{dB} \right)_{\mathbf{B}=0} = -\frac{2}{\mathcal{V}} \text{Im} \left(J_i^x \left| \left(\frac{1}{\mathcal{L}} \right)'' \right. \mathcal{M} \left(\frac{1}{\mathcal{L}} \right)'' \right. | J_j^y \rangle + \mathcal{O}(\varepsilon) \quad . \quad (208)$$

It is possible to evaluate Eq. (208) by inserting two Krylov bases resolutions of identity,

$$\sum_{n=0}^{\infty} |n; J_i^\alpha\rangle \langle n; J_i^\alpha| = \mathbb{1}_{i\alpha} \quad , \quad (209)$$

where $\mathbb{1}_\alpha$ is the projector onto OHS subspace spanned by the hyperstates $\mathcal{L}^k |J_i^\alpha\rangle$ for $0 \leq k \leq \infty$. Using the C_4 symmetry, we obtain

$$\begin{aligned} \left(\frac{dL_{ij}^{xy}(\varepsilon, \mathcal{V})}{dB} \right)_{\mathbf{B}=0} &= -\frac{2\chi_{\text{csr}}}{\mathcal{V}} \text{Im} \sum_{nm} \langle 0; J_i^x | \left(\frac{1}{\mathcal{L}} \right)'' | n; J_i^x \rangle \mathcal{M}_{nm}^{ij} \langle m; J_j^y | \left(\frac{1}{\mathcal{L}} \right)'' | 0; J_j^y \rangle \\ &= -\frac{2\chi_{\text{csr}}}{\mathcal{V}} \text{Im} \sum_{nm} G''_{0,n} \mathcal{M}_{nm}^{ij} G''_{m,0} \quad . \end{aligned} \quad (210)$$

where \mathcal{M}_{nm}^{ij} are the z -hypermagnetization normalized matrix elements between Krylov hyperstates,

$$\mathcal{M}_{nm}^{ij} = \text{Im} \langle n; J_i^x | \mathcal{M} | m; J_j^y \rangle \quad . \quad (211)$$

By Eq. (163),

$$\text{Im} G_{0,n}^i = \delta_{n,2k} R_k^i \text{Im} G_{00}^i, \quad R_k^i = \prod_{k'=1}^k \left(-\frac{\Delta_{2k'-1}^i}{\Delta_{2k'}^i} \right) \quad , \quad (212)$$

and by Eq. (53),

$$\text{Re} L_{ii}^{xx} = \text{Re} L_{ii}^{yy} = -\chi_{\text{csr}}^i \text{Im} G_{00}^i \quad . \quad (213)$$

Thus the sum over n, m in Eq. (210) includes only even integers and results in the summation formula,

$$\left(\frac{dL_{ij}^{xy}(\varepsilon, \mathcal{V})}{dB} \right)_{\mathbf{B}=0} = -2 \frac{L_{ii}^{yy}(\varepsilon, \mathcal{V}) L_{jj}^{xx}(\varepsilon, \mathcal{V})}{\sqrt{\chi_{\text{csr}}^i \chi_{\text{csr}}^j}} \sum_{kl} R_k^{(i)} R_l^{(j)} \mathcal{M}_{2k,2l}^{ij} + \mathcal{O}(\varepsilon) \quad . \quad (214)$$

The longitudinal conductivities $L_{ii}^{xx}(\varepsilon)$ and $L_{jj}^{yy}(\varepsilon)$ factor out of the sum in Eq. (214). They produce the non-commuting DC limit of $\varepsilon, 1/\mathcal{V} \rightarrow 0$.

Thus, (unless longitudinal conductivities vanish, or the currents are completely separable as explained in subsection 29.1), the longitudinal conductivities may be divided out and the Hall-type coefficients in Eqs. (198) can be expressed as a ε -independent thermodynamic coefficients.

25. Hall Coefficient

In the double summation over the Krylov bases we separate out the $n = 0, m = 0$ term write the electric Hall coefficient as a sum of two terms,

$$R_{\text{H}} = R_{\text{H}}^{(0)} + R_{\text{H}}^{\text{corr}} \quad , \quad (215)$$

where

$$\begin{aligned}
R_{\text{H}}^{(0)} &= \frac{\chi_{\text{cmc}}}{\chi_{\text{csr}}^2} \quad , \\
\chi_{\text{csr}} &= \lim_{\mathbf{q} \rightarrow 0} \lim_{\mathcal{V} \rightarrow \infty} \frac{\hbar}{\mathcal{V}} (j^x | j^x) \quad , \\
\chi_{\text{cmc}} &= -2 \lim_{\mathbf{q} \rightarrow 0} \lim_{\mathcal{V} \rightarrow \infty} \frac{\hbar}{\mathcal{V}} \text{Im}(j^x | \mathcal{M} | j^y) \quad , \\
R_{\text{H}}^{\text{corr}} &= -\frac{2}{\chi_{\text{csr}}} \sum_{kl} R_k R_l \mathcal{M}_{2k,2l} (1 - \delta_{k,0} \delta_{l,0}) \quad .
\end{aligned} \tag{216}$$

χ_{csr} is the zeroth moment of the longitudinal conductivity, which was defined in Section 21. It represents the kinetic energy of the constituent charge carriers. The current-magnetization-current (CMC) susceptibility, χ_{cmc} , measures the effect of the Lorentz force on the currents, as shown below. $R_{\text{H}}^{(0)}$ reproduces Boltzmann's equation result for energy dependent scattering time [71].

The correction term $R_{\text{H}}^{\text{corr}}$ involves higher order recurrences and hypermagnetization matrix elements, \mathcal{M}_{nm}^{ij} defined in (210). The recurrences and Krylov operators involve current non-conservation, caused by disorder, hard core interactions and lattice Umklapp scattering. These terms are increasingly difficult to compute. In order to be allowed to neglect them, they must be estimated to be smaller in magnitude than $R_{\text{H}}^{\text{corr}}$. In Section 31 and Section 34, such estimates are obtained by calculation of the lowest order terms for certain lattice models of strongly interacting electrons and hard core bosons.

The current-magnetization-current (CMC) susceptibility, χ_{cmc} , measures the effect of the Lorentz force on the currents, as shown below. $R_{\text{H}}^{(0)}$ reproduces Boltzmann's equation result for energy dependent scattering time [71]. $R_{\text{H}}^{\text{corr}}$ includes the higher order corrections due to disorder, hard core interactions and lattice Umklapp scattering. For Hard Core Bosons, $R_{\text{H}}^{\text{corr}}$ will be partially evaluated in subsection 34.4.

25.1. Weak scattering limit

For non-interacting band electrons with dispersion $\epsilon_{\mathbf{k}}$, the CSR is given by Eq. (15), and the CMC is

$$\chi_{\text{cmc}} = \frac{e^3}{c} \sum_{\mathbf{k}} \left(-\frac{\partial f_{\mathbf{k}}^0}{\partial \epsilon} \right) \left(v_{\mathbf{k}}^y \left(v_{\mathbf{k}}^y \frac{\partial}{\partial k^x} - v_{\mathbf{k}}^x \frac{\partial}{\partial k^y} \right) v_{\mathbf{k}}^x \right) \quad . \tag{217}$$

Thus, $R_{\text{H}}^{(0)} = \chi_{\text{cmc}} / \chi_{\text{csr}}^2$ recovers Boltzmann equation result (16) for isotropic lifetime. $R^{\text{corr}} \propto \Delta_1$, which depends on $[H, j^x] \neq 0$. Therefore the correction is relatively suppressed at low disorder.

26. Modified Nernst Coefficient

The Modified Nernst Coefficient \bar{N} for C_4 symmetric Hamiltonians is

$$\bar{N} = \frac{1}{\sigma_{xx}^{\text{dc}} \kappa_{xx}^{\text{dc}}} \frac{d\alpha_{xy}}{dB} = \frac{1}{\kappa_{xx}^{\text{dc}}} (N + R_{\text{H}} \alpha_{xx}) \quad . \tag{218}$$

\bar{N} can be expressed by the summation formula,

$$\bar{N} = \bar{N}^{(0)} + \bar{N}^{\text{corr}} \quad , \tag{219}$$

where

$$\begin{aligned}
\bar{N}^{(0)} &= \frac{\chi_{\text{cmc}}^{\text{th-el}}}{\chi_{\text{csr}} \chi_{\text{csr}}^{\text{th}}} , \\
\chi_{\text{csr}}^{\text{th}} &= \lim_{V \rightarrow \infty} \frac{\hbar}{\mathcal{V}} (J_Q^x | J_Q^x) , \\
\chi_{\text{cmc}}^{\text{th-el}} &= -\frac{2}{V} \text{Im} (J_Q^x | \mathcal{M} | J_Q^y) , \\
\bar{N}_{\text{H}}^{\text{corr}} &= -\frac{2}{\sqrt{\chi_{\text{csr}}^{\text{th}} \chi_{\text{csr}}}} \sum_{kl} R_k^{\text{th}} R_l \mathcal{M}_{2k,2l}^{\text{th-el}} (1 - \delta_{k,0} \delta_{l,0}) , \\
\mathcal{M}_{nm}^{\text{th-el}} &= \text{Im} \langle n; J_Q^x | \mathcal{M} | m; J_Q^y \rangle .
\end{aligned} \tag{220}$$

$\chi_{\text{csr}}^{\text{th}}$ and $\mathcal{M}_{nm}^{\text{th-el}}$ are the thermal CSR, and thermoelectric hypermagnetization matrix elements respectively. \bar{N} is therefore expressed as a thermodynamic coefficient similar to R_{H} , and R_{TH} which follows below.

27. Thermal Hall coefficient

The thermal Hall coefficient is,

$$R_{\text{TH}} = R_{\text{TH}}^{(0)} + R_{\text{TH}}^{\text{corr}} , \tag{221}$$

where

$$\begin{aligned}
R_{\text{TH}}^{(0)} &= T \frac{\chi_{\text{cmc}}^{\text{th}}}{(\chi_{\text{csr}}^{\text{th}})^2} \\
R_{\text{TH}}^{\text{corr}} &= -\frac{2T}{\chi_{\text{csr}}^{\text{th}}} \sum_{kl} R_k^{\text{th}} R_l^{\text{th}} \mathcal{M}_{2k,2l}^{\text{th-th}} (1 - \delta_{k,0} \delta_{l,0}) \\
\mathcal{M}_{nm}^{\text{th-th}} &= \text{Im} \langle n; J_Q^x | \mathcal{M} | m; J_Q^y \rangle .
\end{aligned} \tag{222}$$

28. Calculating the correction terms

The correction terms in Eqs. (216,220,222) depend on recurrences $\Delta_n, n = 1, 2, \dots$, which demand calculations of moments $\chi_{\text{csr}}, \mu_2, \mu_4, \dots$, and hypermagnetization matrix elements $\mathcal{M}_{2k,2l}$. The latter are most conveniently derived from the *non-normalized* magnetization matrix elements

$$\tilde{\mathcal{M}}_{nm} \equiv \text{Im} (\mathcal{L}^n J_i^y | \mathcal{M} | \mathcal{L}^m J_j^x) = -\text{Im} \text{Tr} \rho [\mathcal{L}^{n-1} J_i^y, \mathcal{M} \mathcal{L}^m J_j^x] , \tag{223}$$

which are thermodynamic expectation values of nested commutators. For short range Hamiltonians, the commutators include sums over connected clusters of operators which are easier to trace over than calculating two-operator susceptibilities. These clusters can be generated and traced over by symbolic manipulation, as demonstrated in Sections 31 and 34.

$\tilde{\mathcal{M}}_{nm}$ are related to \mathcal{M}_{nm} of the correction terms by the Gramm-Schmidt matrix K . This matrix is determined as follows. Applying the resolution of identity with the Krylov basis,

$$\begin{aligned}
\mathcal{L}^k |0\rangle &= \sum_{k' \leq k} |k'\rangle \langle k' | \mathcal{L}^k |0\rangle \\
&\equiv \sum_{k'} K_{k,k'} |k'\rangle .
\end{aligned} \tag{224}$$

The matrix K is obtained by powers of the tridiagonal Liouvillian matrix (158), which results in polynomials of the recurrences $\Delta_{k' \leq k}$,

$$K_{k',k} [\Delta_1, \dots, \Delta_k] = (L^k)_{k',0}, \quad k' \leq k . \tag{225}$$

Thus we obtain,

$$\mathcal{M}_{n,m} = \sum_{n' \leq n} \sum_{m' \leq m} K_{n,n'}^{-1}[\Delta] K_{m,m'}^{-1}[\Delta] \tilde{\mathcal{M}}_{n',m'}'' \quad . \quad (226)$$

29. Optimization of thermodynamic approaches

29.1. The Separability problem

The thermodynamic approaches have their limitations. The continued fraction extrapolation can only be performed efficiently if a clear asymptotic power law can be deduced from the dependence of the calculated recurrences on their order. In practice, the fluctuations of the calculated recurrences from an asymptotic power law behavior should decrease monotonically if a reliable termination function is to be found.

Nearly separable currents can significantly slow the convergence of continued fractions and Hall coefficients corrections. For example, the recurrences of a sum of two spectral functions with very different characteristic frequency scales is shown in Fig. 12. We note that the fluctuations about average recurrences do not converge rapidly.

Physically, sums of spectral functions with vastly different frequency scales can be expected for separable currents with different relaxation times. That is to say, if the Hamiltonian and its currents can be written as sum of commuting channels,

$$H = \sum_{r=1}^{N_r} H_r \quad , \quad \mathbf{j} = \sum_r \mathbf{j}_r \quad , \quad [\mathbf{j}_r, H_{r'}] \propto \delta_{rr'} \quad , \quad (227)$$

the resulting conductivities will be sums,

$$\sigma_{\alpha\beta}(\omega) = \sum_r \sigma_{\alpha\beta}^r(\omega) \quad . \quad (228)$$

While their moments are additive,

$$\mu_{2k} = \sum_r \mu_{2k}^r \quad , \quad (229)$$

the recurrences which are obtained by Eqs. (169) are highly entangled functions of the separate μ_{2k}^r 's.

Similarly, the Hall coefficient summation formulas are formally correct, but cease to be useful for separable currents. Since the total Hall coefficient is,

$$R_H = \frac{\sum_{r=1}^{N_r} (d\sigma_{xy}^r/dB)}{\left(\sum_{r=1}^{N_r} \sigma_{xx}^r\right)^2} \quad , \quad (230)$$

for multichannel separable currents $N_r > 1$, ratios between different conductivities must enter the Hall coefficient, which therefore cannot be captured accurately just by $R_H^{(0)}$. For example, Fermi surface electrons with strongly dependent \mathbf{k} -dependent lifetime $\tau_{\mathbf{k}}$. At weak scattering, the currents of different wavevectors are separable. While $R_H^{(0)}$ of Eq. (216) recovers the single lifetime expression of Eq. 14, it does not agree (within a factor of order unity) with the \mathbf{k} -dependent lifetime result of Boltzmann's equation in Eq. 13. The difference between $R_H^{(0)}$ and Boltzmann's result is contained in the higher order correction terms, which are unwieldy.

In conclusion, continued fractions and Hall coefficient summation formulas are best suited for a non-separable current governed by one relaxation timescale. Otherwise, in Hamiltonians which support two or more separable currents with different relaxation timescales, the conductivities of each current should be calculated separately and later assembled in Eq. (230) to obtain the total Hall coefficient.⁸

⁸We thank Steve Kivelson for emphasizing the anisotropic lifetime problem in the Hall coefficient formula.

29.2. Renormalized Hamiltonians at low temperatures

Effective Hamiltonians are crucially important for efficient use of thermodynamic approaches to DC transport coefficients. As can be seen from the Lehmann representation of longitudinal conductivities (52), and the DPP formulas of the Hall conductivities (103), the important part of the spectrum and eigenstates resides in an energy window of order T above the ground state. The Hall coefficient formula, which is derived from Eq. (208), also depends on that part of the spectrum as can be seen from,

$$\left(\frac{dL_{ij}^{xy}(\varepsilon, V)}{dB} \right) = -\pi^2 \frac{2}{\mathcal{V}} \text{Im} \sum_{nmn'} W_{nm} \langle n | J_i^x | m \rangle \langle n' | J_j^y | n \rangle \mathcal{M}_{nmn'}^{n'} \delta_\varepsilon(E_n - E_{m'}) \delta_\varepsilon(E_{n'} - E_n) \quad . \quad (231)$$

where $\delta_\varepsilon(x) = \varepsilon/(x^2 + \varepsilon^2)$. Thus, in the DC limit, dL_{ij}^{xy}/dB is also an *on-shell* expression. It is greatly advantageous to replace the microscopic Hamiltonian H^{micro} by an effective Hamiltonian $H^{\text{eff}}(B)$ which operates in the low energy Hilbert space and reproduces the correct spectrum at $\{E_n \leq \text{const } T\}$.

The renormalized currents and magnetization within this reduced Hilbert space are defined by,

$$\begin{aligned} \mathbf{j}_i^{\text{eff}} &= i[H^{\text{eff}}, \mathbf{P}_i^{\text{eff}}] \quad , \\ M^{\text{eff}} &= -\frac{\partial H^{\text{eff}}}{dB} \quad , \end{aligned} \quad (232)$$

where $\mathbf{P}_i^{\text{eff}}$ are also projected onto the reduced Hilbert space. A consequence of renormalization in certain models is to reduce the magnitude of currents' non-conservation, i.e.

$$\| [H^{\text{eff}}, \mathbf{j}_i^{\text{eff}}] \| \leq \| [H^{\text{micro}}, \mathbf{j}_i] \| \quad . \quad (233)$$

The relative magnitude of the first recurrent depends on this commutator. Since all terms in the Hall coefficient's correction terms R_{corr} are proportional to Δ_1 , this ensures reduction of the relative magnitude $R_{\text{corr}}/R_{\text{H}}^{(0)}$.

An simple example of the value of renormalization is demonstrated by comparing the zeroth Hall coefficients of the microscopic Hamiltonian of electrons in a periodic potential, to that of the conduction band effective Hamiltonian. The microscopic Hamiltonian is $H^{\text{particles}}$ given in Eq. (32). Its magnetization is given by

$$M^z = \frac{1}{2c} \sum_{i=1}^{N_p} \mathbf{x}_i \times \frac{\mathbf{p}_i}{m} \quad . \quad (234)$$

The CSR and CMC are completely independent on the potential terms and hence,

$$\begin{aligned} \chi_{\text{csr}}^{\text{particles}} &= \frac{N_p e^2}{\mathcal{V} m} \\ \chi_{\text{cmc}}^{\text{particles}} &= \frac{N_{\text{tot}} e^3}{\mathcal{V} m^2 c} \\ R_{\text{H}}^{(0), \text{particles}} &= \frac{\mathcal{V}}{N_p e c} \quad . \end{aligned} \quad (235)$$

Where N_p includes the electrons in *all* the filled bands and core states. The zeroth Hall coefficient must clearly be very far from the full answer, since we know from Boltzmann's equation (16) that R_{H} depends only on the filling of the *conduction* band. The correction term is therefore expected to be significant. Indeed, the magnitude of the first recurrent, which is a factor in R^{corr} is of order

$$\Delta_1^2 = \frac{1}{\mathcal{V} \chi_{\text{csr}}} \sum_{\mathbf{k}, \mathbf{q}, n, n'} \frac{f_{\mathbf{k}, n} - f_{\mathbf{k}+\mathbf{q}, n'}}{\epsilon_{\mathbf{k}+\mathbf{q}, n} - \epsilon_{\mathbf{k}, n'}} (q^x)^2 |V(\mathbf{q})|^2 \quad , \quad (236)$$

which can be very large for crystal potentials $|V(\mathbf{q})| \gg |\epsilon_F|$.

In comparison, if we use the renormalized conduction band Hamiltonian,

$$\begin{aligned}
H^{\text{eff}} &= \sum_{\mathbf{k}} \frac{\mathbf{k}^2}{2m^*} c_{\mathbf{k}}^\dagger c_{\mathbf{k}} + \frac{1}{\mathcal{V}} \sum_{\mathbf{k}, \mathbf{k}'} U_{\mathbf{k}\mathbf{k}'}^{\text{dis}} c_{\mathbf{k}}^\dagger c_{\mathbf{k}'} \quad , \\
\mathbf{j}^{\text{eff}} &= \sum_{\mathbf{k}} \frac{\mathbf{k}}{m^*} c_{\mathbf{k}}^\dagger c_{\mathbf{k}} \quad .
\end{aligned} \tag{237}$$

where $U^{\text{dis}} \ll \epsilon_F$ is due to impurities, then

$$\begin{aligned}
\chi_{\text{csr}}^{\text{eff}} &= \frac{(e^*)^2 n_{\text{cond}}}{m^*} \quad , \\
\chi_{\text{cmc}}^{\text{eff}} &= \frac{(e^*)^2 n_{\text{cond}}}{(m^*)^2 c} \quad , \\
(R_{\text{H}}^{(0)})^{\text{eff}} &= \frac{1}{n_{\text{cond}} e^* c} \quad .
\end{aligned} \tag{238}$$

n_{cond} is just the density of the partially filled conduction band. $R_{\text{H}}^{(0)}$ recovers Drude-Boltzmann theory (7), with a small correction term which is suppressed by a factor of $U^{\text{dis}}/\epsilon_F \ll 1$.

For dirty semimetals [71], where the interband gap is of the same order as U^{dis} , the Hall coefficient can be well approximated by $R_{\text{H}}^{(0)}$ of the two-band Hamiltonian, including both intraband and interband current matrix elements. The Hall coefficient formula provides a simpler route to the Hall coefficient than the coupled two-band Boltzmann equation [38, 39, 40].

Part VII

Strongly Correlated Electrons

30. The Hubbard Model

Electrons in a tight binding bandstructure, with strong local interactions can be minimally described by the Hubbard model (HM) [72, 73], which on the SL is given by

$$H^{\text{HM}} = -t \sum_{\langle ij \rangle, s=\uparrow, \downarrow} (c_{is}^\dagger c_{js} + c_{js}^\dagger c_{is}) + U \sum_i n_{i\uparrow} n_{i\downarrow} . \quad (239)$$

For historical reasons, the electron filling in the HM is often measured by the “hole concentration” relative to half filling, i.e. $x = \langle n_i^h \rangle$, as defined by $n_i^h = 1 - \sum_{s=\uparrow, \downarrow} n_{is}$.

For $U = 0$ the HM reduces to the non-interacting nn SL model, which was discussed in Section 5.1. As shown in subsection 25.1, $R_H^{(0)}$ reduces to Boltzmann’s equation isotropic scattering time result, which was depicted in Fig. 2.

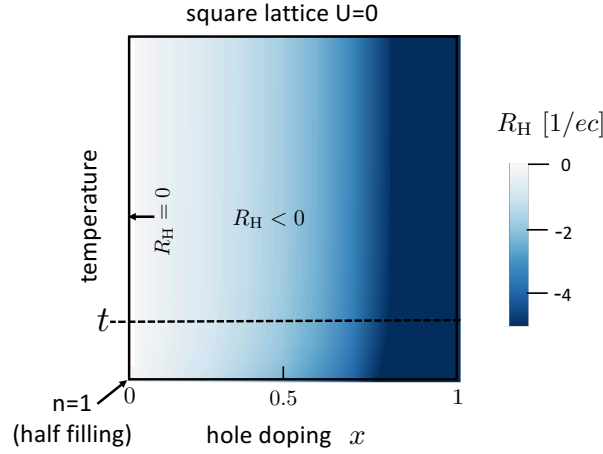


Figure 13: Hall coefficient of weakly disordered ($U = 0$) square lattice. R_H^{SL} given by Eq. (16). The strongest prediction of Boltzmann theory for this model is that $R_H < 0$ for $0 < x < 1$, and does not diverge anywhere except at $x \rightarrow 1$.

The Hall coefficient temperature-doping map of the nn SL model, is depicted in Fig. 13. We note that the Hall sign is negative for all $x > 0$, and vanishes half filling $x_{\text{sign}} = 0$. This Hall map will be contrasted with the Hall map in the $U \gg t$ regime.

31. The tJ Model

In the strong interacting regime of $U \gg t$, the electronic correlations of the HM differ dramatically from the predictions of the weakly interacting model on the SL. This is true especially near half filling $x = 0$, where a charge gap of order U appears between the singly occupied spin and hole configurations, and configurations which contain doubly occupied sites. At zero temperature $T \ll U$, the half filled HM describes a Mott insulator, which orders antiferromagnetically. Away from half filling, the ground state phase diagram is still under debate, with variational studies indicating possible charge and spin density wave order, and/or d -wave superconducting order [5, 23, 73].

As argued in subsection 29.2, at temperatures $T \ll U$, the thermodynamic approaches converge much better after the HM Hamiltonian is renormalized onto its lower energy Gutzwiller-projected (GP) subspace of no-double-occupancies.

There, for $U \gg t$, the HM maps onto the t-J model (tJM) [66, 74], which to second leading order in t/U ,

$$\begin{aligned}
H^{\text{tJM}} &= \mathcal{P}_{\text{GP}}(H^t + H^J + H^{J'})\mathcal{P}_{\text{GP}} + \mathcal{O}(t^3/U^2) \quad , \\
H^t &= -t \sum_{\langle ij \rangle} K_{ij}^+ \quad , \\
H^J &= J \sum_{\langle ij \rangle} \mathbf{s}_i \cdot \mathbf{s}_j (1-n_i^h)(1-n_j^h) \quad , \\
H^{J'} &= -\frac{J}{4} \sum_{\langle ij \rangle \langle jk \rangle} (K_{ik}^+ - 2\Sigma_{ik}^+ \cdot \mathbf{s}_j)(1-n_j^h) \quad .
\end{aligned} \tag{240}$$

The GP bond operators are

$$\begin{aligned}
K_{ij}^\pm &\equiv \sum_s \tilde{c}_{is}^\dagger \tilde{c}_{js} \pm \tilde{c}_{js}^\dagger \tilde{c}_{is} \quad , \\
\Sigma_{ij}^\pm &\equiv \sum_{ss'} \tilde{c}_{is}^\dagger \vec{\sigma}_{ss'} \tilde{c}_{js'} \pm \tilde{c}_{js}^\dagger \vec{\sigma}_{ss'} \tilde{c}_{is'} \quad ,
\end{aligned} \tag{241}$$

where $\tilde{c}_{is}^\dagger \equiv c_{is}^\dagger(1-n_{i,-s})$. K^+ (K^-) describes the bond kinetic energy (current) and Σ^\pm describes the spin-dependent hopping. $J = 4t^2/U$ is Anderson's antiferromagnetic superexchange energy.

31.1. Linear Resistivity slope

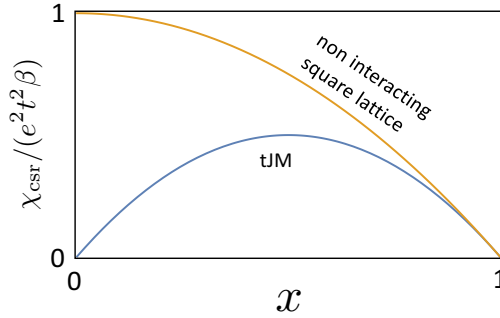


Figure 14: Doping dependent CSRs at intermediate temperatures $t < T \ll U$. In contrast to the non-interacting case, the CSR of the tJM vanishes toward the Mott phase as $x \rightarrow 0$. This results in an interaction induced divergence of R_{H} and the resistivity slope.

The t model, H^t , dominates the metallic charge transport at $U \gg T \gg J$. The doping dependence of the CSR of the t model was calculated by Jaklic [75] and Perepelitsky [76] up to order β^3 :

$$\chi_{\text{csr}} = 2\beta e^2 t^2 x(1-x) + \frac{\beta^3 e^2 t^4}{6} x(1-x)(-9 + 2x + x^2) + \mathcal{O}(\beta^5 t^6) \quad . \tag{242}$$

As depicted in Fig. 14, the CSR vanishes toward $x \rightarrow 0$ as a consequence of the GP. It is also suppressed relative to the non-interacting limit even far from half filling. Vanishing of the CSR produces a divergence of the Hall coefficient by Eq. (289).

The high temperature limit of the first two conductivity recurrences of H^t are,

$$\Delta_1^2 = t^2(3 - 2x - x^2)(1 + \mathcal{O}(\beta t)^2), \quad \Delta_2^2 = t^2 \frac{24(1+x)}{3+x} (1 + \mathcal{O}(\beta t)^2) \quad , \tag{243}$$

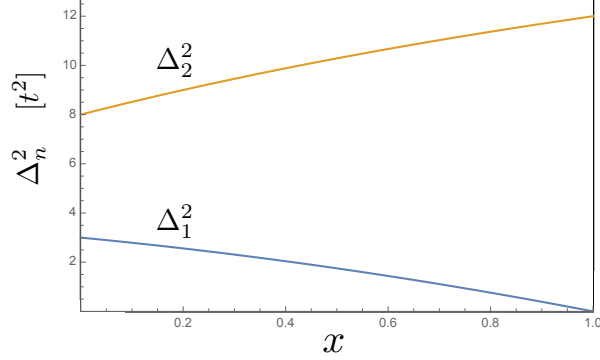


Figure 15: The first two recurrences of H^I . Doping dependence of the first two recurrences of H^I at high temperature.

which yields the CF of the DC conductivity as,

$$\sigma_{xx}(\omega) = -\beta\chi_{\text{csr}} \lim_{\varepsilon \rightarrow 0} \text{Im} \frac{1}{i\varepsilon - \frac{\Delta_1^2}{i\varepsilon - \Delta_2 G_{22}^>(i\varepsilon)}} . \quad (244)$$

Due to lack of higher order recurrences, $G_{22}^>$ is approximated by extrapolating the recurrences using semicircle termina-

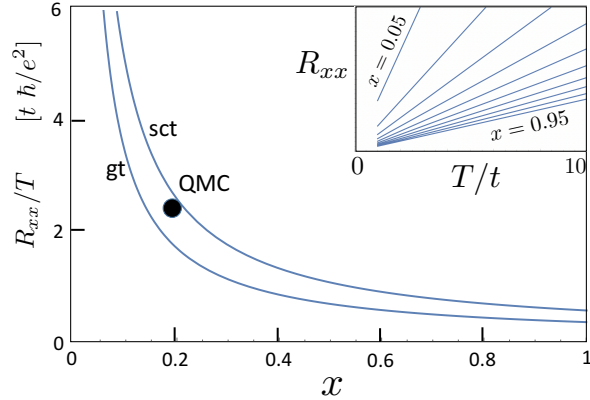


Figure 16: High temperature resistivity slopes of H^I . sct and gt denote two different continued fraction extrapolation schemes (see text). Inset depicts $R_{xx}(T)$ for gt approximation. The solid circle marks the Quantum Monte Carlo result for the $U=8t$ HM, reported in Fig. S3 of Ref. [77].

tion (sct) (see Eq. (186)), and Gaussian termination (gt) (see Eq. (188)),

$$\begin{aligned} (\bar{\Delta}_n^{\text{sct}})^2 &\Rightarrow \Delta_2^2 , \quad n = 2, 3, \dots \infty . \\ (\bar{\Delta}_n^{\text{gt}})^2 &\Rightarrow \frac{1}{2}n\Delta_2^2 , \quad n = 2, 3, \dots \infty . \end{aligned} \quad (245)$$

In Fig. 16, the high temperature DC resistivity slopes of H^I are plotted for both termination approximations. We see that the slopes diverge toward the Mott limit, as expected by the suppression of the CSR depicted in Fig. 14. Interestingly, the resistivity is finite at high temperatures even in the dilute electron density limit $x \rightarrow 1$. The slopes of Fig. 16 are in qualitative agreement with the HM calculation in Ref. [77].

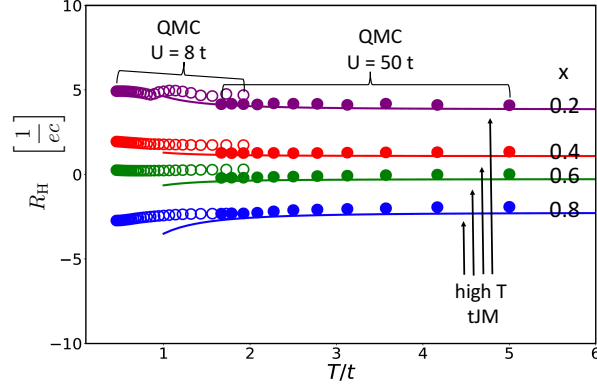


Figure 17: Hall coefficient $R_H^{(0)}$ in the intermediate temperature regime $J \leq T \ll U$. Lines depict the high temperature expansion results for the t -model Eq. (247). Solid and open circles are Quantum Monte Carlo (QMC) results using Boltzmann weights of the HM with two widely different values of U/t . The QMC results are limited to the regions of negligible fermion sign error. We note that the high temperature expansion agrees with the QMC data down to $T \approx 2t$, and the QMC data shows quite weak temperature dependence down to $T \approx 0.5t$.

31.2. Hall map for large U/t

R_H of the t -model was calculated by Eq. (216). The doping dependent CMC was determined up to order $(\beta t)^4$,

$$\begin{aligned} \chi_{\text{cmc}}^t &= \frac{\beta^2 t^4 e^3}{2c} x(1-x)(-5 + 10x + 3x^2) \\ &+ \frac{\beta^4 t^6 e^3}{16c} x(1-x)(45 - 136x + 50x^2 + 48x^3 - 71x^4) \quad . \end{aligned} \quad (246)$$

The zeroth Hall coefficient was determined up to second order in βt ,

$$R_H^{t,(0)} = \frac{1}{ec} \left(\frac{-5 + 10x + 3x^2}{8x(1-x)} \right) + \left((\beta t)^2 \frac{-45 - 53x + 145x^2 + 225x^3}{192x} \right) \quad . \quad (247)$$

The calculation of $R_H^{t,(0)}$ was extended down to the intermediate temperature (IT) regime: $J \leq T \ll U$, by Quantum Monte Carlo (QMC) simulation, using the full HM weights at large U/t . The QMC calculation includes the effects of the spin interactions H^J in the tJM. The QMC data is plotted in Fig. 17, with the analytic curves of Eq. (247) which are depicted by solid lines.

At extremely high temperatures $T \gg U$, one must use the unprojected HM of Eq. (239). The suppression of double occupancies in the HM diminishes since the Boltzmann weights become weakly dependent of U . $R_H^{(0)}$ is then simply given by the high temperature limit of the non-interacting SL, i.e.,

$$\begin{aligned} \chi_{\text{csr}}^{\text{HM}} &\sim \beta e^2 t^2 n(2-n) \quad , \quad \chi_{\text{cmc}}^{\text{HM}} \sim \beta^2 \frac{e^3}{c} t^4 n(2-n)(1-n) \quad , \\ R_H^{(0)} &= \frac{2(1-n)}{n(2-n)ec} + O(\beta U)^2 \simeq R_H^{\text{SL}} \quad , \end{aligned} \quad (248)$$

where $n = 1 - x$ is the electron density.

Interestingly, at lower temperatures, which lie within the applicability of the tJM, the recovery of the $U \approx 0$ behavior at high temperatures is heralded by the effects of H^J in the tJM (240). H^J become important in the CMC susceptibility, by adding to the currents and magnetizations next neighbor hopping terms,

$$\begin{aligned} j_{ijk}^\alpha &= -ieJ(1-n_j^h) \left(K_{jk;\alpha}^- - 2\Sigma_{ik;\alpha}^- \cdot \mathbf{s}_j \right) \\ M' &= \frac{1}{2c} \sum_{(ij)\langle jk \rangle} (x_i j_{ijk}^y - y_i j_{ijk}^x) \quad . \end{aligned} \quad (249)$$

Since $J \ll t$, these terms are unimportant for the CSR. However, for the CMC they contribute one less power of βH than those χ'_{cmc} , since they encircle a magnetic flux with one less Hamiltonian bond. Hence they become dominant at temperatures of order $T \simeq U$,

$$\chi'_{\text{cmc}} = \frac{\beta J e^3}{2} x(1-x)(1+2x-3x^2) \quad . \quad (250)$$

We note that χ'_{cmc} has the opposite sign to χ'_{cmc} , and H^J yields the contribution to $R_{\text{H}}^{(0)}$ of,

$$\Delta R_{\text{H}}' = \frac{4T}{ecU} \left(\frac{1+2x-3x^2}{8x(1-x)} \right) \quad . \quad (251)$$

Therefore, as $x \rightarrow 0$ and $T \rightarrow U$, $\Delta R_{\text{H}}'$ reduces the positive Hall coefficient divergence, and the doping levels of the Hall sign reversal. Its effect is observed in the upper blueish regions of Fig. 1.

31.3. Hall coefficient corrections

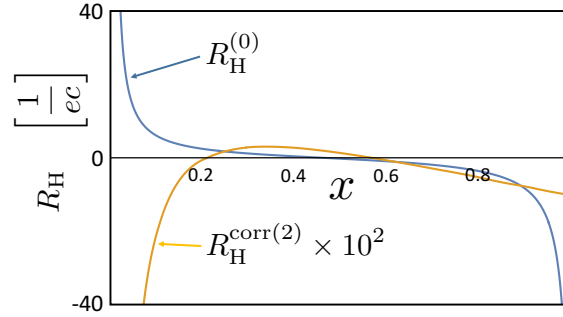


Figure 18: Comparison of the the leading order high temperature Hall coefficient of t -model, defined in Eq. (247) (blue line), with its second order correction term (orange line, multiplied by 100 for visibility) defined in Eq. (252). The ratio of magnitudes vanishes at $x \rightarrow 1$, and approaches 0.06 at $x \rightarrow 0$.

We calculate the correction term up to second order

$$R_{\text{H}}^{\text{corr}(2)} = \frac{1}{\chi_{\text{csr}}} \left(\left(\frac{\Delta_1}{\Delta_2} \right)^2 \mathcal{M}_{2,2} - \left(\frac{\Delta_1}{\Delta_2} \right) (\mathcal{M}_{2,0} + \mathcal{M}_{0,2}) \right) \quad . \quad (252)$$

The three hypermagnetization matrix elements $\mathcal{M}_{0,2}$, $\mathcal{M}_{2,0}$, $\mathcal{M}_{2,2}$ were evaluated numerically. Each application of the Liouvillian or the hypermagnetization can create a new hyperstate by multiplying the individual site operators site-by-site using a multiplication table. The calculation of $\mathcal{M}'_{2,2}$ to leading order in (βt) involved traces over up to 10^5 operator clusters.

In Fig. 18, we plot the final result for $R_{\text{H}}^{\text{corr}(2)}$ for all doping concentrations. We see that in comparison $R_{\text{H}}^{(0)}$, its quantitative effect is negligible, and maximized toward $x \rightarrow 0$ by

$$\lim_{x \rightarrow 0} |R_{\text{H}}^{\text{corr}(2)} / R_{\text{H}}^{(0)}| \rightarrow 6\% \quad . \quad (253)$$

Based on the high temperature ($\mathcal{O}(\beta t)^0$) in Eq. (253), and the weak temperature dependence found for $R_{\text{H}}^{(0)}$ shown in Fig. 17, we may assume that the correction term remains negligible throughout the IT regime. We note that we have not calculated $R_{\text{H}}^{\text{corr}}$ for the HM at $T \geq U$.

32. Discussion

Sign reversal of the Hall coefficient at low doping has been previously obtained by dynamical mean field theory (DMFT) [78, 79], QMC [80, 81] and determinant QMC [82]. These methods have found evidence of hole pockets in the momentum dependent occupation, which is qualitatively consistent with our results at low doping. Refs. [83, 84, 85] calculate (within DMFT) the Hall conductivity of the Hubbard model at strong magnetic fields. They found that the Hall sign is reversed relative to band theory, near half filling. These effects were attributed to the Chern numbers of the non-interacting Hofstadter's butterfly bands of the square lattice. It is interesting that these sign changes which were predicted at strong fields, (as measured in strongly correlated flat bands Moiré systems [86]), are qualitatively similar to the Hall sign we obtain in the weak field limit.

Here however, we find that the sign reversal occurs already at $x \leq 0.45$, which may come as a surprise vis-a-vis the widely used band theoretical approaches at much lower doping. The reason is simply related to the spin and charge entangled commutation relations of GP current operators of the tJM,

$$[K_{12}^-, K_{23}^-] = K_{13}^- \left(\frac{1 + n_2^h}{2} \right) + \Sigma_{13}^- \cdot \mathbf{s}_2 (1 - n_2^h) \quad , \quad (254)$$

which affects the hole density dependence of the CMC, and determines the doping concentration of the sign reversal. Since the hole density operators have coefficients of order unity, it is natural that the sign change occurs at a fraction with a denominator not much larger than unity. The important lesson we can learn from this is that the effects of GP reach far into the high doping and temperature regimes.

Previous QMC calculations of $R_H^{(0)}$ for the HM [80, 87] have used our Eq. (216), and neglected R_H^{corr} . They have also reported a positive Hall sign near half filling (but no apparent divergence) for the square lattice model. However in the regime of $U/t \simeq 16$, $R^{\text{corr}} \propto \|[H, j^x]\| \sim U/t$, is expected to dominate over $R_H^{(0)}$, and hence cannot be ignored.

The difference between $R_H^{(0)}$ (HM) [87] and $R_H^{(0)}$ (tJM) of Eq. (247), can be explained by the fact that $R^{\text{corr}}(\text{tJM}) \ll R^{\text{corr}}(\text{HM})$ in the IT regime.

We can compare $R_H^{(0)}$ of Eq. (247) to the infinite frequency Hall coefficient of the t-model calculated at leading order in β by Shastry, Shriman and Singh [88],

$$R_H^* = \frac{d}{dB} \lim_{\beta \rightarrow 0, \omega \rightarrow \infty} \rho_{xy}(\omega) = \frac{1}{e c} \left(-\frac{1}{4x} + \frac{1}{1-x} - \frac{3}{4} \right) \quad . \quad (255)$$

R_H^* changes sign at $x = 1/3$ and diverges as $1/(4x)$ toward the Mott limit. While Eq. (247) changes sign at $x = 0.4415$ and diverges as $5/(8x)$ at small x . Still, the qualitative similarity we find between the infinite and zero frequencies is surprising, but we cannot infer any general relations from this coincidence. We note that R_H^* may be relevant to the optical Kerr effect [89].

In summary, the calculation of the DC Hall coefficient as a function of hole doping in the IT regime appears to be well controlled. We can learn from it that the Mott insulator phase affects the charge carriers in the nearby metallic phase. This has theoretical implication to any possible ordered phases at lower temperatures, such as superconductivity and/or other orders [3, 23, 24, 90]. The superconducting order parameter should consist of GP holes, with spin entangled commutation relations (254), rather than quasiparticles near the non-interacting Fermi surface. The GP also governs the relation between superfluid stiffness (which is bounded by the CSR), and the electron density [91]. It affects the moving vortex charge and the Hall sign in the flux flow regime [92, 93].

Part VIII

Strongly Correlated Bosons

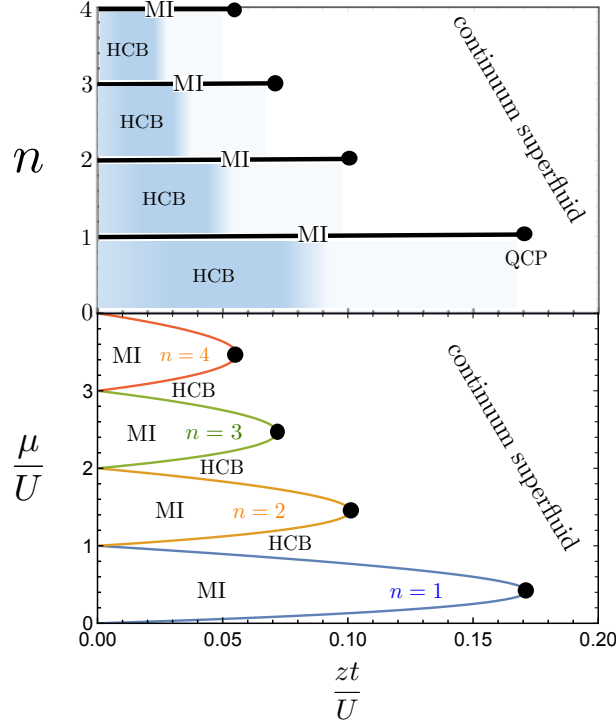


Figure 19: $T = 0$ phase diagram of the Bose Hubbard Model, Eq. (256). At weak interactions $U/zt \rightarrow 0$, the lattice periodicity is unimportant, and the bosons condense into a continuum superfluid ground whose excitations are governed by the Gross-Pitaevskii field theory (257). The quantum critical points (marked by black disks), denote second order transitions into gapped Mott insulators of integer fillings n . Sandwiched between the Mott insulator phases, at fractional average densities, the Hamiltonian renormalizes into Hard Core Bosons (HCB) model Eq. (271), whose boson occupations are constrained to fluctuate between two consecutive integers.

33. The Bose Hubbard model

The Bose Hubbard model (BHM) is a minimal model of interacting lattice bosons,

$$H^{\text{BHM}} = -t \sum_{\langle ij \rangle} (e^{-iqA_{ij}/c} a_i^\dagger a_j + e^{iqA_{ij}/c} a_j^\dagger a_i) + U \sum_i n_i^2 - \mu \sum_i n_i \quad . \quad (256)$$

t is the hopping rate and U is the local repulsive interaction, q is the boson charge, and c is the speed of light. The lattice constant is unity. a_i^\dagger creates a boson on lattice site i , and $n = a_i^\dagger a_i$ is the boson occupation. $A_{ij} = \int_{\mathbf{x}_i}^{\mathbf{x}_j} d\mathbf{x} \cdot \mathbf{A}$, where \mathbf{A} is the electromagnetic vector potential.

H^{BHM} can be realized by cold bosonic atoms trapped in an optical lattice, where \mathbf{A} can be implemented by light induced artificial gauge fields [94].

The BHM also describe a Josephson junction array where the BCS pairing gap in each grain is larger than the Josephson coupling t . U would be the inverse capacitance of each grain.

The BHM has a well known phase diagram [95] which is shown in Fig. 19.

33.1. Weak interactions

We note that for weak interactions, $t/U \rightarrow \infty$, the bosons condense into the $\mathbf{k} \simeq 0$ eigenstates with effective dispersion $\omega_{\mathbf{k}} \simeq \frac{\hbar^2 \mathbf{k}^2}{2m^*}$. The low energy theory is therefore effectively a Galilean symmetric continuum theory described by the Gross-Pitaevskii (GP) action [96],

$$S^{\text{GP}} = \int dt d^d x \left(i\psi^* \dot{\psi} - \frac{1}{2m^*} |\nabla - i\frac{q}{c} \mathbf{A}\psi|^2 + U|\psi|^4 - \mu|\psi|^2 \right) , \quad (257)$$

where $\psi(\mathbf{x}_i)$ is a complex coherent-state field which represents the lattice boson operator a_i . For dimension $d > 2$, S^{GP} describes a superconductor at low temperatures, and a charged bosons gas above a finite transition temperature. In the presence of impurities, the metallic conductivity tensor is described by Drude theory Eq. (6) with scattering rate which vanishes with impurity concentration. Therefore by (7), the Hall coefficient is equal to the Galilean symmetric result,

$$R_{\text{H}}^{\text{GP}} = \frac{1}{nqc} , \quad (258)$$

where n is the boson density. No Hall sign change is expected as a function of density or temperature in the weak interactions regime.

33.2. Strong interaction

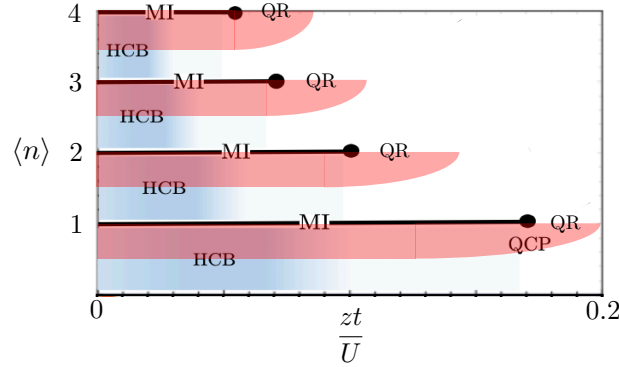


Figure 20: Hall signs (for $q > 0$) for the BHM phase diagram as calculated by the ground state Chern number Eq. (70) [97, 98]. Red regions are negative, and blue and white regions are positive. QR and HCB regions denote the effective strong interaction models (261) and (271) respectively. The BHM ground state Chern number sign agrees with that of R_{H} at high temperatures.

Fig. 20 depicts the BHM ground state Chern number (Eq. (70)) as calculated by Huber and Lindner [97] in the strong interaction regime. We note the red regions of Hall sign reversal at strong interactions. While at zero temperature the ground state is a gapless superfluid with zero Hall resistivity, and the Chern calculation should not apply (see Section 13). Nevertheless, we find that the Hall sign agrees with the Hall coefficient sign in the corresponding metallic phases at higher temperature, as described below.

For strong interactions, $t/U < 1$ there are Mott insulator lobes in which the boson filling is locked into an integer $\langle n_i \rangle = m = 0, 1, 2, \dots$. The mean field boundaries $\mu_{\text{cr}}(U, m)$ for the Mott lobe m , is given by the implicit equation [99],

$$zt \left(\frac{m+1}{Um - \mu} - \frac{m+1}{Um - \mu} \right) = 1 , \quad (259)$$

which also determines the location of the Quantum Critical Points (QCP) $(\mu_{\text{cr}}(m), U_{\text{cr}}(m))$, by the equation $\left(\frac{\partial \mu}{\partial U} \right)^{-1} = 0$.

Near the QCP at density \bar{n} , the BHM maps onto an O(2) quantum field theory [100], described by a complex field $\psi(\mathbf{x}_i) \propto \langle b_i \rangle$. In a dimensionless scaled form [101] the O(2) action is,

$$S^{O(2)} = \frac{1}{g} \int \int d^{d+1}x \sum_{\mu=1, d+1} |(\partial_\mu - i\frac{q}{c}A_\mu)\psi|^2 + \frac{m_0}{8} (|\psi|^2 - 2)^2 \quad . \quad (260)$$

x_{d+1} is the imaginary time coordinate, $A_{d+1} = c\mu/q$. The coupling constant $g \propto U/t$ determines ground state. In $d \geq 2$, $g < g_c$, the field theory describes a superconductor, and for $g > g_c$ it is a Mott insulator. g_c is the QCP. m_0 is the bare Higgs (amplitude mode) mass. The low energy Higgs mass and the superfluid stiffness vanish at the QCP.

In order to obtain operator expression for the currents and magnetization, which are necessary for the CMC and CSR susceptibilities, the BHM near the QCP can be renormalized onto an effective Quantum Rotators (QR) Hamiltonian [99],

$$H^{\text{QR}} = \sum_i \frac{q^2}{2C} (n_i - \chi_c \mu)^2 - J^{\text{eff}} (n_i - \bar{n}) \sum_{\langle ij \rangle} \cos(\phi_i - \phi_j - \frac{q}{c}A_{ij}) \quad , \quad (261)$$

where

$$[n_i, \phi_j] = -i\delta_{ij} \quad . \quad (262)$$

H^{QR} physically describes a Josephson junction array, whose grain capacitance and Josephson couplings are related to the BHM parameters,

$$C \simeq \frac{1}{U} \\ J^{\text{eff}} \simeq 2dt \quad . \quad (263)$$

Near the QCP, J^{eff} is renormalized down to the low energy superfluid stiffness ρ_s , as given by the CSR,

$$\chi_{\text{csr}} = q^2 (j^x | j^x) = q^2 \rho_s(\bar{n}) \quad . \quad (264)$$

ρ_s vanishes at the QCP as $(g_c - g)^\nu$, where ν is the $d+1$ dimensional correlation length exponent of the O(2) model [17]. ρ_s also depends on the electron density n . Expanding the density fluctuations about the integer Mott density \bar{n} in the path integral, we obtain the operator,

$$\rho_s[n_i] = \rho_s(\bar{n}) + \sum_i \frac{d\rho_s(\bar{n})}{d\bar{n}} (n_i - \bar{n}) \quad . \quad (265)$$

Thus, the renormalized current and magnetization operators involve both phase and density operators

$$j^\alpha(\mathbf{x}_i) = \frac{q \sum_i \rho_s[n_i] \nabla^\alpha \phi(\mathbf{x}_i) + \text{h.c.}}{2} \\ m(\mathbf{x}_i) = \frac{\frac{q}{2c} \rho_s[n_i] (x_i j^y - y_i j^x) + \text{h.c.}}{2} \quad . \quad (266)$$

The CMC can be calculated using the canonical commutations in Eq. (262):

$$\chi_{\text{cmc}} = \frac{2}{\mathcal{V}} (j^y, [M^z, j^x]) = \frac{q}{\mathcal{V}} \left(j^y, x \partial_x \left(\frac{d\rho_s}{dn} \right) j^y \right) = \frac{q^3}{c} \rho_s \frac{d\rho_s}{d\bar{n}} \quad , \quad (267)$$

which according to Eq. (289):

$$R_{\text{H}}^{(0)} = \frac{\chi_{\text{cmc}}}{\chi_{\text{csr}}^2} = \frac{1}{qc} \frac{d \log \rho_s}{d\bar{n}} \quad , \quad (268)$$

which qualitatively agrees with similar expressions found for the reactive Hall constant near a Mott insulator [102], and for the Hall coefficient of a two leg Luttinger-liquid [103]. R^{corr} may be assumed to be small near the QCP since it depends on current relaxation which scales with the ratio of lattice constant to the longer correlation length.

Since the Mott densities \bar{n} minimize $\rho_s[\bar{n}]$, The Hall coefficient vanishes at extrema of $\rho_s(n)$. Near the QCP, R_{H}/q changes from negative to positive at the Mott density $\bar{n} = 1, 2, \dots$, since the superfluid stiffness vanishes at the QCP. The switch from $R_{\text{H}}/q > 0$ (given by Eq. (258) at low densities) to $R_{\text{H}}/q < 0$ is expected around midpoint between two Mott lobes. This behavior is captured by the Hard Core Bosons model below.

34. Hard Core Bosons on the square lattice

Between consecutive Mott lobes, at temperatures below $T \ll |\mu_{\text{cr}}(n) - \mu_{\text{cr}}(n+1)|$, there is a superfluid phase with constrained density fluctuations.

These fluctuations can be described by the renormalizing the BHM onto the projected space between two Mott lobes, $n_i \in (m, m+1)$. The projected charge fluctuations are described hard core bosons (HCB) operators,

$$\begin{aligned} \tilde{a}_i, \tilde{a}_i^\dagger, \quad (\tilde{a})^2 = (\tilde{a}^\dagger)^2 = 0, \\ 0 \leq \tilde{n}_i \leq 1. \end{aligned} \quad (269)$$

These operators are faithfully represented by SU(2) spin-half operators,

$$\tilde{a}_i^\dagger \rightarrow S_i^+, \quad \tilde{n}_i - \frac{1}{2} \rightarrow S_i^z, \quad \mathbf{S}^2 = \frac{3}{4}. \quad (270)$$

which can be used to represent the HCB hamiltonian by the gauged quantum XY model of spin half,

$$H^{\text{HCB}} = -t \left(\sum_{\langle ij \rangle} e^{-i\frac{q}{c}A_{ij}} S_i^+ S_j^- + h.c. \right) - \mu \sum_i S_i^z, \quad (271)$$

where μ, t , which depend on $U/t, m$ are renormalized from the corresponding BHM values. The HCB charge polarizations, currents and magnetization operators are respectively represented by,

$$\begin{aligned} \mathbf{P} &= q \sum_i \mathbf{x}_i S_i^z, \quad \mathbf{j} = i[H, \mathbf{P}] = \sum_{\langle ij \rangle} \mathbf{j}_{ij}, \\ j_{ij}^\alpha &= -iqt(S_i^+ S_j^- - S_i^- S_j^+)(x_j^\alpha - x_i^\alpha), \\ M &= \frac{1}{4c} \sum_{\langle ij \rangle} (\mathbf{x}_i + \mathbf{x}_j) \times \mathbf{j}_{ij}. \end{aligned} \quad (272)$$

Here \mathbf{r}_i denotes the position of site i . For the square lattice, the density dependent BKT transition temperature for HCB on the square lattice has been evaluated by QMC: [104, 105, 106]

$$T_{\text{BKT}}(n) \simeq 2.8tn(1-n). \quad (273)$$

34.1. Superconducting phase

HCB on the square lattice exhibit long range superfluid order below the Berezinskii, Kosterlitz and Thouless [107, 108] transition (BKT) transition temperature $T - \text{BKT}$. At $T \geq 0$ the two dimensional superfluid stiffness ρ_s in the classical (large S approximation) is,

$$\rho_s \equiv q^{-2} \frac{d^2 F^{\text{cl}}(T, n)}{(dA_x)^2} \Big|_{A=0} > 0, \quad (274)$$

which yields a maximum at half filling,

$$\rho_s^{\text{cl}}(0, n) = 2tn(1-n). \quad (275)$$

Quantum corrections to $\rho_s^{\text{cl}}(0, \frac{1}{2})$ enhance it by about 7% [109, 110].

The zero temperature AC longitudinal conductivity at half filling $n = \frac{1}{2}$, is evaluated by computing the conductivity moments μ_0, \dots, μ_{12} in Eq. (148) by ED. The resulting 6 recurrences $\Delta_1, \dots, \Delta_6$ are depicted in Fig. 21(a). The large odd > even oscillations of the recurrences indicates that the conductivity is suppressed at low frequencies. In fact, the continuous form of $\sigma_{xx}(\omega)$, shown in Fig. 21(a), exhibits a threshold at around $\omega = 5t$. This threshold behavior is supported by an ED calculation for the Kubo formula on a 4×4 lattice.

$$\sigma_{xx}(A, \varepsilon) = \frac{1}{A} \sum_{n>0} |\langle \Psi_0 | j^x | \Psi_n \rangle|^2 \frac{\varepsilon}{(E_n - E_0 - \omega)^2 + \varepsilon^2}. \quad (276)$$

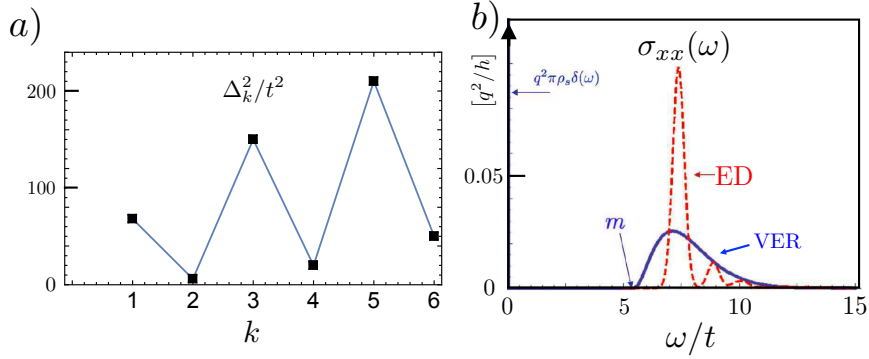


Figure 21: Dynamical conductivity $\sigma_{xx}(\omega)$ of HCB in the superfluid phase. a) 6 ground state recurrences, computed by ED on 4×4 lattice. Even-Odd alternation of the recurrences indicates a strong suppression of σ_{xx} at low frequencies. b) ρ_s is the zero temperature superconducting stiffness. Blue line: Conductivity by continued fraction extrapolation by Variation extrapolation of recurrences. Red line: Exact Diagonalization calculation of Kubo formula. The apparent threshold energy m is interpreted as Higgs-amplitude mode's mass.

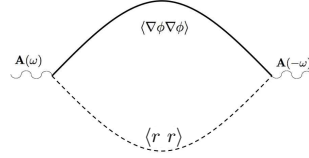


Figure 22: Dynamical conductivity of the Relativistic Gross Pitaevskii model Eq. (277), at zero temperature in the superconducting phase at weak coupling. r is the amplitude/Higgs mode with mass m , and ϕ the massless Goldstone mode. The conductivity exhibits a threshold at $\omega = m$ as shown in Eq. (279).

We note that this threshold feature is not expected by BCS theory in a single band, weak coupling superconductor without disorder. By Mattis and Bardeen [111], such a threshold would appear at 2Δ , where Δ is the pairing gap only if there is sufficient disorder. For HCB model (271) $\Delta = \infty$, and there is no disorder!

This threshold was argued to be the Higgs-amplitude mode of the particle-hole symmetric Relativistic Gross-Pitaevskii (RGP) theory [17, 101] with Euclidean action,

$$S^{\text{RGP}} = \frac{1}{2g} \int_{\Lambda} d^{2+1}x \left[\left| (\nabla - i\frac{q}{c}\mathbf{A})\vec{\Phi} \right|^2 + \frac{m_0^2}{4} (|\vec{\Phi}|^2 - 1)^2 \right]. \quad (277)$$

Here, $\vec{\Phi}$ is the two component rotator field, defined at wavevectors below the cut-off Λ . The imaginary time component is $x_3 = c\tau$, where $c = \sqrt{\rho_s/\chi}$, $\rho_s \sim t$ is the microscopic stiffness, and $\chi \sim \frac{1}{t}$ is the local compressibility. g is the quantum parameter, which drives a quantum phase transition [99] into a bosonic Mott insulator as it grows toward $g \rightarrow g_c$.

At weak coupling and zero temperature, $\vec{\Phi}(\mathbf{x}) = \vec{\Phi}_0$, and the conductivity is evaluated by fluctuations of the amplitude r and phase ϕ ,

$$\vec{\Phi} = \Phi_0(1+r)\hat{\mathbf{r}} + \phi\hat{\mathbf{z}} \times \hat{\mathbf{r}}. \quad (278)$$

At lowest order in g^0 , the bubble diagram in Fig. 22 yields a threshold AC conductivity given by [101],

$$\sigma_{xx}^{\text{RGP}}(\omega) \sim \omega^5 \Theta(\omega^2 - m^2), \quad (279)$$

where m is the mass-gap of the amplitude field r . $m(g) \sim |g - g_c|^\nu$ is the analogue of the Higgs particle mass, which vanishes at the critical point with the three dimensional XY model's correlation length exponent $\nu \simeq 0.671$.

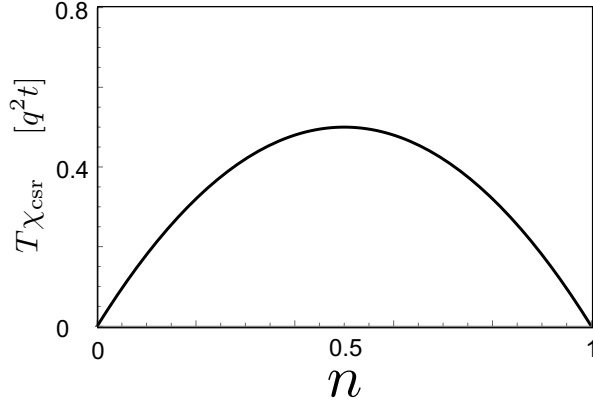


Figure 23: CSR of HCB at order, $O(\beta)$, as give by Eq. (280).

34.2. Metallic phase: longitudinal conductivity

The longitudinal conductivity is evaluated for the metallic phase of H^{HCB} on the square lattice, at $T > T_{\text{BKT}}$. The CF expansion is extrapolated following the Variational Extrapolation of Recurrents described in subsection 23.5.

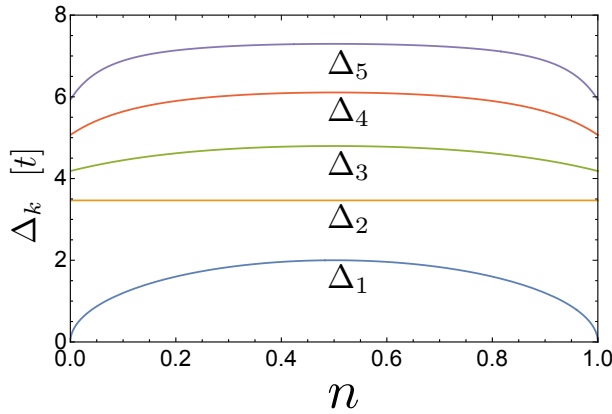


Figure 24: Density dependence of the five lowest recurrents. The cancellation of the density dependence of $\Delta_1(n)$ and $\chi_{\text{csr}}(n)$ leads to the weak density dependence of the linear resistivity slopes.

The leading orders CSR is,

$$\chi_{\text{csr}} = 2q^2\beta t^2 n(1-n) + O(\beta t)^3 \quad . \quad (280)$$

$\mu_{2k}, k = 0, \dots, 5$ were also evaluated to leading order in βt , which yields recurrents of order $O(\beta^0)$. In Fig. 24, the recurrents are plotted for densities $0 < n < 1$.

According to (177) and Fig. 7, the termination function appears to be well fit by the stretched exponential form i.e.

$$\begin{aligned} \tilde{G}_{00}''(\omega, \alpha) &= N_\alpha \exp\left(-\left|\frac{\omega}{\Omega_\alpha}\right|^\alpha\right) \quad , \\ \tilde{G}_{00}'(\omega, \alpha) &= \frac{1}{\pi} \text{PV} \int_{-\infty}^{\infty} d\omega' \frac{\tilde{G}_{00}''(\omega', \alpha)}{\omega - \omega'} \quad , \end{aligned} \quad (281)$$

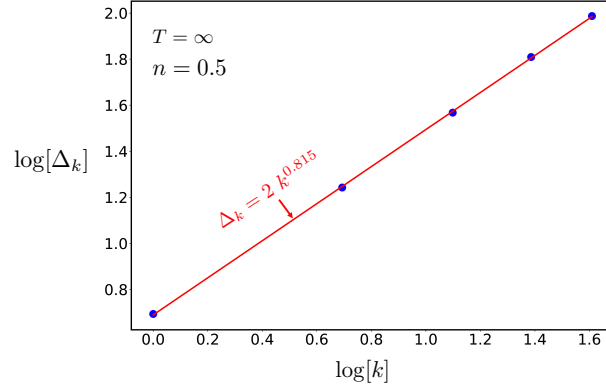


Figure 25: Order dependence of HCB recurrences (in units of t) at half filling, and infinite temperature

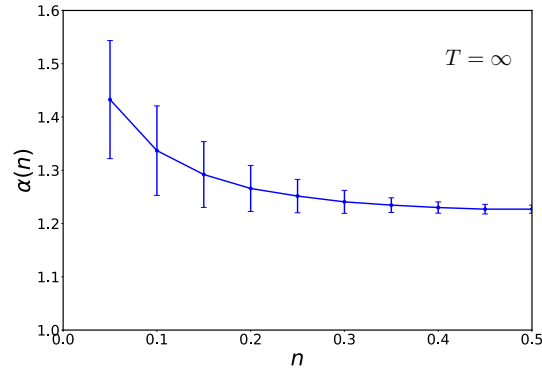


Figure 26: The fit exponent α as a function of HCB filling n , which determines the termination function $G_2^>$ of the AC conductivity. Error bars describe the mean square deviations for the power law fits of $\Delta_k \sim k^\alpha$, $k = 2, \dots, 5$.

where the normalization

$$N_\alpha = \frac{\pi\alpha}{2\Omega_\alpha \Gamma\left(\frac{1}{\alpha}\right)} \quad (282)$$

ensures that $\int d\omega \bar{G}_{00}''(\omega, \alpha) = \pi$.

The $S^z \rightarrow -S^z$ symmetry of the HCB hamiltonian leads to $\sigma_{xx}(n) = \sigma_{xx}(1-n)$. For $n \neq 0.5$, Δ_1 is an outlier of the power law line, since it vanishes as $n \rightarrow 0, 1$. The higher recurrences are fit by

$$\bar{\Delta}_k = \Omega_\alpha a_\alpha k^{\alpha(n)} \quad , \quad k = 2, \dots \quad (283)$$

where $\alpha(n)$ is obtained by least square fit in Fig. 26. The error bars increase away from half filling. We find that fluctuations of the recurrences about Eq. (283) induces large uncertainty in the extrapolated $\sigma_{xx}(\omega)$. Hence the use of Eq. (283) to the regime $0.35 \leq n \leq 0.5$.

The high temperature dynamical conductivities are plotted in Fig. 27. Since the first two recurrences are,

$$\Delta_1^2 = 16n(1-n)t^2 \quad , \quad \Delta_2^2 = 12t^2 \quad . \quad (284)$$

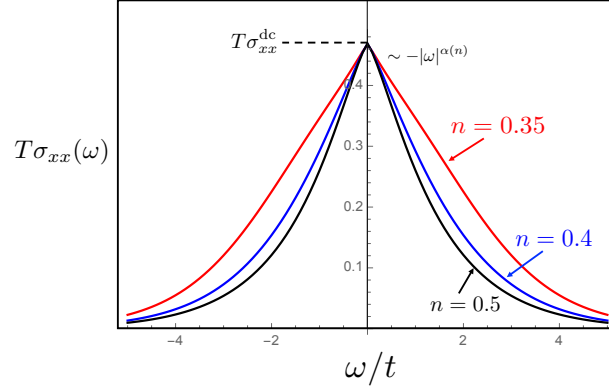


Figure 27: HCB dynamical conductivity at high temperatures. The DC value of $T\sigma_{xx}(0)$ is independent of boson density n , while the width of the conductivity increases away from half filling. The singularity at zero frequency depends on α as determined by Fig. 26.

The conductivity is proportional to the density independent ratio,

$$\sigma_{xx} \propto \frac{\chi_{\text{csr}}(n)\Delta_2}{\Delta_1^2(n)} . \quad (285)$$

Eq. (285) is interpreted as the ratio of kinetic energy ($\chi_{\text{csr}}(n)$) to scattering rate ($\Delta_1^2(n)/\Delta_2$), which have a similar density dependence. Hence, since α changes very little ($\sim 1\%$ in the range $n \in (0.35, 0.5)$), the linear resistivity slope in this regime is very weakly density dependent, and given by

$$R_{xx}^{\text{dc}} \simeq 0.33 \frac{T}{t} R_Q \quad , \quad R_Q \equiv \frac{h}{q^2} . \quad (286)$$

The CF extrapolation also yields a singular frequency dependence at low frequencies, as shown in Fig. (27),

$$\frac{\sigma_{xx}(\omega) - \sigma_{xx}^{\text{dc}}}{\sigma_{xx}^{\text{dc}}} \sim - \left| \frac{\omega}{\Omega_\alpha} \right|^\alpha . \quad (287)$$

The sharp zero frequency cusp is consistent with Mukerjee, Oganessian, and Huse [112], (MOH) who found a similar singularity in the high temperature conductivity of a one dimensional non-integrable fermion model, and predicted similar behavior in higher dimensional models.

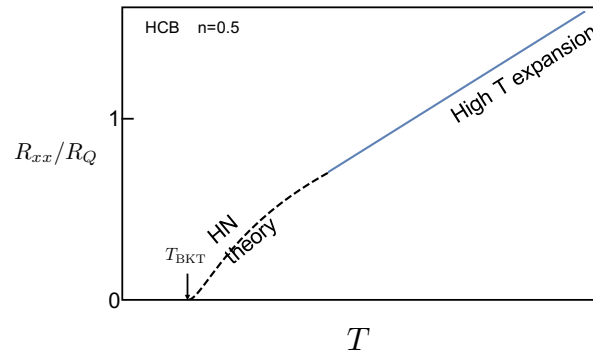


Figure 28: Resistivity versus temperature of HCB at half filling. The high temperature linear slope of Eq. (286) (solid line) is matched toward the superconducting transition temperature $T - \text{BKT}$ using Halperin and Nelson's (HN) free vortices theory, Eq. (288) (Dashed line).

The high temperature linear temperature slope of the HCB resistivity can be connected to the superconducting transition at $T_{\text{BKT}} \approx 0.7t$. Halperin and Nelson (HN) [113] described the superconducting fluctuation region just T_{BKT} , where the resistivity rises as

$$\begin{aligned} R_{\alpha\beta}^{\text{HN}} &\simeq 2.7R_{\alpha\beta}^n(T) \left(\frac{\xi_+}{\xi_c} \right)^{-2} \\ &= 2.7R_{\alpha\beta}^n(T) \exp \left(-2b \left(\frac{T_{\text{BKT}}}{T - T_{\text{BKT}}} \right)^{\frac{1}{2}} \right) . \end{aligned} \quad (288)$$

ξ_+ is the BKT correlation length, and ξ_c is of the order of the HCB lattice constant and $b \approx 1$. For the HCB model, the “normal state” resistivity $R_{xx}^n(T)$ is obtained from our Eq. (286). We use these values to plot the crossovers from HN theory Eq. (288) to higher temperatures as dashed lines in Fig. 28.

34.3. Metallic phase: Hall coefficient

The zeroth term,

$$R_{\text{H}}^{(0)} = \frac{\chi_{\text{cmc}}}{\chi_{\text{csr}}^2} . \quad (289)$$

is calculated by the high temperature expansions of the CSR, Eq. (280) and the CMC susceptibility. The leading order in β is,

$$\begin{aligned} \chi_{\text{cmc}} &= \frac{2}{c} q^3 t^2 \text{Tr} \left(\rho(\beta, n) (S_1^+ S_3^- + S_1^- S_3^+) S_2^z \right) \\ &= \frac{1}{c} \beta^2 q^3 t^4 (1 - 2n)(1 - (2n - 1)^2) . \end{aligned} \quad (290)$$

One observes that χ_{csr} (χ_{cmc}) is “particle-hole” symmetric (antisymmetric) under $n \rightarrow 1 - n$. Thus we obtain,

$$R_{\text{H}}^{(0)} = \frac{1}{qc} \left(\frac{2n - 1}{n(n - 1)} + \frac{2}{3} (\beta t)^2 \left(n - \frac{1}{2} \right) \right) . \quad (291)$$

Notably at low density, the Hall coefficient recovers the continuum Galilean invariant result $R_{\text{H}}^{(0)} \rightarrow (nqc)^{-1}$. Near half-filling, $R_{\text{H}} \sim -8(n - \frac{1}{2})/(qc)$, reflecting the effects of lattice Umklapp and hard core scattering.

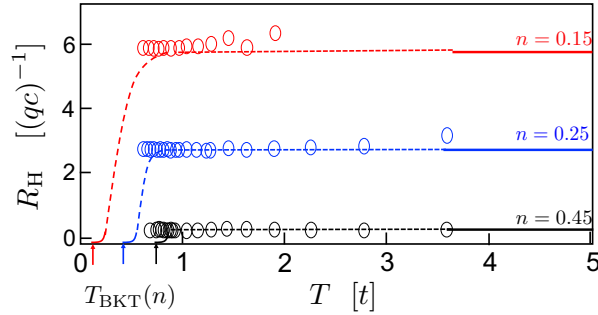


Figure 29: Metallic Hall resistivity of HCB. High temperature asymptotes $R_{\text{H}}^{(0)}$ of Eq. (291) (solid lines), and lower temperature extension by QMC calculations (circles). Dashed lines interpolate between $R_{\text{H}}^{(0)}(T)$ and HN theory near $T_{\text{BKT}}(n)$.

Eq. (291) was extended to lower temperatures numerically [114] by a path-integral based QMC for bosonic lattice models which are devoid of a sign problem. For this purpose, the DSQSS package [115], which employs a path-integral based Monte Carlo scheme for bosons was employed, with a Directed Loop Algorithm (DLA) [116]. In Fig. 29, the solid lines are the analytical results of Eq. (291), while the QMC data are depicted by open circles. We see that the Hall coefficients above the HN regime, rapidly saturate to their high temperature limit.

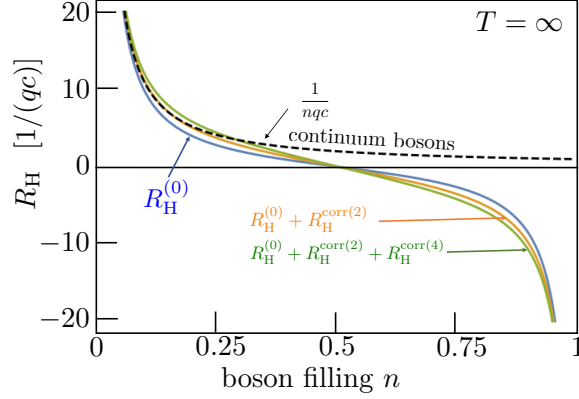


Figure 30: Density dependent Hall coefficient $R_H(n)$ of HCB on a square lattice at high temperature. $R_H^{(0)}$, R_H^{corr} are defined in Eqs. (289) and (292). Convergence up to fourth order corrections is shown by the yellow and green curves. The Hall sign change at half filling is a consequence of the the hard core interactions on the lattice.

34.4. Hall coefficient corrections

In general, R^{corr} can be a cumbersome calculation. The relative simplicity of the HCB Hamiltonian permits a feasible computation of R^{corr} up to fourth Krylov order. The calculated correction [114] is the truncated sum,

$$\begin{aligned}
 R_H^{\text{corr}(4)} &= \frac{1}{\chi_{\text{csr}}} \sum_{i,j=0}^4 R_i R_j (1 - \delta_{i,0} \delta_{j,0}) \mathcal{M}_{2i,2j} \\
 \mathcal{M}_{2i,2j} &= \text{Im} \left(\langle 2i; y | \mathcal{M} | 2j; x \rangle - \langle 2i; x | \mathcal{M} | 2j; y \rangle \right) \quad , \\
 R_{i>1} &= \prod_{r=1}^i \left(-\frac{\Delta_{2r-1}}{\Delta_{2r}} \right) \quad , \quad R_0 = 1 \quad . \quad (292)
 \end{aligned}$$

The hypermagnetization matrix elements $\mathcal{M}_{2i,2j}$ are calculated as described in Section 28. The fourth order matrix element \mathcal{M}_{44} involved traces over up to $\sim 10^7$ operator products. The corrected density dependent high temperature Hall coefficient is depicted in Fig. 30.

We see that these corrections do not qualitatively change the zeroth term's behavior especially near the densities $n = 0, 1, \frac{1}{2}$, although they converge slower around intermediate densities $n = 0.25, 0.75$. Since the Hall coefficient is finite for any metal, the summation over higher order corrections must converge. Thus, $R_H^{(0)}$ appears to be qualitatively correct at high temperatures. At lower temperatures $R_H^{(0)}$, as evaluated by QMC in Fig. 29, appears to be blind to the onset of long range superconducting phase correlations and vortices, as described by HN theory. Therefore toward $T \rightarrow T_{\text{BKT}}$, the correction term is expected to grow relative to $R_H^{(0)}$ and cancel it completely at T_{BKT} .

35. Discussion

From the calculations shown above, one concludes that near half filling, the 'weakly interacting continuum bosons' description fails for HCB. The quantum mechanical effects of lattice periodicity and constraints of no-double occupancies play a crucial role in the transport coefficients.

We note that metallic phases of HCB and the tJM electrons [117] share their proximity to Mott insulators. As shown in Part VII, the Hall sign of the tJM also diverges toward the Mott phase, and reverses its sign relative to that predicted by models of weak interactions.

Part IX

Summary and Future Directions

This report reviews recent theoretical advances in quantum transport theory with particular emphasis on application to strongly interacting, gapless phases of matter. The DPP formulas for DC Hall-type conductivities can reduce the computational cost of Kubo formulas in the Lehmann representation. They also help clarify conceptual dilemmas about the role of gapless eigenstates in carrying the Hall currents on OBC, and the ultimate irrelevancy of the magnetization subtractions in thermal Hall conductivities. The DPP formulas generalize the Berry curvature expressions derived in Section 17, for clean non interacting models. This may help us understand the interplay between Berry curvatures and effects of boundaries and disorder [53] within the Kubo formula framework, without appealing to semiclassical approximations.

A significant fraction of this report is devoted to thermodynamic approaches which include continued fractions for AC conductivities, and thermodynamic summation formulas for the electric, thermoelectric and thermal Hall coefficients. These approaches converge better by first renormalizing the Hamiltonian down to the temperature scale of interest, and calculating conductivities which do not consist of separable contributions.

As examples, continued fractions and Hall coefficient summation formulas are applied to basic models of interacting lattice fermions and bosons: the Hubbard, t-J, and HCB Hamiltonians. Conductivities of strongly interacting models are contrasted with their weakly interacting limits in order to illuminate the qualitative effects of strong interactions.

In future studies, thermodynamic approaches can take advantage of reliable variational ground states, e.g. DMRG [3], to obtain low temperature dynamical correlations in other strongly correlated lattice models of spins, fermions and bosons. For example: thermal Hall coefficient formula of strongly frustrated magnetic insulators [60], the Hall conductivity of Heavy fermion metals [118], and nearly ferroelectric material SrTiO_4 [119], conductivities of interacting flat band multilayers of graphene [120] and transition metal dichalcogenides [121, 122].

Experimental measurements of conductivities of cold fermionic and bosonic atoms trapped in optical lattices with artificial gauge fields [123] could test the accuracy of thermodynamic calculations. On the mathematical side, further understanding of the relation between low order recurrences and the low frequency behavior of conductivities would be very worthwhile.

36. Acknowledgements

We thank Gil Refael for his encouragement to write the Report. We are indebted to Netanel Lindner, Snir Gazit, Ilia Khait, Noga Bashan, Abhisek Samanta and Ari Turner, whose results are reviewed in this Report. We are grateful for critical comments by Steve Kivelson, Steve Simon, Bruno Uchoa, and Daniel Arovas, which improved the readability of the manuscript. A.A. acknowledges the Israel Science Foundation (ISF) Grant No. 2081/20. This Report was written in part at the Aspen Center for Physics, which is supported by National Science Foundation grant PHY-2210452, and at the Kavli Institute for Theoretical Physics, supported by Grant Nos. NSF PHY-1748958, NSF PHY-1748958 and NSF PHY-2309135.

References

- [1] A. W. Sandvik, Stochastic series expansion method with operator-loop update, *Physical Review B* 59 (22) (1999) R14157.
- [2] N. Prokof'ev, B. Svistunov, Worm algorithms for classical statistical models, *Phys. Rev. Lett.* 87 (2001) 160601. doi:10.1103/PhysRevLett.87.160601.
URL <https://link.aps.org/doi/10.1103/PhysRevLett.87.160601>
- [3] S. R. White, Density matrix formulation for quantum renormalization groups, *Phys. Rev. Lett.* 69 (1992) 2863–2866. doi:10.1103/PhysRevLett.69.2863.
URL <https://link.aps.org/doi/10.1103/PhysRevLett.69.2863>
- [4] U. Schollwöck, The density-matrix renormalization group in the age of matrix product states, *Annals of Physics* 326 (1) (2011) 96 – 192, January 2011 Special Issue. doi:<http://dx.doi.org/10.1016/j.aop.2010.09.012>.
URL <http://www.sciencedirect.com/science/article/pii/S0003491610001752>
- [5] P. Corboz, S. R. White, G. Vidal, M. Troyer, Stripes in the two-dimensional t-j model with infinite projected entangled-pair states, *Physical Review B* 84 (4) (2011) 041108.
- [6] M. Fishman, S. White, E. Stoudenmire, The itensor software library for tensor network calculations, *SciPost Physics Codebases* (2022) 004.
- [7] W. Kohn, J. Luttinger, Quantum theory of electrical transport phenomena, *Physical Review* 108 (3) (1957) 590.
- [8] J. Ziman, *Electrons and phonons: the theory of transport phenomena in solids*, Oxford university press, 1960.
- [9] G. Mahan, *Many-Particle Physics, Physics of Solids and Liquids*, Springer, 2000.
URL <https://books.google.co.il/books?id=xzSgZ4-yyMEC>
- [10] M. E. Cage, K. Klitzing, A. Chang, F. Duncan, M. Haldane, R. B. Laughlin, A. Pruisken, D. Thouless, *The quantum Hall effect*, Springer Science & Business Media, 2012.
- [11] B. A. Bernevig, *Topological Insulators and Topological Superconductors*, Princeton University Press, Princeton, 2013 [cited 2024-02-20]. doi:doi:10.1515/9781400846733.
URL <https://doi.org/10.1515/9781400846733>
- [12] D. J. Thouless, M. Kohmoto, M. P. Nightingale, M. den Nijs, Quantized hall conductance in a two-dimensional periodic potential, *Phys. Rev. Lett.* 49 (1982) 405–408. doi:10.1103/PhysRevLett.49.405.
URL <https://link.aps.org/doi/10.1103/PhysRevLett.49.405>
- [13] J. E. Avron, R. Seiler, Quantization of the hall conductance for general, multiparticle schrödinger hamiltonians, *Physical review letters* 54 (4) (1985) 259.
- [14] P. Streda, L. Smrcka, Thermodynamic derivation of the hall current and the thermopower in quantising magnetic field, *Journal of Physics C: Solid State Physics* 16 (24) (1983) L895.
URL <http://stacks.iop.org/0022-3719/16/i=24/a=005>
- [15] V. Emery, S. Kivelson, Superconductivity in bad metals, *Physical Review Letters* 74 (16) (1995) 3253.
- [16] R. Kubo, Statistical-Mechanical Theory of Irreversible Processes. I. General Theory and Simple Applications to Magnetic and Conduction Problems, *Journal of the Physical Society of Japan* 12 (6) (1957) 570–586. arXiv:<https://doi.org/10.1143/JPSJ.12.570>, doi:10.1143/JPSJ.12.570.
URL <https://doi.org/10.1143/JPSJ.12.570>
- [17] S. Gazit, D. Podolsky, A. Auerbach, D. P. Arovas, Dynamics and conductivity near quantum criticality, *Phys. Rev. B* 88 (2013) 235108. doi:10.1103/PhysRevB.88.235108.
URL <https://link.aps.org/doi/10.1103/PhysRevB.88.235108>
- [18] N. R. Cooper, B. I. Halperin, I. M. Ruzin, Thermoelectric response of an interacting two-dimensional electron gas in a quantizing magnetic field, *Phys. Rev. B* 55 (1997) 2344–2359. doi:10.1103/PhysRevB.55.2344.
URL <https://link.aps.org/doi/10.1103/PhysRevB.55.2344>
- [19] T. Qin, Q. Niu, J. Shi, Energy magnetization and the thermal hall effect, *Physical review letters* 107 (23) (2011) 236601.
- [20] N. H. Lindner, A. Auerbach, Conductivity of hard core bosons: A paradigm of a bad metal, *Physical Review B* 81 (5) (2010) 054512.
- [21] V. Viswanath, G. Müller, *The recursion method: application to many body dynamics*, Vol. 23, Springer Science & Business Media, 1994.
- [22] I. Khait, S. Bhattacharyya, A. Samanta, A. Auerbach, Hall map and breakdown of fermi liquid theory in the vicinity of a mott insulator, arXiv: 2211.15711 (2022).
- [23] S. Sorella, The phase diagram of the Hubbard model by Variational Auxiliary Field quantum Monte Carlo, Preprint at: <https://arxiv.org/abs/2101.07045> (2021). doi:10.48550/ARXIV.2101.07045.
URL <https://arxiv.org/abs/2101.07045>
- [24] A. Dorneich, M. Troyer, Accessing the dynamics of large many-particle systems using the stochastic series expansion, *Phys. Rev. E* 64 (2001) 066701. doi:10.1103/PhysRevE.64.066701.
URL <https://link.aps.org/doi/10.1103/PhysRevE.64.066701>
- [25] N. W. Ashcroft, N. D. Mermin, *Solid state physics*, Cengage Learning, 2022.
- [26] S. M. Girvin, K. Yang, *Modern condensed matter physics*, Cambridge University Press, 2019.
- [27] M.-C. Chang, Q. Niu, Berry phase, hyperorbits, and the hofstadter spectrum: Semiclassical dynamics in magnetic bloch bands, *Phys. Rev. B* 53 (1996) 7010–7023. doi:10.1103/PhysRevB.53.7010.
URL <https://link.aps.org/doi/10.1103/PhysRevB.53.7010>
- [28] H. Mori, Transport, collective motion, and brownian motion, *Progress of theoretical physics* 33 (3) (1965) 423–455.
- [29] R. Zwanzig, *Nonequilibrium statistical mechanics*, Oxford university press, 2001.
- [30] N. Das, P. Bhalla, N. Singh, Memory function approach to correlated electron transport: A comprehensive review, *International Journal of Modern Physics B* 30 (23) (2016) 1630015. arXiv:<https://doi.org/10.1142/S0217979216300152>, doi:10.1142/S0217979216300152.
URL <https://doi.org/10.1142/S0217979216300152>

- [31] W. Götze, P. Wölfle, Homogeneous dynamical conductivity of simple metals, *Physical Review B* 6 (4) (1972) 1226.
- [32] P. W. Anderson, Absence of diffusion in certain random lattices, *Phys. Rev.* 109 (1958) 1492–1505. doi:10.1103/PhysRev.109.1492. URL <https://link.aps.org/doi/10.1103/PhysRev.109.1492>
- [33] E. Abrahams, P. Anderson, D. Licciardello, T. Ramakrishnan, Scaling theory of localization: Absence of quantum diffusion in two dimensions, *Physical Review Letters* 42 (10) (1979) 673.
- [34] E. Abrahams, 50 years of Anderson Localization, Vol. 24, world scientific, 2010.
- [35] E. Akkermans, G. Montambaux, Mesoscopic physics of electrons and photons, Cambridge university press, 2007.
- [36] A. Ioffe, A. Regel, Non-crystalline, amorphous, and liquid electronic semiconductors, *Progress in semiconductors* (1960) 237–291.
- [37] K. T. N. E. Hussey, H. Takagi, Universality of the mott-ioffe-regel limit in metals, *Philosophical Magazine* 84 (27) (2004) 2847–2864. arXiv:<https://doi.org/10.1080/14786430410001716944>, doi:10.1080/14786430410001716944. URL <https://doi.org/10.1080/14786430410001716944>
- [38] P. B. Allen, B. Chakraborty, Infrared and dc conductivity in metals with strong scattering: Nonclassical behavior from a generalized boltzmann equation containing band-mixing effects, *Phys. Rev. B* 23 (1981) 4815–4827. doi:10.1103/PhysRevB.23.4815. URL <https://link.aps.org/doi/10.1103/PhysRevB.23.4815>
- [39] A. Sekine, D. Culcer, A. H. MacDonald, Quantum kinetic theory of the chiral anomaly, *Phys. Rev. B* 96 (2017) 235134. doi:10.1103/PhysRevB.96.235134. URL <https://link.aps.org/doi/10.1103/PhysRevB.96.235134>
- [40] C. H. Wong, Y. Tserkovnyak, Quantum kinetic equation in phase-space textured multiband systems, *Phys. Rev. B* 84 (2011) 115209. doi:10.1103/PhysRevB.84.115209. URL <https://link.aps.org/doi/10.1103/PhysRevB.84.115209>
- [41] J. M. Luttinger, Theory of thermal transport coefficients, *Phys. Rev.* 135 (1964) A1505–A1514. doi:10.1103/PhysRev.135.A1505. URL <https://link.aps.org/doi/10.1103/PhysRev.135.A1505>
- [42] B. S. Shastry, Sum rule for thermal conductivity and dynamical thermal transport coefficients in condensed matter, *Physical Review B* 73 (8) (2006) 085117.
- [43] T. Qin, J. Zhou, J. Shi, Berry curvature and the phonon hall effect, *Physical Review B* 86 (10) (2012) 104305.
- [44] H. Katsura, N. Nagaosa, P. A. Lee, Theory of the thermal hall effect in quantum magnets, *Physical review letters* 104 (6) (2010) 066403.
- [45] S. H. Simon, M. S. Rudner, Contrasting lattice geometry dependent versus independent quantities: Ramifications for berry curvature, energy gaps, and dynamics, *Phys. Rev. B* 102 (2020) 165148. doi:10.1103/PhysRevB.102.165148. URL <https://link.aps.org/doi/10.1103/PhysRevB.102.165148>
- [46] F. D. M. Haldane, Model for a quantum hall effect without landau levels: Condensed-matter realization of the “parity anomaly”, *Physical review letters* 61 (18) (1988) 2015.
- [47] A. Auerbach, Equilibrium formulae for transverse magnetotransport of strongly correlated metals, *Physical Review B* 99 (11) (2019) 115115.
- [48] A. Yacoby, H. Hess, T. Fulton, L. Pfeiffer, K. West, Electrical imaging of the quantum hall state, *Solid state communications* 111 (1) (1999) 1–13.
- [49] D. Xiao, Y. Yao, Z. Fang, Q. Niu, Berry-phase effect in anomalous thermoelectric transport, *Phys. Rev. Lett.* 97 (2006) 026603. doi:10.1103/PhysRevLett.97.026603. URL <https://link.aps.org/doi/10.1103/PhysRevLett.97.026603>
- [50] R. Matsumoto, S. Murakami, Rotational motion of magnons and the thermal hall effect, *Phys. Rev. B* 84 (2011) 184406. doi:10.1103/PhysRevB.84.184406. URL <https://link.aps.org/doi/10.1103/PhysRevB.84.184406>
- [51] G. Sundaram, Q. Niu, Wave-packet dynamics in slowly perturbed crystals: Gradient corrections and berry-phase effects, *Phys. Rev. B* 59 (1999) 14915–14925. doi:10.1103/PhysRevB.59.14915. URL <https://link.aps.org/doi/10.1103/PhysRevB.59.14915>
- [52] T. Jungwirth, Q. Niu, A. MacDonald, Anomalous hall effect in ferromagnetic semiconductors, *Physical review letters* 88 (20) (2002) 207208.
- [53] N. Sinitsyn, Q. Niu, J. Sinova, K. Nomura, Disorder effects in the anomalous hall effect induced by berry curvature, *Physical Review B* 72 (4) (2005) 045346.
- [54] M. P. Marder, *Condensed matter physics*, John Wiley & Sons, 2010.
- [55] J.-i. Inoue, G. E. W. Bauer, L. W. Molenkamp, Suppression of the persistent spin hall current by defect scattering, *Phys. Rev. B* 70 (2004) 041303. doi:10.1103/PhysRevB.70.041303. URL <https://link.aps.org/doi/10.1103/PhysRevB.70.041303>
- [56] K. Nomura, J. Sinova, T. Jungwirth, Q. Niu, A. MacDonald, Nonvanishing spin hall currents in disordered spin-orbit coupling systems, *Physical Review B* 71 (4) (2005) 041304.
- [57] A. Shytov, E. Mishchenko, H.-A. Engel, B. Halperin, Small-angle impurity scattering and the spin hall conductivity in two-dimensional semiconductor systems, *Physical Review B* 73 (7) (2006) 075316.
- [58] N. Bashan, A. Auerbach, Degeneracy-projected polarization formulas for hall-type conductivities, *Physical Review Letters* 128 (3) (2022) 036601.
- [59] J. Chalker, P. Coddington, Percolation, quantum tunnelling and the integer hall effect, *Journal of Physics C: Solid State Physics* 21 (14) (1988) 2665.
- [60] Y. Kasahara, K. Sugii, T. Ohnishi, M. Shimozawa, M. Yamashita, N. Kurita, H. Tanaka, J. Nasu, Y. Motome, T. Shibauchi, Y. Matsuda, Unusual thermal hall effect in a kitaev spin liquid candidate α - ruCl_3 , *Phys. Rev. Lett.* 120 (2018) 217205. doi:10.1103/PhysRevLett.120.217205. URL <https://link.aps.org/doi/10.1103/PhysRevLett.120.217205>
- [61] X. Li, B. Fauqué, Z. Zhu, K. Behnia, Phonon thermal Hall effect in strontium titanate, *Physical review letters* 124 (10) (2020) 105901.
- [62] G. Grissonnanche, S. Thériault, A. Gourgout, M. E. Boulanger, E. Lefrançois, A. Ataei, F. Laliberté, M. Dion, J. S. Zhou, S. Pyon, T. Takayama, H. Takagi, N. Doiron-Leyraud, L. Taillefer, Chiral phonons in the pseudogap phase of cuprates, *Nature Physics* 16 (11)

- (2020) 1108–1111. doi:10.1038/s41567-020-0965-y.
URL <https://doi.org/10.1038/s41567-020-0965-y>
- [63] R. P. Feynman, Atomic theory of the two-fluid model of liquid helium, *Physical Review* 94 (2) (1954) 262.
- [64] S. M. Girvin, A. H. MacDonald, P. M. Platzman, Magneto-roton theory of collective excitations in the fractional quantum hall effect, *Phys. Rev. B* 33 (1986) 2481–2494. doi:10.1103/PhysRevB.33.2481.
URL <https://link.aps.org/doi/10.1103/PhysRevB.33.2481>
- [65] D. P. Arovas, A. Auerbach, F. Haldane, Extended heisenberg models of antiferromagnetism: Analogies to the fractional quantum hall effect, *Physical review letters* 60 (6) (1988) 531.
- [66] A. Auerbach, *Interacting electrons and quantum magnetism*, Springer Science & Business Media, 2012.
- [67] G. Freud, On the coefficients in the recursion formulae of orthogonal polynomials, in: *Proceedings of the Royal Irish Academy. Section A: Mathematical and Physical Sciences*, JSTOR, 1976, pp. 1–6.
- [68] D. Lubinsky, H. Mhaskar, E. Saff, A proof of freud’s conjecture for exponential weights, *Constructive Approximation* 4 (1988) 65–83.
- [69] A. Auerbach, Hall number of strongly correlated metals, *Physical Review Letters* 121 (6) (2018) 066601.
- [70] N. Lindner, A. Auerbach, D. P. Arovas, Vortex dynamics and hall conductivity of hard-core bosons, *Physical Review B* 82 (13) (2010) 134510.
- [71] A. Samanta, D. P. Arovas, A. Auerbach, Hall coefficient of semimetals, *Physical Review Letters* 126 (7) (2021) 076603.
- [72] J. Hubbard, Electron correlations in narrow energy bands, *Proc. R. Soc. Lond.* (1963). doi:10.1103/PhysRevLett.111.036401.
URL <http://doi.org/10.1098/rspa.1963.0204>
- [73] D. P. Arovas, E. Berg, S. A. Kivelson, S. Raghu, The hubbard model, *Annual Review of Condensed Matter Physics* 13 (1) (2022) 239–274. arXiv:<https://doi.org/10.1146/annurev-conmatphys-031620-102024>, doi:10.1146/annurev-conmatphys-031620-102024.
URL <https://doi.org/10.1146/annurev-conmatphys-031620-102024>
- [74] J. Spałek, Effect of pair hopping and magnitude of intra-atomic interaction on exchange-mediated superconductivity, *Phys. Rev. B* 37 (1988) 533–536. doi:10.1103/PhysRevB.37.533.
URL <https://link.aps.org/doi/10.1103/PhysRevB.37.533>
- [75] J. Jaklič, P. Prelovšek, Charge dynamics in the planar t-J model, *Physical Review B* 52 (9) (1995) 6903.
- [76] E. Perepelitsky, A. Galatas, J. Mravlje, E. Khatami, B. S. Shastry, A. Georges, et al., Transport and optical conductivity in the Hubbard model: A high-temperature expansion perspective, *Physical Review B* 94 (23) (2016) 235115.
- [77] E. W. Huang, R. Sheppard, B. Moritz, T. P. Devereaux, Strange metallicity in the doped hubbard model, *Science* 366 (6468) (2019) 987–990. arXiv:<https://www.science.org/doi/pdf/10.1126/science.aau7063>, doi:10.1126/science.aau7063.
URL <https://www.science.org/doi/abs/10.1126/science.aau7063>
- [78] W. Xu, K. Haule, G. Kotliar, Hidden Fermi Liquid, Scattering Rate Saturation, and Nernst Effect: A Dynamical Mean-Field Theory Perspective, *Phys. Rev. Lett.* 111 (2013) 036401. doi:10.1103/PhysRevLett.111.036401.
URL <https://link.aps.org/doi/10.1103/PhysRevLett.111.036401>
- [79] E. Z. Kuchinskii, N. A. Kuleeva, D. I. Khomskii, M. V. Sadovskii, Hall effect in a doped mott insulator: Dmft approximation, *JETP Letters* 115 (7) (2022) 402–405.
- [80] W. O. Wang, J. K. Ding, B. Moritz, Y. Schattner, E. W. Huang, T. P. Devereaux, Numerical approaches for calculating the low-field dc Hall coefficient of the doped Hubbard model, *Phys. Rev. Research* 3 (2021) 033033. doi:10.1103/PhysRevResearch.3.033033.
URL <https://link.aps.org/doi/10.1103/PhysRevResearch.3.033033>
- [81] Imaginary time QMC conductivities require analytic continuation, which is limited to frequencies higher than temperature (see Appendix B in [17]). The DC conductivities are often deduced by proxies to the analytical continuation [80].
- [82] W. Wu, M. S. Scheurer, S. Chatterjee, S. Sachdev, A. Georges, M. Ferrero, Pseudogap and fermi-surface topology in the two-dimensional hubbard model, *Phys. X* 8 (2018) 021048. doi:10.1103/PhysRevX.8.021048.
URL <https://link.aps.org/doi/10.1103/PhysRevX.8.021048>
- [83] A. A. Markov, G. Rohringer, A. N. Rubtsov, Robustness of the topological quantization of the Hall conductivity for correlated lattice electrons at finite temperatures, *Phys. Rev. B* 100 (2019) 115102. doi:10.1103/PhysRevB.100.115102.
URL <https://link.aps.org/doi/10.1103/PhysRevB.100.115102>
- [84] J. Vučićević, R. Žitko, Electrical conductivity in the Hubbard model: Orbital effects of magnetic field, *Phys. Rev. B* 104 (2021) 205101. doi:10.1103/PhysRevB.104.205101.
URL <https://link.aps.org/doi/10.1103/PhysRevB.104.205101>
- [85] Y. Shi, J. Schirmer, L.-Q. Chen, Hall coefficient and resistivity in the doped bilayer hubbard model, Preprint at: <https://arxiv.org/abs/2308.03862> (2023).
- [86] R. Krishna Kumar, X. Chen, G. Auton, A. Mishchenko, D. A. Bandurin, S. V. Morozov, Y. Cao, E. Khestanova, M. Ben Shalom, A. Kretinin, et al., High-temperature quantum oscillations caused by recurring Bloch states in graphene superlattices, *Science* 357 (6347) (2017) 181–184.
- [87] W. O. Wang, J. K. Ding, B. Moritz, E. W. Huang, T. P. Devereaux, Dc hall coefficient of the strongly correlated hubbard model, *npj Quantum Materials* 5 (1) (2020) 51.
- [88] B. Shastry, B. Shraiman, R. Singh, Faraday rotation and the hall constant in strongly correlated fermi systems, *Physical review letters* 70 (13) (1993) 2004.
- [89] P. Hosur, A. Kapitulnik, S. A. Kivelson, J. Orenstein, S. Raghu, W. Cho, A. Fried, Erratum: Kerr effect as evidence of gyrotropic order in the cuprates [*Phys. Rev. B* 87, 115116 (2013)], *Phys. Rev. B* 91 (2015) 039908. doi:10.1103/PhysRevB.91.039908.
URL <https://link.aps.org/doi/10.1103/PhysRevB.91.039908>
- [90] P. W. Anderson, The Resonating Valence Bond State in LaCuO and Superconductivity, *Science* 235 (4793) (1987) 1196–1198. arXiv:<https://www.science.org/doi/pdf/10.1126/science.235.4793.1196>, doi:10.1126/science.235.4793.1196.
URL <https://www.science.org/doi/abs/10.1126/science.235.4793.1196>

- [91] Y. J. Uemura, G. M. Luke, B. J. Sternlieb, J. H. Brewer, J. F. Carolan, W. N. Hardy, R. Kadono, J. R. Kempton, R. F. Kiefl, S. R. Kreitzman, P. Mulhern, T. M. Riseman, D. L. Williams, B. X. Yang, S. Uchida, H. Takagi, J. Gopalakrishnan, A. W. Sleight, M. A. Subramanian, C. L. Chien, M. Z. Cieplak, G. Xiao, V. Y. Lee, B. W. Statt, C. E. Stronach, W. J. Kossler, X. H. Yu, Universal Correlations between T_c and $\frac{n_s}{m^*}$ (Carrier Density over Effective Mass) in High- T_c Cuprate Superconductors, *Phys. Rev. Lett.* 62 (1989) 2317–2320. doi:10.1103/PhysRevLett.62.2317.
URL <https://link.aps.org/doi/10.1103/PhysRevLett.62.2317>
- [92] S. Y. F. Zhao, N. Poccia, M. G. Panetta, C. Yu, J. W. Johnson, H. Yoo, R. Zhong, G. D. Gu, K. Watanabe, T. Taniguchi, S. V. Postolova, V. M. Vinokur, P. Kim, Sign-Reversing Hall Effect in Atomically Thin High-Temperature $\text{Bi}_{2.1}\text{Sr}_{1.9}\text{CaCu}_{2.0}\text{O}_{8+\delta}$ Superconductors, *Phys. Rev. Lett.* 122 (2019) 247001. doi:10.1103/PhysRevLett.122.247001.
URL <https://link.aps.org/doi/10.1103/PhysRevLett.122.247001>
- [93] A. Auerbach, D. P. Arovas, Hall anomaly and moving vortex charge in layered superconductors, *SciPost Phys.* 8 (2020) 061. doi:10.21468/SciPostPhys.8.4.061.
URL <https://scipost.org/10.21468/SciPostPhys.8.4.061>
- [94] Y. J. Lin, R. L. Compton, K. Jiménez-García, J. V. Porto, I. B. Spielman, Synthetic magnetic fields for ultracold neutral atoms, *Nature* 462 (7273) (2009) 628–632. doi:10.1038/nature08609.
URL <https://doi.org/10.1038/nature08609>
- [95] R. T. Scalettar, G. G. Batrouni, G. T. Zimanyi, Localization in interacting, disordered, bose systems, *Physical review letters* 66 (24) (1991) 3144.
- [96] L. Pitaevskii, S. Stringari, Bose-Einstein condensation and superfluidity, Vol. 164, Oxford University Press, 2016.
- [97] S. D. Huber, N. H. Lindner, Topological transitions for lattice bosons in a magnetic field, *Proceedings of the National Academy of Sciences* 108 (50) (2011) 19925–19930.
- [98] N. H. Lindner, A. Auerbach, D. P. Arovas, Vortex quantum dynamics of two dimensional lattice bosons, *Physical review letters* 102 (7) (2009) 070403.
- [99] S. Sachdev, Quantum phase transitions, second ed. Edition, Cambridge University Press, Cambridge, 2011.
- [100] M. P. Fisher, P. B. Weichman, G. Grinstein, D. S. Fisher, Boson localization and the superfluid-insulator transition, *Physical Review B* 40 (1) (1989) 546.
- [101] D. Podolsky, A. Auerbach, D. P. Arovas, Visibility of the amplitude (higgs) mode in condensed matter, *Physical Review B* 84 (17) (2011) 174522.
- [102] X. Zotos, F. Naef, M. Long, P. Prelovšek, Drude Weight, Integrable Systems and the Reactive Hall Constant, Springer Netherlands, Dordrecht, 2001, pp. 273–282.
- [103] R. Citro, T. Giamarchi, E. Orignac, Hall response in interacting bosonic and fermionic ladders (2024). [arXiv:2404.16973](https://arxiv.org/abs/2404.16973).
- [104] H.-Q. Ding, M. Makivic, Kosterlitz-thouless transition in the two-dimensional quantum xy model, *Physical Review B* 42 (10) (1990) 6827.
- [105] H.-Q. Ding, Phase transition and thermodynamics of quantum xy model in two dimensions, *Phys. Rev. B* 45 (1992) 230–242. doi:10.1103/PhysRevB.45.230.
URL <https://link.aps.org/doi/10.1103/PhysRevB.45.230>
- [106] K. Harada, N. Kawashima, Universal jump in the helicity modulus of the two-dimensional quantum xy model, *Phys. Rev. B* 55 (1997) R11949–R11952. doi:10.1103/PhysRevB.55.R11949.
URL <https://link.aps.org/doi/10.1103/PhysRevB.55.R11949>
- [107] V. Berezinskii, Destruction of long-range order in one-dimensional and two-dimensional systems having a continuous symmetry group i. classical systems, *Sov. Phys. JETP* 32 (3) (1971) 493–500.
- [108] J. M. Kosterlitz, D. J. Thouless, Ordering, metastability and phase transitions in two-dimensional systems, *Journal of Physics C: Solid State Physics* 6 (7) (1973) 1181.
- [109] A. W. Sandvik, C. J. Hamer, Ground-state parameters, finite-size scaling, and low-temperature properties of the two-dimensional $s = 1/2$ xy model, *Physical Review B* 60 (9) (1999) 6588.
- [110] K. Bernardet, G. Batrouni, J.-L. Meunier, G. Schmid, M. Troyer, A. Dorneich, Analytical and numerical study of hardcore bosons in two dimensions, *Physical Review B* 65 (10) (2002) 104519.
- [111] D. C. Mattis, J. Bardeen, Theory of the anomalous skin effect in normal and superconducting metals, *Physical Review* 111 (2) (1958) 412.
- [112] S. Mukerjee, V. Oganesyan, D. Huse, Statistical theory of transport by strongly interacting lattice fermions, *Physical Review B* 73 (3) (2006) 035113.
- [113] B. Halperin, D. R. Nelson, Resistive transition in superconducting films, *Journal of low temperature physics* 36 (1979) 599–616.
- [114] S. Bhattacharyya, A. De, S. Gazit, A. Auerbach, Metallic transport of hard core bosons, [arXiv:2309.14479](https://arxiv.org/abs/2309.14479) (2023). [arXiv:2309.14479](https://arxiv.org/abs/2309.14479).
- [115] Y. Motoyama, K. Yoshimi, A. Masaki-Kato, T. Kato, N. Kawashima, Dsqss: Discrete space quantum systems solver, *Computer Physics Communications* 264 (2021) 107944. doi:<https://doi.org/10.1016/j.cpc.2021.107944>.
URL <https://www.sciencedirect.com/science/article/pii/S0010465521000692>
- [116] O. F. Syljuåsen, A. W. Sandvik, Quantum monte carlo with directed loops, *Phys. Rev. E* 66 (2002) 046701. doi:10.1103/PhysRevE.66.046701.
URL <https://link.aps.org/doi/10.1103/PhysRevE.66.046701>
- [117] I. Khait, S. Bhattacharyya, A. Samanta, A. Auerbach, Hall map and breakdown of Fermi liquid theory in the vicinity of a Mott insulator, [arXiv:2211.15711](https://arxiv.org/abs/2211.15711) (2022).
- [118] N. Maksimovic, D. H. Eilbott, T. Cookmeyer, F. Wan, J. Ruzs, V. Nagarajan, S. C. Haley, E. Maniv, A. Gong, S. Faubel, I. M. Hayes, A. Bangura, J. Singleton, J. C. Palmstrom, L. Winter, R. McDonald, S. Jang, P. Ai, Y. Lin, S. Ciocys, J. Gobbo, Y. Werman, P. M. Oppeneer, E. Altman, A. Lanzara, J. G. Analytis, Evidence for a delocalization quantum phase transition without symmetry breaking in CeCoIn₅, *Science* 375 (6576) (2022) 76–81. [arXiv:https://www.science.org/doi/pdf/10.1126/science.aaz4566](https://arxiv.org/abs/https://www.science.org/doi/pdf/10.1126/science.aaz4566), doi:10.1126/science.aaz4566.
- [119] X. Li, B. Fauqué, Z. Zhu, K. Behnia, Phonon thermal Hall effect in strontium titanate, *Physical review letters* 124 (10) (2020) 105901.

- [120] E. Y. Andrei, A. H. MacDonald, Graphene bilayers with a twist, *Nature Materials* 19 (12) (2020) 1265–1275. doi:10.1038/s41563-020-00840-0.
URL <https://doi.org/10.1038/s41563-020-00840-0>
- [121] M. M. Scherer, D. M. Kennes, L. Classen, Chiral superconductivity with enhanced quantized Hall responses in moiré transition metal dichalcogenides, *npj Quantum Materials* 7 (1) (2022) 100. doi:10.1038/s41535-022-00504-z.
URL <https://doi.org/10.1038/s41535-022-00504-z>
- [122] J. Pizarro, S. Adler, K. Zantout, T. Mertz, P. Barone, R. Valentí, G. Sangiovanni, T. O. Wehling, Deconfinement of Mott localized electrons into topological and spin-orbit-coupled Dirac fermions, *npj Quantum Materials* 5 (1) (2020) 79. doi:10.1038/s41535-020-00277-3.
URL <https://doi.org/10.1038/s41535-020-00277-3>
- [123] P. T. Brown, D. Mitra, E. Guardado-Sanchez, R. Nourafkan, A. Reymbaut, C.-D. Hébert, S. Bergeron, A.-M. Tremblay, J. Kokalj, D. A. Huse, et al., Bad metallic transport in a cold atom Fermi-Hubbard system, *Science* 363 (6425) (2019) 379–382.